INSIGHT INTO GLOBAL GROUND-LEVEL AIR QUALITY USING SATELLITES, MODELING AND IN SITU MEASUREMENTS

by

Sajeev Philip

Submitted in partial fulfilment of the requirements
for the degree Doctor of Philosophy

at

Dalhousie University
Halifax, Nova Scotia
October 2015

TABLE OF CONTENTS

LIST OF TABLES

LIST OF FIGURES

ABSTRACT

Ground-level air quality depends on the ambient concentration of atmospheric aerosols and trace gases. We applied information on aerosols and trace gases gathered from satellite remote sensing, in situ observations, and atmospheric chemistry modelling to improve estimates of air quality. We inferred fine particulate matter ($PM_{2.5}$) chemical composition at 0.1^o x 0.1^o spatial resolution for 2004-2008 by combining aerosol optical depth retrieved from the MODIS and MISR satellite instruments, with coincident profile and composition information from the GEOS-Chem global chemical transport model. Evaluation of the satellite-model $PM_{2.5}$ composition dataset with North American in situ measurements indicated significant spatial agreement. We found that global population-weighted $PM_{2.5}$ concentrations were dominated by particulate organic mass (11.9 ± 7.3 $\mu g/m^3$), secondary inorganic aerosol (11.1 ± 5.0 $\mu g/m^3$), and mineral dust (11.1 ± 7.9 $\mu g/m^3$). Secondary inorganic $PM_{2.5}$ concentrations exceeded 30 $\mu g/m^3$ over East China. Sensitivity simulations suggested that population-weighted ambient $PM_{2.5}$ from biofuel burning (11 $\mu g/m^3$) could be almost as large as from fossil fuel combustion sources (17 $\mu g/m^3$).

We developed a simple method to derive an estimate of the spatially and seasonally resolved global, lower tropospheric, ratio between organic mass (OM) and organic carbon (OC). We used the Aerosol Mass Spectrometer-measured organic aerosol data, and the ground-level nitrogen dioxide concentrations derived from the OMI satellite instrument, to develop the OM/OC estimate. The global OM/OC ratio ranged from 1.3 to 2.1 $\mu g/\mu gC$, with distinct spatial variation between urban and rural regions. The seasonal OM/OC ratio had a summer maximum and a winter minimum over regions dominated by combustion emissions.

We assessed the sensitivity of chemical transport models to the duration of the chemical and transport operators used to calculate the mass continuity equation. Increasing the transport timestep increased the concentrations of emitted species, and the production of ozone. Increasing the chemical timestep increased hydroxyl radical and chemical feedbacks. The simulation error from changing spatial resolution exceeds that from changing temporal resolution.

LIST OF ABBREVIATIONS AND SYMBOLS USED

ACENET	Atlantic Computational Excellence Network
AERONET	Aerosol Robotic Network
AMS	Aerosol Mass Spectrometer
AOD	Aerosol Optical Depth
BC	Black Carbon
BRAVO	Big Bend Regional Aerosol and Visibility Observational Inventory
CALIOP	Cloud-Aerosol Lidar with Orthogonal Polarization
CALIPSO	Cloud-Aerosol Lidar and Infrared Pathfinder Satellite Observations
CAPMON	Canadian Air and Precipitation Monitoring Network
CASTNET	Clean Air Status and Trends Network
CPU	Central Processing Unit
CTM	Chemical Transport Model
DJF	December-January-February
DRH	Deliquescence Relative Humidity
EANET	Acid Deposition Monitoring Network in East Asia
EDGAR	Emission Database for Global Atmospheric Research
EMEP	European Monitoring and Evaluation Programme
EPA-AQS	U.S. Environmental Protection Agency Air Quality System
EPA-NEI	Environmental protection Agency-National Emissions Inventory
f_{POA}	Fraction of Primary Organic Aerosol
FTIR	Fourier Transform Infrared Spectroscopy
GAMAO	Global Modeling Assimilation Office
GEOS	Goddard Earth Observing System
GFED	Global Fire Emissions Database
HOA	Hydrocarbon-like Organic Aerosol
I	Intensity of light (W m^{-2})
I_0	Source intensity (W m^{-2})
IMPROVE	Interagency Monitoring of Protected Visual Environments
IPCC	Intergovernmental Panel on Climate Change
JJA	June-July-August
LIDAR	Light Detection and Ranging Instruments

MAM	March-April-May
MISR	Multiangle Imaging Spectroradiometer
MODIS	Moderate Resolution Imaging Spectroradiometer
N	Number of observations
NAPS	National Air Pollution Surveillance Network
NASA	National Aeronautics and Space Administration
NE	Normalized Error
NO_x	$NO + NO_2$
NSERC	National Science and Engineering Research Council
OA	Organic Aerosol
OC	Organic Carbon
OM	Organic Mass (a synonym of Organic Aerosol)
OMI	Ozone Monitoring Instrument
OOA	Oxygenated Organic Aerosol
PM_1	Fine particulate matter with aerodynamic diameter less than 1 μm (μm m^{-3})
$PM_{2.5}$	Fine particulate matter with aerodynamic diameter less than 2.5 μm (μm m^{-3})
PM_{10}	Fine particulate matter with aerodynamic diameter less than 10 μm (μm m^{-3})
POA	Primary Organic Aerosol
$P(\Theta)$	Aerosol phase function
R	Reflectance
R_a	Aerosol induced reflectance
R_m	Reflectance by molecular scattering
R_s	Surface reflectance
RMSE	Root Mean Square Error
SIA	Secondary Inorganic Aerosol
SOA	Secondary Organic Aerosol
SON	September-October-November
TEOM	Tapered Element Oscillating Monitor
VOC	Volatile Organic Compounds
WHO	World Health Organization

θ	Viewing angle (^{o})
Θ	Scattering angle (^{o})
σ	Trace gas absorption cross section (m^2 $molecule^{-1}$)
Ω	Column abundance of the trace gas (molecules cm^{-2})
ϖ	Aerosol single scattering albedo
τ	Optical depth

ACKNOWLEDGEMENTS

I would like to thank my supervising professor, Dr. Randall V. Martin for his profound guidance. I am thankful to my supervisory committee, Dr. Ian A. Folkins, Dr. Jeffrey R. Pierce, and Dr. Rachel Y.-W. Chang, and the members of the Atmospheric Composition Analysis Group at Dalhousie University for their contributions. I would like to acknowledge the coauthors, Dr. Aaron van Donkelaar, Mr. Jason Wai-Ho Lo, Dr. Yuxuan Wang, Dr. Dan Chen, Dr. Lin Zhang, Dr. Prasad S. Kasibhatla, Dr. Siwen Wang, Dr. Qiang Zhang, Dr. Zifeng Lu, Dr. David G. Streets, Dr. Shabtai Bittman, Dr. Douglas J. Macdonald, Dr. Jose-Luis Jimenez, Dr. Qi Zhang, Dr. Manjula. R. Canagaratna, Dr. Dominick. V. Spracklen, Dr. Caroline. R. Nowlan, Dr. Lok N. Lamsal, Mr. Matthew. J. Cooper, Dr. Nickolay A. Krotkov and Dr. Christoph A. Keller, and several anonymous reviewers. I am grateful to the MODIS, MISR, CALIOP, AERONET, NAPS, CAPMoN, CASTNET, IMPROVE, EPA-AQS, EMEP, and EANET teams for making their data publicly available. I am thankful for the research funding from Dr. Randall V. Martin, and from Health Canada, the National Science and Engineering Research Council of Canada, the Atlantic Computational Excellence Network, and the U.S. National Institutes of Health.

CHAPTER 1: INTRODUCTION

A byproduct of human technological advances over the last three centuries is an enormous increase in atmospheric aerosols and trace gases (IPCC, 2013) that deteriorate ground-level air quality. Ambient air pollution from anthropogenic and natural sources is a major human health burden (e.g., Dockery et al., 1993; Lim et al., 2012; WHO, 2013). Assessing atmospheric chemistry and improving air quality requires an in depth understanding of the distribution and composition of aerosols (e.g., Andreae and Crutzen, 1997).

1.1 Ground-level air quality and aerosols

The outdoor air which we breathe contains a heterogeneous combination of numerous gases and particles, some of which create health problems. The relative risks of various pollutants are determined by their size, chemical composition, toxicity, and its relative abundance in the atmosphere. Epidemiologic studies identified the major pollutant as aerosols, which are small particles suspended in the atmosphere. Other pollutants include ozone (O_3), nitrogen oxides ($NO_x = NO_2 + NO$), sulfur dioxide (SO_2) and carbon monoxide (CO). In fact, trace gases undergo chemical reactions in the atmosphere and play a key role in determining the abundance of aerosols.

Fine particles induce systemic and airway inflammatory, and other vascular responses, and affect neural pathways (Health Effects Institute, 2004; Brook et al., 2010). Fine particles can enter into human lungs, deposit into the respiratory tract, and lead to cardiac and respiratory inflammation. People with pre-existing diseases become more susceptible to increased risk of mortality on further exposures (Health Effects Institute, 2004). Reduction

of $PM_{2.5}$ (fine particulate matter with aerodynamic diameter less than 2.5 micrometers) by 10 $\mu g/m^3$ could increase life expectancy by 0.61 ± 0.2 years (Pope et al., 2009).

In addition, aerosols and their precursor trace gases have a wide range of impacts on climate, ecosystem and visibility (e.g., Ramanathan and Carmichael, 2008; IPCC, 2013). An insight into the processes determining their atmospheric abundance is needed to understand air quality and climate.

1.2 Sources and properties of aerosols

Atmospheric aerosols exist in different size ranges and chemical compositions. Based on the size distribution, aerosols are broadly divided into three categories, namely ultrafine (particles with aerodynamic diameter < 0.1 μm), accumulation (0.1 –1 μm) and coarse (> 1 μm) particles (Seinfeld and Pandis, 2006). The ultrafine particles in the atmosphere are formed by the clustering of gas molecules (aerosol nucleation) or the condensation of hot vapors during combustion. The growth of these particles through 1) condensation of gases, 2) collisions (coagulation), and 3) non-precipitating cloud processing (Hoppel et al., 1986) leads to accumulation mode aerosols. The size transition of accumulation particles to coarse mode is slow as the condensation and coagulation rates diminish with increasing mass. Accumulation mode particles have a lifetime of days to weeks before removal (primarily through scavenging by cloud droplets and precipitation).

The coarse particles, such as mineral dust and sea spray are formed by the mechanical action of wind on the Earth's surface, and ocean wave breaking. Vegetative debris, biological materials, microorganisms, and toxic elements are also part of this coarse aerosol category. The condensation of semi volatile gases forms a coating on dust and sea spray.

The coarse particles settle out within a short time due to their high sedimentation velocity. Precipitation is also a major removal process.

Atmospheric aerosols contain water. The phase transition of aerosols from their solid state at a low relative humidity (RH) to the liquid phase happens at a transition point known as deliquescence RH (DRH) (Seinfeld and Pandis, 2006). The hygroscopic growth of aerosols is due to the condensation of water onto the aerosol-solution. For some salts (e.g., ammonium sulfate), the decrease of RH does not crystallize the salt at DRH; rather it remains supersaturated until it crystallizes at a lower RH (DRH is ~62% for ammonium nitrate, and ~80% for ammonium sulfate). Internal aerosol mixtures such as salts and organics in the atmosphere exhibit even lower crystallization points.

Epidemiological literatures typically distinguish the aerosol size ranges as $PM_{0.1}$ (particulate matter < 0.1 μm), $PM_{2.5}$ (< 2.5 μm), and PM_{10} (<10 μm). $PM_{2.5}$ is most consistently found to be deleterious to health (e.g., Chen et al., 2008) due to its small size to penetrate into human respiratory tracts. The effects of $PM_{0.1}$ are more uncertain.

The chemical components of $PM_{2.5}$ include sulfate, nitrate and ammonium ions (secondary inorganic aerosols), black carbon (BC), organic carbon (OC), and mechanically driven particles (such as, dust, sea salt and trace metals). Sulfur dioxide and primary sulfate particles are emitted into the atmosphere mainly from the combustion of fossil fuels. The majority of the H_2SO_4 in the atmosphere is oxidized from SO_2. Sulfuric acid then condenses to form aqueous sulfate particles owing to its low vapor pressure over the H_2SO_4-H_2O solution. These particles can be neutralized with ammonia gas to form ammonium sulfate particles. The atmospheric oxidation of NO_x forms nitric acid through a series of chemical

reactions. The reversible reaction of excess NH_3 with HNO_3 leads to ammonium nitrate formation, at low temperature and high relative humidity conditions. The excess NH_3 exists as NH_4^+ ions. The degree of ammonia neutralization varies spatially and temporally.

The majority of secondary inorganic aerosols are formed from the emissions of trace gases, such as NO_x, SO_2 and NH_3 from various anthropogenic and natural sources. The major anthropogenic emission sources include fossil fuel combustion and biofuel burning. Power plants and smelters produce much of the SO_2, while NO_x is emitted mainly from the transportation sources. Soil, fertilizers and lightning are the other sources of NO_x. Biomass burning, wild fires and other combustion sources release a certain amount of SO_2 and NO_2. Ammonia is emitted from agriculture, fertilizers and livestock.

Organic aerosols (OA) are mainly emitted by combustion processes, and from vegetation. In addition to primary organic aerosols, the volatile organic compounds (VOC) in the atmosphere lead to secondary organic aerosol (SOA) formation. The particulate organic mass (OM) contains organic carbon, and additional elements such as N, O, and H. Black carbon aerosols are emitted by incomplete combustion processes and from fires.

1.3 Monitoring of aerosols

Scientific understanding of the distribution and properties of aerosols developed in part through direct atmospheric measurements (McMurry, 2000). Ground level in situ measurements of aerosols provide size and mass distributions, aerosol composition, and optical properties. There are extensive operational aerosol monitoring networks especially across North America and Europe (e.g., Dabek-Zlotorzynska et al., 2011; Hand et al., 2011).

In situ samplers usually collect aerosols on a filter pack over sampling periods of 24-hr or 3 to 6 days (Hand et al., 2011). The different aerosol size ranges are separated out using various size inlets of the filter. Total $PM_{2.5}$ and PM_{10} mass concentrations are typically analyzed gravimetrically by weighing a teflon filter before and after sampling. A nylon filter preceded by a sodium carbonate coated denuder is used to measure anions and cations through ion chromatography. The denuder avoids the condensation of nitric acid and organic gases. The carbon mass, imbedded in the quartz filter, is analyzed by thermal optical reflectance or thermal optical transmittance techniques. The elemental compositions are determined using the X-ray fluorescence methods. Assumptions about the oxides of these elements are used to estimate dust (e.g., Al, Si, Fe) and sea salt (e.g., Na, Cl) particles.

The Tapered Element Oscillating Monitor (TEOM) provides hourly measurements of $PM_{2.5}$. It utilizes the frequency of vibration of an oscillator by aerosols to determine the mass (Allen et al., 1997). Trace gases like NO_2 and SO_2 are also measured by continuous gas monitors on an hourly basis through measurement networks.

These in situ measurement networks provide high quality concentration data which often is considered as the 'truth'. However, there are inherent uncertainties and limitations in these measurements. Volatilization of gases from the filter, and the trapping of organic gases in quartz filters induce negative and positive biases respectively (e.g., Hand et al., 2011). Other limitations of in situ monitoring are the need for manual labor and the high cost of instrument deployment. Many developing countries are nearly devoid of routine network measurements despite their being afflicted by high pollution levels. The vertical

mixing, horizontal transport and distribution of aerosols and trace gases could also be studied through the measurements of their vertical profiles. Aircraft campaigns (e.g., Kim et al., 2015) are usually conducted over specific regions.

The global distribution of aerosols cannot be determined through sparse measurements or campaigns. Remote sensing techniques offer insights into vertically resolved aerosol properties. For example, ground-based light detection and ranging instruments (LIDAR) provide the vertical backscatter profile of aerosols. However this valuable insight into the vertical distribution of aerosols is local in nature (spatially sparse). A nadir pointing active LIDAR aboard the CALIPSO (Cloud-Aerosol Lidar and Infrared Pathfinder Satellite Observations) satellite encircling the Earth in a sun synchronous polar orbit, is providing aerosol and cloud information backscatter profiles in spatially extensive sheets under the orbit line (Winker et al., 2007).

Remore sensing techniques generally retrieve the total atmospheric column abundance of aerosol and trace gases. Beer's law describes the scattering and absorption of light traversing a medium,

$$I = I_0 \exp(-\tau) \tag{1.1}$$

where, I_o and I are the source and scattered intensity of light respectively, at a particular wavelength. τ is the optical depth of the traversing medium which depends on the viewing angle θ, wavelength and other parameters. The optical thickness of aerosols in the light path is referred to aerosol optical depth (AOD). The AERONET (Aerosol Robotic Network) is a global collection of ground-based sun photometers providing reliable and accurate AOD measurements (Holben et al., 1998).

Aerosol optical depth can be retrieved through the solar backscatter measurements of satellite instruments (e.g., Martin, 2008). The downward viewing satellite monitors typically measure the total reflectance, $R(\Theta)$ (where Θ is the scattering angle) at specific wavelengths. For dark scenes, and small value of AOD, aerosol induced reflectance, $R_a(\Theta)$ can be calculated by,

$$R_a(\Theta) \approx R(\Theta) - R_m(\Theta) - R_s(\Theta) \tag{1-2}$$

where, $R_m(\Theta)$ and $R_s(\Theta)$ are the molecular reflectance and surface reflectance respectively. If R_a is isolated, then the AOD is retrieved by accounting for the scattering properties of the aerosols,

$$AOD \approx \frac{R_a(\Theta)}{P(\Theta)\varpi} \tag{1-3}$$

where, $P(\Theta)$ is the aerosol phase function which quantifies the angular distribution of scattering (Hansen and Travis, 1974). ϖ is the aerosol single scattering albedo which quantifies the scattered fraction of the incident radiation.

The two MODIS (Moderate Resolution Imaging Spectroradiometer) instruments onboard the National Aeronautics and Space Administration's (NASA) Terra and Aqua satellites provide near-daily global-scale observations of AOD at a resolution of 10 km x 10 km (Levy et al., 2007). The MISR (Multiangle Imaging Spectroradiometer) instrument aboard the Terra satellite uses multi-angle, multi-spectral observations to provide AOD and other aerosol optical properties at a spatial resolution of 18 km x 18 km (Kahn et al., 2007).

Solar backscatter measurements by satellites in the UV-visible region of the spectrum are used for retrieving trace gas column density. The trace gas optical depth, τ can be written

as, $$\tau = \sigma\Omega \quad (1\text{-}4)$$

where, σ is the trace gas absorption cross section. Ω is the column abundance of the trace gas. A suite of satellites currently measure the column density of trace gases using UV spectrometry. For example, the OMI (Ozone Monitoring Instrument) sensor aboard NASA's Aura satellite provides reliable NO_2 column density data with a near daily coverage at spatial resolution of up to 13 km x 24 km. Satellite retrievals based on thermal infrared wavelengths generally have reduced sensitivity to ground-level trace gas species (e.g., NASA's Tropospheric Emission Spectrometer satellite).

1.4 Atmospheric chemistry modeling

Modeling of atmospheric chemistry is another useful way to understand the global distribution and transport of atmospheric trace gases and aerosols (e.g., Fiore et al., 2009). Global chemical transport models (CTMs) solve the continuity equation of the chemical species for individual grid boxes defined in the Eulerian model (e.g., Bey et al., 2001; Horowitz et al., 2003; Huijnen et al., 2010). The major inputs needed for a CTM are the meteorological information and emission inventories of various species. A microphysics model is needed to simulate the size distribution of aerosols. CTMs simulate the temporal and spatial evolution of trace gases and aerosols at various resolutions.

The basic radical and oxidant processes controlling the distribution of tropospheric chemicals are simulated through the ozone-NO_x-hydrocarbon chemistry. The secondary inorganic aerosols are simulated by computing H_2SO_4-HNO_3-NH_3 thermodynamics (Fontoukis and Nenes, 2007). The simulation of organic species involves both primary BC

and OC emissions, and SOA formation from the oxidation of VOCs. Sea spray and dust emissions are parameterized using meteorological variables (e.g., wind fields).

The loss processes for gas-aerosol species involve dry deposition, and wet deposition (scavenging in wet convective updrafts and by precipitation).

Chemical transport models have critical roles in satellite AOD retrievals (e.g., Drury et al., 2010) and interpretation, and in deriving the ground-level concentrations of aerosols through the coupling of satellite column observations with simulated ratio of column to ground-level concentrations (van Donkelaar et al., 2006; 2010). CTMs also contain information on speciated aerosols and emission sources.

1.5 Outline of the thesis

Epidemiologic and health impact studies clearly associate ambient outdoor concentrations of $PM_{2.5}$ and its chemical composition with adverse health impacts (Lepeule et al., 2012; Bell et al., 2012). The extent and cause of these health risks, the differential toxicity of fine particulates, the chemical and emission sources of aerosols are not yet well understood due to the inadequacy of aerosol measurements. Spatial mapping of $PM_{2.5}$ chemical composition could help in elucidating the health impacts of fine particulate matter.

Several studies have found close relationships between satellite-retrieved AOD and ground-level $PM_{2.5}$ (Wang and Christopher, 2003; Kloog et al., 2011). Chemical transport models are capable of simulating the atmospheric distribution of aerosols, and can offer information about the local, coincident relationship of satellite-retrieved AOD with ground-level $PM_{2.5}$ (Liu et al., 2004; van Donkelaar et al., 2010). Moreover, model

sensitivity simulations can be used to quantify the contributions of specific emission sources to $PM_{2.5}$. The first and major stage of this thesis was to estimate the chemical composition and emission sources of $PM_{2.5}$ by combining satellite-retrieved AOD with CTM-simulated aerosol vertical profile and composition. This contribution was published (Philip et al., 2014b) in the journal "Environmental Science and Technology".

Particulate organic matter is of interest for air quality and climate research (Kanakidou et al., 2005). Ambient organic aerosol is a complex mix of thousands of different organic molecules. OA contains organic carbon as its major constituent. Traditional ground-based impaction or filter-based instruments measure organic carbon (e.g., Hand et al., 2012), but not OM due to difficulties in characterizing different components of OM. Moreover, most of the global models simulate primary organic aerosol as OC (e.g., Park et al., 2003). A common practice is to interpret OC through the use of a continental mean value of OM/OC (ranges from 1.4 to 2.1 μg/μgC).

The characterization of organic aerosol requires spatially and seasonally resolved information about the ratio of OM to OC. The second stage of this thesis was to estimate the spatially and seasonally resolved global OM/OC ratio by combining Aerosol Mass Spectrometer measurements of submicron OA, and satellite-derived nitrogen dioxide concentrations. This contribution was published (Philip et al., 2014a) in the journal "Atmospheric Environment".

Chemical transport models involve considerable computational cost as temporal and spatial resolution increases. Fine temporal resolution offers simulation accuracy at the expense of computation time. Moreover, the concentrations of the simulated species are sensitive to

temporal resolution (Mallet et al., 2007; Santillana et al., 2016). Assessment is needed to understand how temporal resolution affects model performance. The third stage of this thesis was to examine the sensitivity of chemical transport models to temporal resolution, and to develop a practical strategy for optimizing model performance with minimal computational expense.

CHAPTER 2: GLOBAL CHEMICAL COMPOSITION OF AMBIENT FINE PARTICULATE MATTER FOR EXPOSURE ASSESSMENT

Authors: Sajeev Philip[1*], Randall V. Martin[1, 2], Aaron van Donkelaar[1], Jason Wai-Ho Lo[1], Yuxuan Wang[3], Dan Chen[4], Lin Zhang[5], Prasad S. Kasibhatla[6], Siwen Wang[7], Qiang Zhang[8], Zifeng Lu[9], David G. Streets[9], Shabtai Bittman[10] and Douglas J. Macdonald[11]

[1]Department of Physics and Atmospheric Science, Dalhousie University, Halifax, Nova Scotia, Canada

[2]Also at Harvard-Smithsonian Center for Astrophysics, Cambridge, Massachusetts, USA

[3]Ministry of Education Key Laboratory for Earth System Modeling, Center for Earth System Science, Institute for Global Change Studies, Tsinghua University, Beijing, China

[4]Department of Atmospheric and Oceanic Sciences, University of California, Los Angeles, California, USA.

[5]Department of Atmospheric and Oceanic Sciences, School of Physics, Peking University, China

[6]Nicholas School of the Environment and Earth Sciences, Duke University, Durham, North Carolina, USA.

[7]State Key Joint Laboratory of Environment Simulation and Pollution Control, School of Environment, Tsinghua University, Beijing, China.

[8]Center for Earth System Science, Tsinghua University, Beijing, China.

[9]Decision and Information Sciences Division, Argonne National Laboratory, Argonne, IL, USA

[10]Agriculture and Agri-Food Canada, Agassiz, British Columbia, Canada

[11]Environment Canada, Canada

*Sajeev Philip conducted the research and wrote the manuscript

2.1 ABSTRACT

Epidemiologic and health impact studies are inhibited by the paucity of global, long-term measurements of the chemical composition of fine particulate matter. We inferred $PM_{2.5}$ chemical composition at 0.1^o x 0.1^o spatial resolution for 2004-2008 by combining aerosol optical depth retrieved from the MODIS and MISR satellite instruments, with coincident profile and composition information from the GEOS-Chem global chemical transport model. Evaluation of the satellite-model $PM_{2.5}$ composition dataset with North American in situ measurements indicated significant spatial agreement for secondary inorganic aerosol, particulate organic mass, black carbon, mineral dust and sea salt. We found that global population-weighted $PM_{2.5}$ concentrations were dominated by particulate organic mass (11.9 ± 7.3 $\mu g/m^3$), secondary inorganic aerosol (11.1 ± 5.0 $\mu g/m^3$), and mineral dust (11.1 ± 7.9 $\mu g/m^3$). Secondary inorganic $PM_{2.5}$ concentrations exceeded 30 $\mu g/m^3$ over East

China. Sensitivity simulations suggested that population-weighted ambient $PM_{2.5}$ from biofuel burning (11 $\mu g/m^3$) could be almost as large as from fossil fuel combustion sources (17 $\mu g/m^3$). These estimates offer information about global population exposure to the chemical components and sources of $PM_{2.5}$.

2.2 INTRODUCTION

A large body of evidence has established that short-term human exposure to various chemical constituents of particulate matter (PM) with aerodynamic diameter less than 2.5 μm ($PM_{2.5}$) is associated with adverse health effects including increased hospital admissions (e.g., Bell et al., 2009; Ito et al., 2011; Kim et al., 2012), cardiovascular, respiratory, and all-cause mortality (e.g., Burnett et al., 2000; Ostro et al., 2010; Zhou e al., 2011; Cao et al., 2012; Son et al., 2012). However, the health impacts of long-term exposure to $PM_{2.5}$ chemical components are less well understood, in contrast to the well-established relationship of the total $PM_{2.5}$ mass with adverse health effects (e.g., Pope et al., 2009; Brook et al., 2010; Lepeule et al., 2012). Epidemiologic and health impact assessments of $PM_{2.5}$ composition have been impeded by the paucity of long-term measurements of global $PM_{2.5}$ composition. Spatial mapping of aerosol composition could help in elucidating the health impacts of fine particulate matter components.

Satellite remote sensing for surface air quality has developed rapidly over the last decade (Martin, 2008; Hoff and Christopher, 2009). Aerosol optical depth (AOD), an optical measure of the column integrated aerosol abundance in the atmosphere, can now be reliably retrieved from satellite remote sensing over land. Several studies have demonstrated close

relationships between AOD and $PM_{2.5}$ (e.g., Wang and Christopher, 2003; Engel-Cox et al., 2004; Kloog et al., 2011) to the point that AOD is being used for operational air quality forecasting (Al-Saadi et al., 2005; van Donkelaar et al., 2012). However, the relation of AOD with $PM_{2.5}$ is complex (Paciorek and Liu, 2009), and despite progress in retrieving aerosol composition from satellite (Liu et al., 2007; Kahn et al., 2007), current satellite instrumentation provides incomplete information on the chemical composition of $PM_{2.5}$ (Hoff and Christopher, 2009).

Chemical transport models (CTMs) also have developed markedly over the last decade. Current CTMs are capable of simulating the atmospheric distribution of aerosols and of calculating the local, coincident relationship of satellite AOD with ground-level $PM_{2.5}$ concentration at a regional (Liu et al., 2004) and global (van Donkelaar et al., 2010) scale. CTMs also offer the capability of simulating the major chemical components of $PM_{2.5}$, including secondary inorganic aerosol (sulfate, nitrate and ammonium), primary and secondary organic aerosol, black carbon, mineral dust, sea salt and aerosol water. These model developments offer information about the relation of AOD with ground-level $PM_{2.5}$ and its chemical composition. CTMs are also being used to quantify the contributions of specific emission sources to $PM_{2.5}$ to inform mitigation strategies (e.g., Wang et al., 2009; Anenberg et al., 2011).

Scientific understanding of $PM_{2.5}$ chemical composition has been closely coupled with advances in measurements. For example, several in situ monitoring networks across the U.S. and Canada routinely measure the major components of $PM_{2.5}$ (e.g., Malm et al., 1994; Dabek-Zlotorzynska et al., 2011). Numerous studies combined these in situ data to study

the spatial and temporal variation of $PM_{2.5}$ chemical composition (e.g., Bell et al., 2007; Hand et al., 2011, 2012). Other established networks are the European Monitoring and Evaluation Programme (EMEP; http://www.emep.int/) and the Acid Deposition Monitoring Network in East Asia (EANET; http://www.eanet.cc/) which measure some components of $PM_{2.5}$. Research measurements offer additional valuable data. These in situ measurements are too sparse to fully represent population exposure across the world. However, they provide an opportunity to evaluate $PM_{2.5}$ composition inferred from satellite remote sensing and modeling (hereafter, satellite-model).

We combined satellite-derived AOD with global modeling of coincident aerosol vertical profile and composition to produce a global long-term (2004-2008) mean ambient outdoor satellite-model $PM_{2.5}$ composition dataset at a spatial resolution of 0.1^{o} x 0.1^{o}. We evaluated this dataset with in situ measurements across North America, and where available in the rest of the world. We combined model sensitivity simulations with satellite-derived AOD to estimate three major emission sources of total $PM_{2.5}$ mass. We subsequently estimated the population-weighted concentrations of ambient $PM_{2.5}$ chemical components and its major emission sources.

2.3 MATERIALS AND METHODS

2.3.1 PROCESSING SATELLITE AOD OBSERVATIONS

We began with AOD retrievals from the two Moderate Resolution Imaging Spectroradiometer (MODIS) instruments onboard the Terra and Aqua satellites and the Multiangle Imaging Spectroradiometer (MISR) instrument onboard Terra. Aerosol retrievals (collection 5) from each MODIS instrument provide near-daily global-scale

coverage of cloud-free regions at a resolution of 10 km × 10 km (Levy et al., 2007). The MISR retrieval algorithm (version 22) uses multiangle, multispectral observations to provide aerosol optical properties at a spatial resolution of 18 km × 18 km and global coverage of cloud-free regions within 9 days (Kahn et al., 2007). The operational MODIS and MISR retrievals together provide more reliable global AOD than from either instrument alone (van Donkelaar et al., 2010).

Following van Donkelaar et al. (2010), we collected daily AOD retrievals of these three satellite sensors from 2004 to 2008 and regridded them separately onto a resolution of 0.1° × 0.1°. We then divided the world into nine regions with distinct surface type based on the MODIS BRDF/Albedo product (MOD43, Collection 5, Schaaf et al., 2002). We used the available ground-based sun photometer AOD measurements (Aerosol Robotic Network, AERONET, Holben et al., 1998) over these regions to identify the average monthly bias of satellite AOD for each region. We retained the daily satellite AOD observations with a local monthly bias less than ± (20% or 0.1). We included two textural filters for MODIS AOD to reduce cloud contamination by excluding data with no adjacent retrievals and grids with AOD and coefficient of variation greater than 0.5 (Zhang and Reid, 2006; Hyer et al., 2011). These three different (MODIS/Terra, MODIS/Aqua, MISR/Terra) AOD data sets at 0.1° × 0.1° resolution are the major observational inputs for this study.

2.3.2 INFERRING $PM_{2.5}$ CHEMICAL COMPOSITION FROM AOD

Our approach to infer the 24-hr average ground-level dry $PM_{2.5}$ concentrations of each chemical component, i from the observed aerosol optical depth, AOD_{Sat}, involved a chemical transport model (GEOS-Chem) to calculate that relationship,

$$component^{i}_{Sat} = \frac{component^{i}_{CTM}}{AOD_{CTM}} \times AOD_{Sat} \quad (2\text{-}1)$$

The major $PM_{2.5}$ components included sulfate (SO_4^{2-}), nitrate (NO_3^-), ammonium (NH_4^+), total secondary inorganic aerosol (SIA, sum of SO_4^{2-} , NO_3^- and NH_4^+ ions), particulate organic mass (OM), black carbon (BC), mineral dust and sea salt. The subscript *CTM* indicates values from a chemical transport model. The simulated conversion factor for the i^{th} component, defined as the ratio of the i^{th} component to AOD, relates the observed AOD to the ground-level $PM_{2.5}$ components. The approach of distributing the observed AOD across simulated aerosol composition has similarity to AOD assimilation methods (e.g. Saide et al., 2013).

We used the GEOS-Chem global CTM (http://geos-chem.org) to calculate the local conversion factors coincident with each satellite observation. The GEOS-Chem model simulates the temporal and three-dimensional spatial distributions of various aerosol components and gases using assimilated meteorology and emission inventories as major inputs [details in the Supporting Information (SI), section 2.6.1]. We conducted a global simulation at 2^o x 2.5^o spatial resolution and three nested regional simulations at 0.5^o x 0.667^o resolution from 2004 to 2008 using assimilated meteorological data from the Goddard Earth Observing System (GEOS-5) at the NASA Global Modeling Assimilation Office (GMAO). The global simulation outputs are overwritten with nested regional simulations over North America, Europe and East Asia. The top left panel of Figure 2-2 provides the boundaries of these regions. These nested simulations improve over the 2^o x 2.5^o resolution used by van Donkelaar et al. (2010). The $PM_{2.5}$ dry mass composition of the lowest layer of the model centered approximately at 70 meters above ground was taken to

represent the ground-level concentration. We averaged the simulated AOD between 10:00 and 12:00 hrs local solar time to correspond with Terra overpass, and 13:00 and 15:00 hours local solar time to correspond with Aqua overpass. We calculated the daily local Terra and Aqua conversion factors as the ratio of 24 hr average $PM_{2.5}$ components to the corresponding AOD at satellite overpass period.

We applied equation 2-1 to produce $PM_{2.5}$ components from individual AOD observations from the two MODIS and the MISR instruments from 2004 to 2008. We accounted for incomplete sampling by scaling the monthly data with the ratio of monthly mean simulated composition sampled continuously versus sampled coincidently with satellite observations. We capped the variation from the monthly mean simulated composition at the species-dependent uncertainties calculated by van Donkelaar et al. (2013). This cap represents a level of confidence in the simulation and avoids unrealistic conditions that can arise from the correlation of sensor sampling with $PM_{2.5}$ composition. We required 20 successful satellite observations for each 0.1^{o} grid box per five-year monthly mean; otherwise monthly mean simulated composition was used as occurred for 0.5% of the global population. We averaged the monthly data to obtain the long-term mean satellite-model combined $PM_{2.5}$ composition.

We evaluated the satellite-model estimate with $PM_{2.5}$ composition measurements from networks over North America, Europe, East Asia and elsewhere with annually representative composition measurements from publications as described in the SI (section 2.6.2).

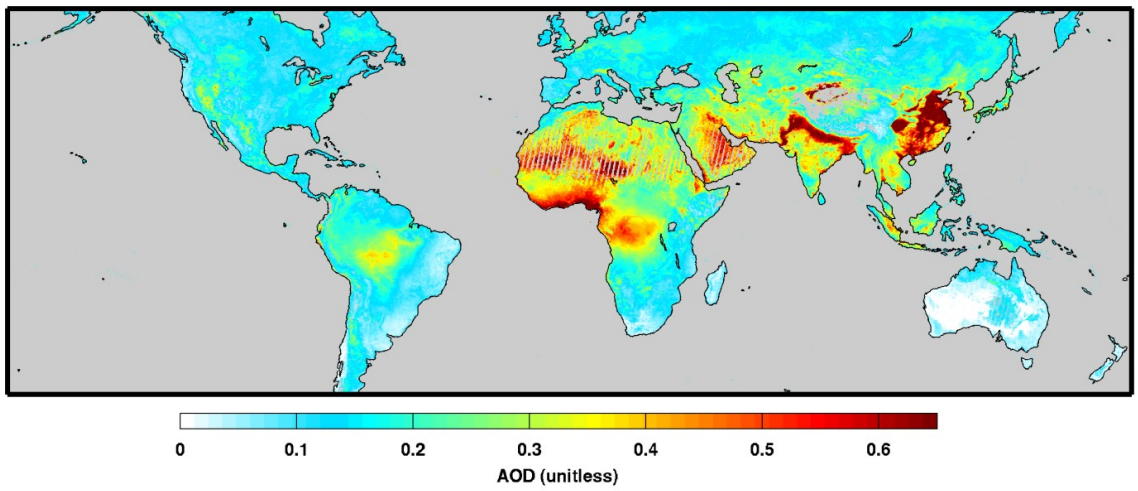

Figure 2-1: Combined aerosol optical depth (AOD) from the MODIS and MISR satellite instruments for 2004-2008. Gray denotes water or missing satellite AOD observations.

The uncertainty associated with the satellite-model $PM_{2.5}$ composition arises from bias in the satellite AOD retrieval, from simulating the $PM_{2.5}$/AOD ratio, from the simulated $PM_{2.5}$ fractional composition, and from incomplete sampling. We represented the uncertainty in the satellite AOD retrieval bias as the maximum of either an absolute AOD of 0.1 or a relative value of 20%, since AERONET was used to identify and exclude regions and time periods with larger expected bias. We estimated the uncertainty in the model vertical profile bias as the annual mean difference in the $PM_{2.5}$/AOD ratio if observations from the CALIOP (Cloud-Aerosol Lidar with Orthogonal Polarization) satellite instrument (Winker et al., 2007) were used to adjust the ratio following van Donkelaar et al. (2013). We assessed the bias in the simulated $PM_{2.5}$ fractional composition for each component (ratio of $PM_{2.5}$ components to total $PM_{2.5}$ mass) by comparison with available in situ observations. Uncertainty due to incomplete sampling was estimated as the difference

between the long-term mean simulated $PM_{2.5}$ composition sampled continuously versus coincidently with the satellite observations. We assumed 100% sampling error for grids without satellite observations. The estimated uncertainty from a quadrature sum of these uncertainty terms may be underestimated since the errors contain systematic components, can be asymmetric, and can be correlated with each other and with $PM_{2.5}$ composition. Thus we added the median global $PM_{2.5}$ composition to the quadrature sum to better represent the unresolved contributions to total uncertainty especially in the regions with low values of $PM_{2.5}$ composition.

2.3.3 ESTIMATING THE $PM_{2.5}$ EMISSION SOURCES

$PM_{2.5}$ constituents arise from different emission source sectors such as fossil fuel combustion, biofuel combustion and biomass burning. Fossil fuel combustion includes burning of coal, oil, and gas from vehicular and industrial sources. Biofuel combustion includes burning of wood and crop residue for domestic cooking and heating. Biomass burning includes both natural open fires and anthropogenic activities such as land cleaning and burning in fields. Quantitative determination of these sectoral contributions to $PM_{2.5}$ can inform mitigation strategies.

We therefore estimated the sectoral sources of total $PM_{2.5}$ using sensitivity simulations to exclude specific emission sectors. For this, we performed three global simulations (sensitivity simulations) for a year (2005) by excluding fossil fuel combustion, biofuel combustion and biomass burning sources. We scaled the $PM_{2.5}$ relative variation from sensitivity simulations (compared with a base simulation) to the total $PM_{2.5}$ mass (sum of

satellite-model $PM_{2.5}$ composition estimates). We calculated sectoral contributions of $PM_{2.5}$ at 35% relative humidity to conform with $PM_{2.5}$ measurement standards.

We calculated the regional population exposure for the GBD regions (Global Diseases, Injuries, and Risk Factors 2010 study; the top panel of Figure 2-9 shows the 21 GBD regions) using the population data at 0.1° resolution for 2005 described in Brauer et al. (2012), and the satellite-model $PM_{2.5}$ composition and emission sources.

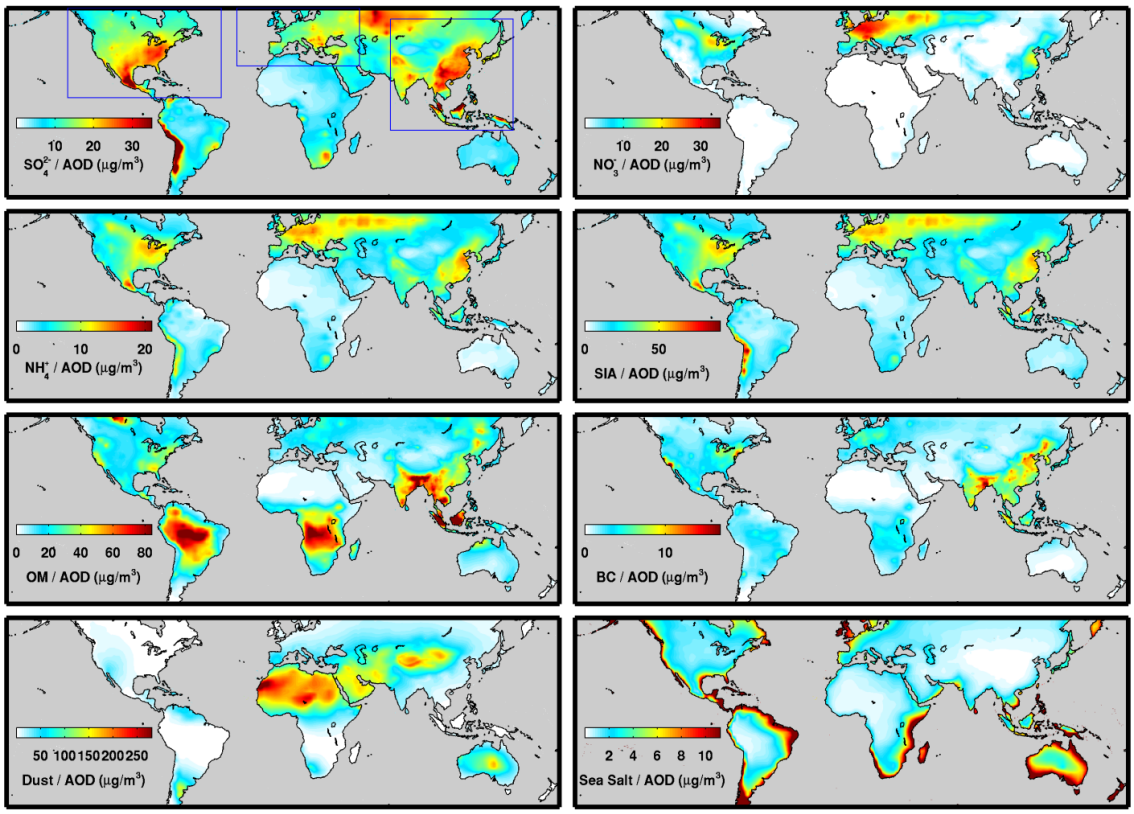

Figure 2-2: Mean ratio of $PM_{2.5}$ composition to AOD for 2004-2008. $PM_{2.5}$ composition is represented as dry mass. Abbreviations are Secondary Inorganic Aerosol (SIA; the sum of SO_4^{2-}, NO_3^- and NH_4^+), Organic Mass (OM), and Black Carbon (BC). Gray denotes water. The top-left panel contains the boundaries of the three nested GEOS-Chem regions.

2.4 RESULTS AND DISCUSSION

Figure 2-1 contains a map of the long-term (2004-2008) mean AOD from the MODIS and MISR satellite instruments. Enhancements exist over anthropogenic pollution sources of South and East Asia, over mineral dust source regions of the Sahara, and over biomass burning regions of South America, Central Africa, and Equatorial and Southeast Asia.

Figure 2-2 shows the long-term (2004-2008) mean GEOS-Chem simulated ratio of $PM_{2.5}$ components to AOD. The ratio represents the relative importance of various $PM_{2.5}$ components to the total AOD over different regions of the globe. The mass/AOD ratio is high over regions with relatively large abundance of a given $PM_{2.5}$ component near the ground. Non-hygroscopic components (e.g. mineral dust) exhibit high conversion factors due to the low contribution of aerosol water to AOD. The high mass/AOD ratios for secondary inorganic, OM and mineral dust indicate that these components are the dominant contributors to global AOD over land. Secondary inorganic $PM_{2.5}$ dominates over industrial regions. Particulate organic mass from biomass burning is the primary contributor to AOD over the Amazon, Central Africa, Northern India and Oceania. Mineral dust is the primary contributor to AOD over deserts. Black carbon is a small component of AOD, but is more apparent in local hotspots. Sea salt generally has the lowest conversion factor over land.

Figure 2-3 shows the satellite-model and in situ observations of North American $PM_{2.5}$ composition. The in situ observation of a large sulfate burden in the East is reproduced in the satellite-model product. Nitrate and ammonium are enhanced south of the Great Lakes where intense agriculture sources of ammonia and weak sulfur sources contribute to excess ammonia gas that is available for forming ammonium nitrate. The Californian nitrate

enhancements are under-predicted reflecting difficulties in representing this heterogeneous region (Walker et al., 2012; Heald et al., 2012). Together these secondary inorganic ions comprise a major fraction of the total $PM_{2.5}$ in the Eastern U.S., reaching concentrations of approximately 10 $\mu g/m^3$. The spatial pattern of particulate organic mass over the southeastern U.S. is generally captured in the satellite-model product. Black carbon concentrations exhibit hotspots in industrial regions; performance elsewhere is more variable given the stochastic nature of fires. Fine-mode dust and fine sea salt emissions are weak contributors to $PM_{2.5}$ mass throughout the continent with typical mass concentrations below 1 $\mu g/m^3$. The primary exception is for mineral dust over deserts in the southwest.

Figure 2-4 shows scatter plots of satellite-model $PM_{2.5}$ components with North American in situ observations, and Table 2-1 contains detailed comparison statistics of in situ with either the satellite-model or pure GEOS-Chem $PM_{2.5}$ composition. The correlation between satellite-model sulfate and ground monitors is high ($r = 0.95$, slope = 0.89). Concentrations are also well predicted for nitrate ($r = 0.68$, slope = 1.01) and ammonium ($r = 0.89$, slope = 0.98). The performance for OM is weaker ($r = 0.45$, slope = 1.17) likely due to the difficulty in simulating secondary organic aerosol and fires, and due to sporadic measurements of stochastic fire events. Black carbon, mineral dust and sea salt have modest agreement with in situ measurements with correlations of 0.56, 0.58 and 0.62 respectively. The bias for all components is within 35% (Figure 2-4). The in situ observations are similarly correlated with the satellite-model product and the GEOS-Chem simulation, with noteworthy improvements in the slope versus the GEOS-Chem simulation for secondary inorganic ions.

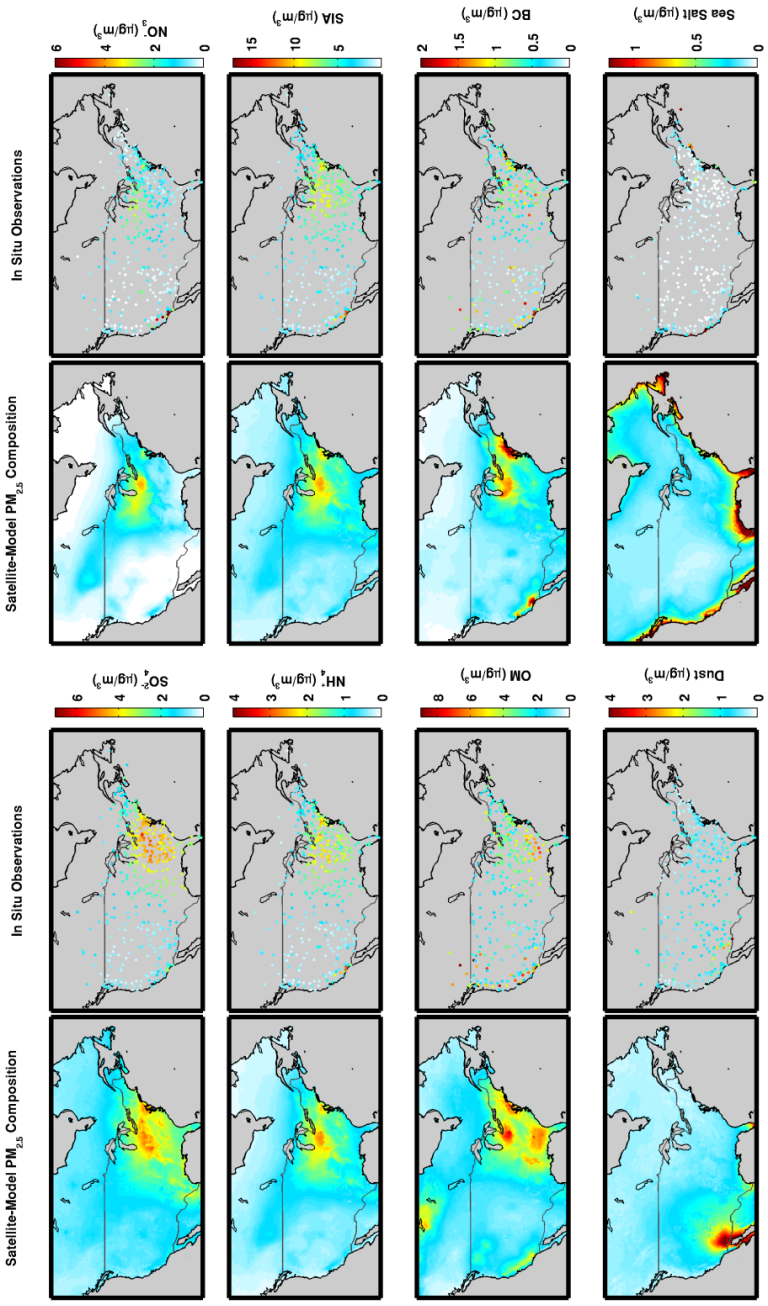

Figure 2-3: $PM_{2.5}$ composition from satellite-model and in situ observations across North America. $PM_{2.5}$ composition is represented as dry mass. Abbreviations are Secondary Inorganic Aerosol (SIA; the sum of SO_4^{2-}, NO_3^- and NH_4^+), Organic Mass (OM), and Black Carbon (BC). Gray denotes water or missing in situ measurement data. Scatter plots are in Figure 2-4.

Figure 2-5 shows the global satellite-model estimate of long-term mean $PM_{2.5}$ composition where the differently colored circles represent the location and value of the in situ observations used to evaluate the dataset outside of North America. Detailed statistics are given in Table 2-1. Secondary inorganic aerosol concentrations over East China exceed 30 $\mu g/m^3$ (Figure 2-5). About half of the simulated secondary inorganic aerosol is sulfate which is consistent with in situ measurements (Yang et al., 2011). The Indo-Gangetic Plain, China, and biomass burning regions of South America and Central Africa are highlighted in the OM map. Previous studies have also noted pronounced OM in these regions (Chawdhury, 2004; Fu et al., 2012). Hotspots of black carbon are most apparent in China and the Indo-Gangetic Plain where in situ measurements also indicate enhancements (Fu et al., 2012; Hopke et al., 2008).

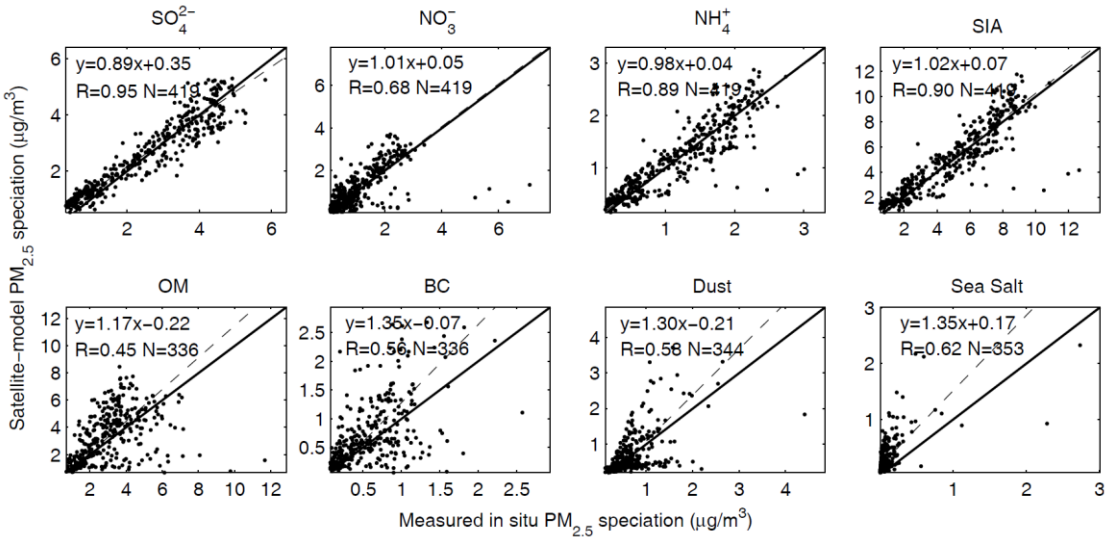

Figure 2-4: Comparison of $PM_{2.5}$ composition from the satellite-model product versus in situ observations across North America. The solid black line is the 1:1 line, and the dashed line is the best fit line. The inset contains the Pearson correlation coefficient as well as the slope and intercept from reduced major axis regression (Miller and Kahn, 1962).

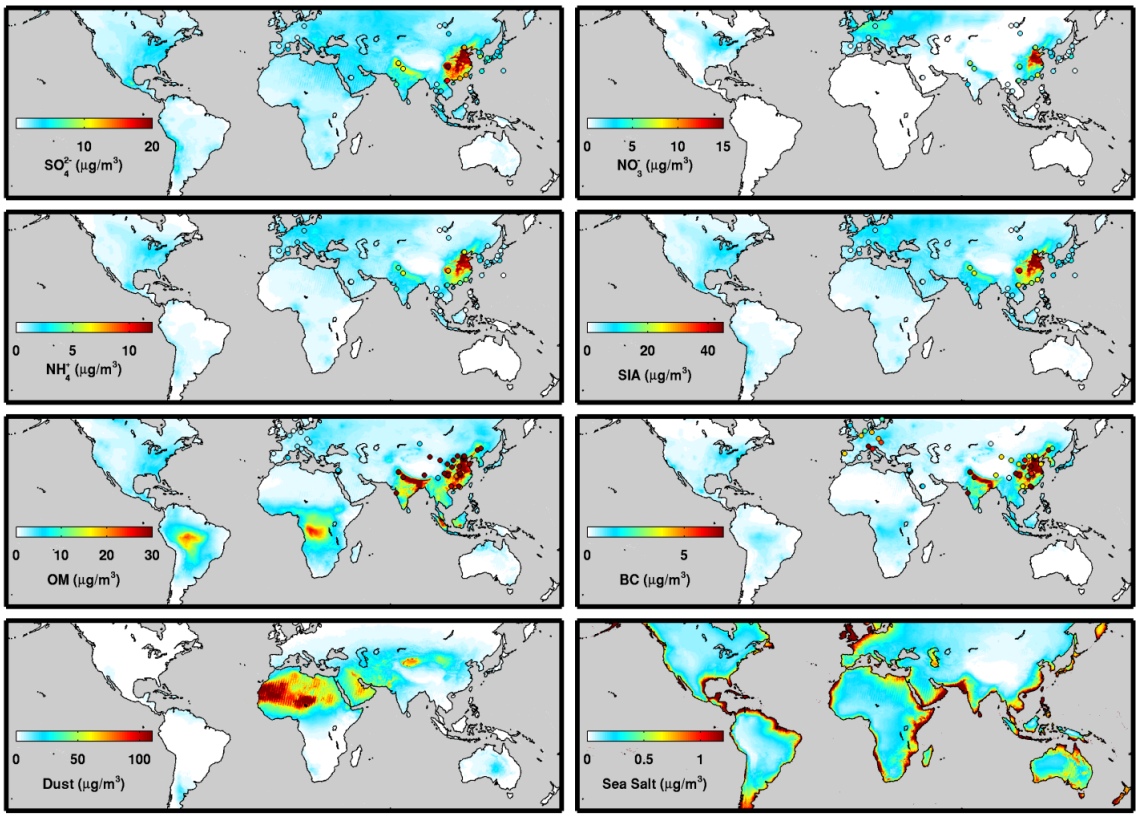

Figure 2-5: Satellite-model global long-term mean (2004-2008) $PM_{2.5}$ composition. $PM_{2.5}$ composition is represented as dry mass. Gray denotes water. Values from in situ observations are overlaid as colored circles. Table 2-1 contains the detailed comparison statistics.

Mineral dust is the largest contributor to $PM_{2.5}$ over the desert regions of North Africa, Middle East, and Central Asia with concentrations greater than 50 $\mu g/m^3$ over broad regions. The satellite-model product exhibits high correlations for secondary inorganic aerosol ($r = 0.93$) and its components, with slopes within 20% of unity (Table 2-1). Carbonaceous aerosols are again less well estimated; sparse in situ monitors may play a role for fires. The satellite-model product outperforms the pure model simulation for all

components (e.g., for secondary inorganic aerosols the slope improved from 0.64 to 0.91; for organic matter the correlation improved from 0.61 to 0.67).

Table 2-2 summarizes the global and regional statistics of long-term (2005-2008) population exposure to ambient $PM_{2.5}$ composition. Our estimates suggest that particulate organic mass is the dominant form of ambient $PM_{2.5}$ with a global population-weighted concentration of 12 $\mu g/m^3$. Other major contributors to global population-weighted $PM_{2.5}$ mass are secondary inorganic components (11 $\mu g/m^3$) and mineral dust (11 $\mu g/m^3$). The secondary inorganic components are dominated by sulfate (6.2 $\mu g/m^3$), followed by ammonium (2.7 $\mu g/m^3$) and nitrate (2.2 $\mu g/m^3$). On a regional scale, secondary inorganic $PM_{2.5}$ concentrations are noteworthy in East Asia (28 $\mu g/m^3$) and South Asia (11 $\mu g/m^3$). The mean ambient particulate organic mass concentration is 22 $\mu g/m^3$ in both South Asia and East Asia. Mineral dust concentrations exceed 20 $\mu g/m^3$ in West Africa, North Africa, Middle East, and Central Asia. These $PM_{2.5}$ values are higher than previous work (van Donkelaar et al., 2010; 2012) arising from our use of satellite AOD for all fine mode fraction values, and increased carbonaceous aerosol emissions over East Asia as described in the SI (section 2.6).

Figure 2-6 shows the total estimated absolute uncertainty of the satellite-model $PM_{2.5}$ composition as determined by propagation of error. For many species, the primary source of uncertainty arose from the simulated $PM_{2.5}$ fractional composition. These uncertainties were 27% for sulfate, 38% for nitrate, 29% for ammonium, 29% for SIA, 45% for OM, 36% for BC, 52% for dust, and 122% for sea salt. In regions of low AOD (below 0.1), uncertainty in the satellite AOD retrieval can exceed 100%. Uncertainty due to model

vertical profile bias was 10% - 30% in most regions with more severe exceptions in convective regions (Figure 2-7).

Table 2-1: Comparison of $PM_{2.5}$ composition from the simulation and satellite-model product versus in situ observations across North America, and globally (non-North American). Abbreviations are Secondary Inorganic Aerosol (SIA; the sum of SO_4^{2-}, NO_3^- and NH_4^+), Organic Mass (OM), and Black Carbon (BC). "Satellite" and "Simulation" in the second column represents satellite-model composition, and complete model simulation respectively at a spatial resolution of 0.1^o x 0.1^o. Correlation statistics are calculated with reduced major axis regression (Miller and Kahn, 1962).

$PM_{2.5}$ Composition	Data	North America				Global			
		r	Slope	Offset ($\mu g/m^3$)	N	r	Slope	Offset ($\mu g/m^3$)	N
SO_4^{2-}	Satellite	0.95	0.89	0.35	419	0.92	0.88	0.93	55
	Simulation	0.97	0.73	0.23	419	0.94	0.61	0.80	55
NO_3^-	Satellite	0.68	1.01	0.05	419	0.73	0.83	-0.26	55
	Simulation	0.63	0.80	0.11	419	0.69	0.64	-0.24	55
NH^+	Satellite	0.89	0.98	0.04	419	0.92	1.08	0.13	55
	Simulation	0.89	0.79	0.04	419	0.93	0.77	0.12	55
SIA	Satellite	0.90	1.02	0.07	419	0.93	0.91	0.85	55
	Simulation	0.90	0.82	0.10	419	0.92	0.64	0.70	55
OM	Satellite	0.45	1.17	-0.22	336	0.67	0.42	-0.73	56
	Simulation	0.42	0.99	-0.34	336	0.61	0.30	-0.47	56
BC	Satellite	0.56	1.35	-0.07	336	0.65	1.05	-1.83	65
	Simulation	0.53	1.04	-0.04	336	0.56	0.68	-1.15	65

Table 2-2: Population-weighted regional $PM_{2.5}$ composition and three major emission sources contributing to $PM_{2.5}$. The top panel of Figure 2-9 shows the borders of GBD (Global Diseases, Injuries, and Risk Factors 2010 study) regions. Abbreviations are Secondary Inorganic Aerosol (SIA; the sum of SO_4^{2-}, NO_3^- and NH_4^+), Organic Mass (OM), and Black Carbon (BC).

Region	$PM_{2.5}$ Composition								$PM_{2.5}$ Emission			Population
	SO_4^{2-}	NO_3^-	NH_4^+	SIA	OM	BC	Dust	Seasalt	Fossilfuel	Biofuel	Biomass	
	($\mu g/m^3$)											(%)
World	6.2	2.2	2.7	11.1	11.9	2.5	11.1	0.6	17.1	11.2	1.3	100.0
Asia Pacific, High Income	5.5	1.5	2.0	9.0	4.8	1.9	3.7	0.9	16.2	2.1	0.3	2.7
Asia, Central	3.2	0.6	1.3	5.1	3.7	0.5	21.3	0.1	7.2	6.5	0.3	1.3
Asia, East	14.5	6.6	7.0	28.0	21.7	5.7	11.7	0.5	45.8	20.2	0.3	21.2
Asia, South	6.9	1.1	2.8	10.8	21.6	3.9	14.3	0.5	15.8	24.1	0.6	22.9
Asia, South East	3.6	0.2	1.1	5.0	8.0	1.2	1.6	1.0	6.7	5.4	3.2	8.7
Australasia	0.7	0.1	0.2	1.0	0.8	0.1	1.1	1.0	1.1	0.2	0.2	0.4
Caribbean	1.2	0.2	0.2	1.6	1.0	0.2	4.8	1.7	1.8	0.1	0.2	0.5
Europe, Central	3.8	3.6	2.5	9.9	4.1	0.8	3.2	0.3	13.7	4.4	0.2	1.9
Europe, Eastern	2.9	2.3	1.7	6.9	2.9	0.4	2.8	0.2	9.0	2.8	0.3	3.3
Europe, Western	2.3	3.2	1.7	7.2	2.1	0.7	3.3	0.8	10.6	1.4	0.2	6.1
Latin America, Andean	2.1	0.0	0.6	2.7	3.2	0.2	0.1	0.5	2.8	0.6	2.9	0.8
Latin America, Central	3.1	0.4	1.0	4.4	2.5	0.5	1.6	0.7	5.2	0.4	1.4	3.4
Latin America, Southern	1.9	0.1	0.5	2.4	2.7	0.3	2.4	0.5	3.0	1.2	1.0	0.9
Latin America, Tropical	1.1	0.1	0.4	1.6	3.4	0.3	0.2	0.6	2.1	1.6	1.8	2.9
North Africa/Middle East	3.5	0.3	1.2	4.9	1.7	0.4	29.0	0.6	6.7	0.8	0.2	6.4
North America, High Income	2.9	1.3	1.3	5.6	3.9	0.9	0.7	0.4	10.2	0.5	0.2	5.0
Oceania	0.5	0.0	0.1	0.6	0.2	0.0	0.1	0.5	0.1	0.1	0.1	0.1
Sub-Saharan Africa, Central	1.6	0.0	0.5	2.1	14.8	0.8	4.9	0.3	1.3	3.9	14.4	1.3
Sub-Saharan Africa, East	1.1	0.1	0.3	1.4	4.6	0.5	9.2	0.6	1.0	3.7	2.7	4.8
Sub-Saharan Africa, Southern	1.9	0.1	0.6	2.6	3.4	0.3	0.7	0.6	3.2	0.9	2.8	1.0
Sub-Saharan Africa, West	1.5	0.1	0.5	2.1	5.1	0.4	45.7	0.3	2.4	2.5	5.4	4.4

Figure 2-9 shows the contributions to long-term mean $PM_{2.5}$ from fossil fuel combustion, biofuel combustion, and biomass burning. Enhanced anthropogenic sources are apparent over industrial and populated regions. Biofuel sources over Asia reflect domestic cooking and heating with non-fossil fuel sources. Biomass burning dominates in Central Africa and the Amazon. Biogenic sources, mineral dust, and sea salt constitute the remaining portion of $PM_{2.5}$.

However, uncertainty on a monthly basis could be even higher due to seasonal differences in vertical mixing (Ford and Heald, 2012). Sampling uncertainty was below 30%

throughout low latitudes except for seasonally convective regions (Figure 2-8) with cloud cover that inhibits observations. Decreases in observation frequency at high latitudes increased uncertainty as a result of incomplete sampling especially for nitrate and carbonaceous components that have large seasonal variation. The global population-weighted mean uncertainty for sulfate (2.8 $\mu g/m^3$), nitrate (1.2 $\mu g/m^3$), ammonium (1.2 $\mu g/m^3$), secondary inorganic $PM_{2.5}$ (5.0 $\mu g/m^3$), organic mass (7.3 $\mu g/m^3$), black carbon (1.2 $\mu g/m^3$), mineral dust (7.9 $\mu g/m^3$), and sea salt (0.8 $\mu g/m^3$) ranged from ~45% of the population-weighted concentrations for many species (Table 2-2) to ~142% for sea salt.

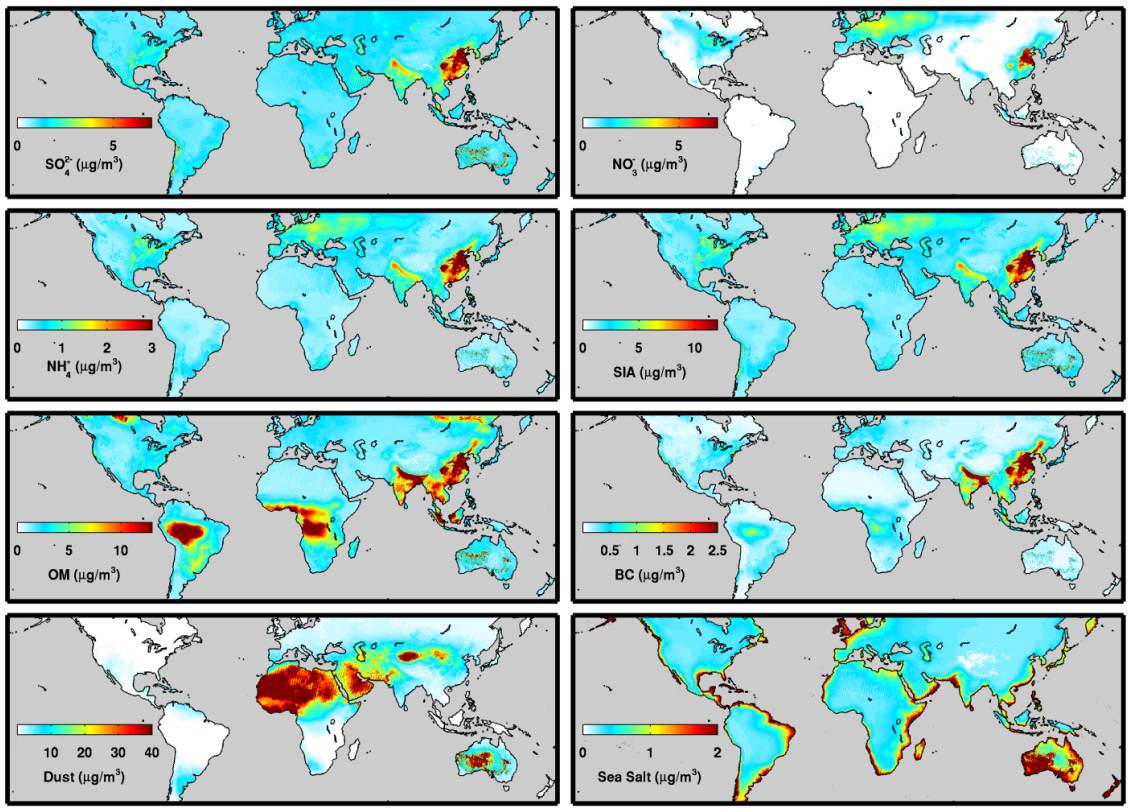

Figure 2-6: Absolute uncertainty of satellite-model $PM_{2.5}$ composition determined by propagation of error. Gray denotes water.

Table 2-2 contains the global and regional statistics of population exposure to various source sectors of $PM_{2.5}$. Population-weighted $PM_{2.5}$ is dominated by fossil fuel combustion (17 $\mu g/m^3$) followed by biofuel combustion (11 $\mu g/m^3$) and biomass burning (1.3 $\mu g/m^3$). $PM_{2.5}$ is high from emissions of fossil fuel combustion over East Asia (46 $\mu g/m^3$), biofuel combustion over South Asia (24 $\mu g/m^3$) and East Asia (20 $\mu g/m^3$), and biomass burning over Central Africa (14 $\mu g/m^3$). Although these sensitivity simulations are uncertain, it is noteworthy that outdoor $PM_{2.5}$ from biofuel combustion is comparable to that from fossil fuel combustion in South Asia. This is in line with previous findings of high ambient $PM_{2.5}$ exposure from biofuel burning (Lim et al., 2012; Stone et al., 2010), in addition to $PM_{2.5}$ exposure from household air pollution (Balakrishnan et al., 2013).

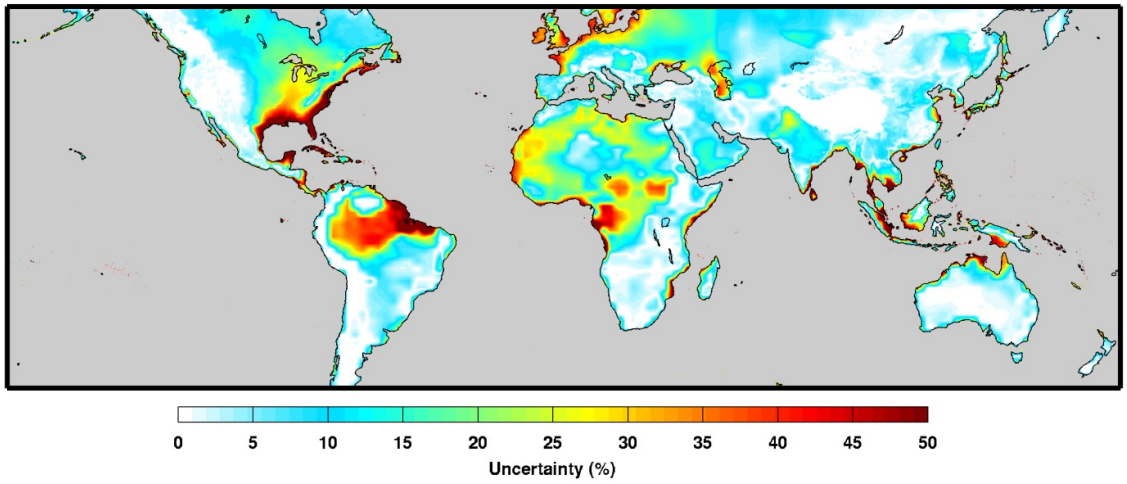

Figure 2-7: Uncertainty in $PM_{2.5}$ due to GEOS-Chem model vertical profile bias determined by comparison with CALIOP satellite observations of aerosol extinction following van Donkelaar et al. (2013). Gray denotes water.

The chemical composition of ambient ground-level fine particulate mass is of relevance for epidemiological and health impact studies (Health Effects Institute, 2004; National Research Council, 2004; Bell et al., 2012; U.S. EPA., 2009). To our knowledge, these estimates, developed from satellite AOD observations and CTM simulations, offer the first assessment of the long-term exposure to all major $PM_{2.5}$ chemical components throughout the world.

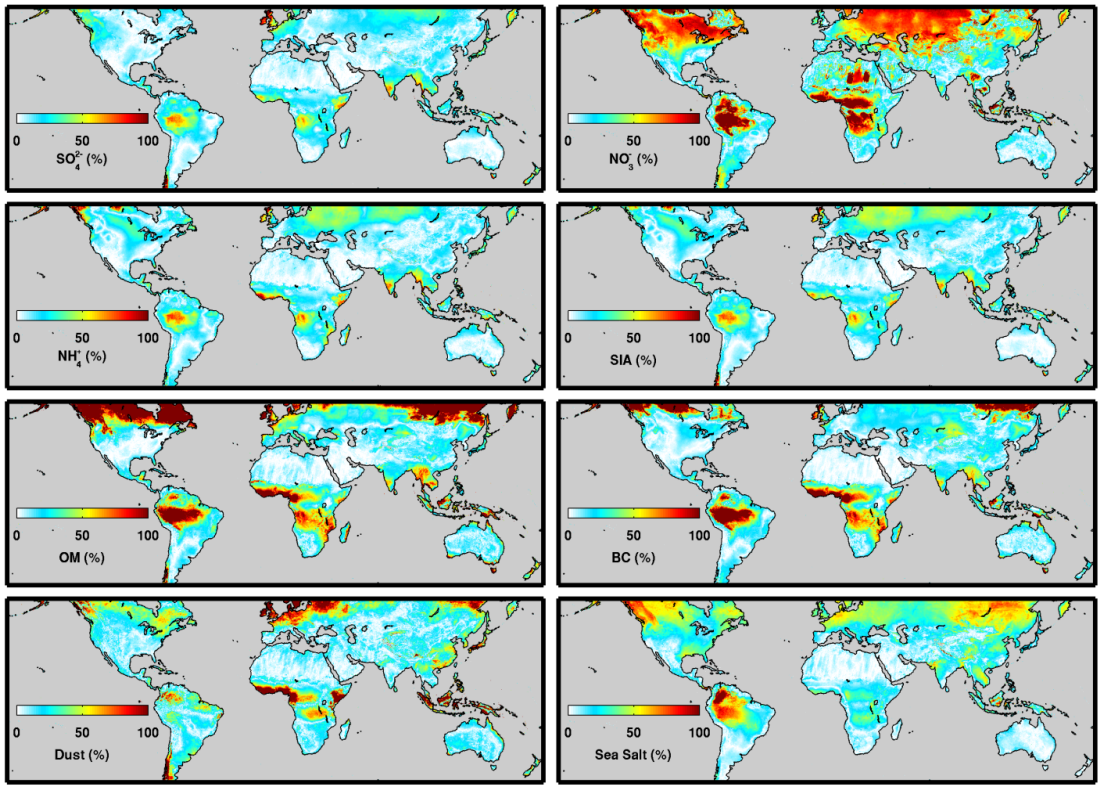

Figure 2-8: Uncertainty in satellite-model $PM_{2.5}$ composition due to incomplete sampling estimated as the difference between the long-term mean simulated $PM_{2.5}$ composition sampled continuously versus coincidently with the satellite observations. Gray denotes water.

Multiple opportunities exist to improve the estimates. Advances in satellite remote sensing (Mishchenko et al., 2007) could yield more observational information on aerosol components. Future developments in the modeling of aerosol composition such as organic mass are needed. Other emerging sources of information on the sources of aerosol precursors include satellite observations of trace gases (Streets et al., 2013) such as NO_2 (Boersma et al., 2011), SO_2 (Lee et al., 2011), and NH_3 (Clarisse et al., 2009). Assimilation of these components into a chemical transport model would provide additional constraints on $PM_{2.5}$ composition. Finer resolution satellite retrievals and simulations would better resolve intra-urban gradients. Trace metals are an important $PM_{2.5}$ component that should be added as their simulation capability improves.

2.5 ACKNOWLEDGEMENTS

This work was supported by Health Canada, the Natural Sciences and Engineering Research Council of Canada, and the U. S. National Institute of Health. Sajeev Philip was supported by an ACEnet Fellowship. Computational facilities are partially provided by ACEnet, the regional high performance computing consortium for universities in Atlantic Canada. We are grateful to the MODIS, MISR, CALIOP, AERONET, NAPS, CAPMoN, CASTNET, IMPROVE, EPA-AQS, EMEP, and EANET teams for making their data publicly available.

2.6 SUPPORTING INFORMATION: GLOBAL CHEMICAL COMPOSITION OF AMBIENT FINE PARTICULATE MATTER FOR EXPOSURE ASSESSMENT

2.6.1 DESCRIPTION OF THE GEOS-CHEM AEROSOL SIMULATION

We used the GEOS-Chem global three-dimensional chemical transport model (version 9-01-03; http://geos-chem.org) to calculate the local conversion factors (ratio of component to AOD) coincident with each satellite observation of AOD. The GEOS-Chem uses assimilated meteorological data from the Goddard Earth Observing System (GEOS-5) at the NASA Global Modeling Assimilation Office (GMAO). The meteorological data includes instantaneous fields, surface variables (e.g., mixed layer depth) at a temporal resolution of 3 hours, and other variables at 6 hours. We reduced the stratospheric layers of the native GEOS-5 vertical grids (72 hybrid eta levels) to 47 for computational expediency. The vertical layers of the current model extend from the Earth's surface to the top of the atmosphere (0.01 hPa) with 47 vertical grids. The lowest layer of the model is centered at approximately 70 meters, and used here to represent the ground-level aerosol concentrations.

The native horizontal resolution for the GEOS-5 meteorological data is 0.5^{o} x 0.667^{o}. First, we used data regridded to a coarser resolution of 2^{o} x 2.5^{o} for computational expediency, and performed the global simulation at this resolution. Second, we conducted three regional (nested) simulations at the native horizontal resolution of 0.5^{o} x 0.667^{o} for three regions of the globe: North America (140^{o}W–40^{o}W, 10^{o}N–70^{o}N), Europe (30^{o}W–50^{o}E, 30^{o}N–70^{o}N) and East Asia (70^{o}W–150^{o}W, 11^{o}S–55^{o}N). This higher resolution simulation preserves the finer spatial patterns of the chemical components (Chen et al., 2009; van Donkelaar et al., 2012). The global simulation outputs were used as boundary conditions for the regional grids. We spun up the model for one month before each global and regional simulation to remove the effects of initial conditions on the aerosol simulation. The dynamical processes (transport and convection) have a temporal resolution of 10 minutes for the nested

simulations, and 15 minutes for the global simulation. We used a timestep of 60 minutes for chemical processes and emissions for both nested and global resolutions. We used full mixing of species below the mixed layer, with a correction to the GEOS-5 predicted nocturnal mixed layer depth as described in Heald et al. (2012) and Walker et al. (2012).

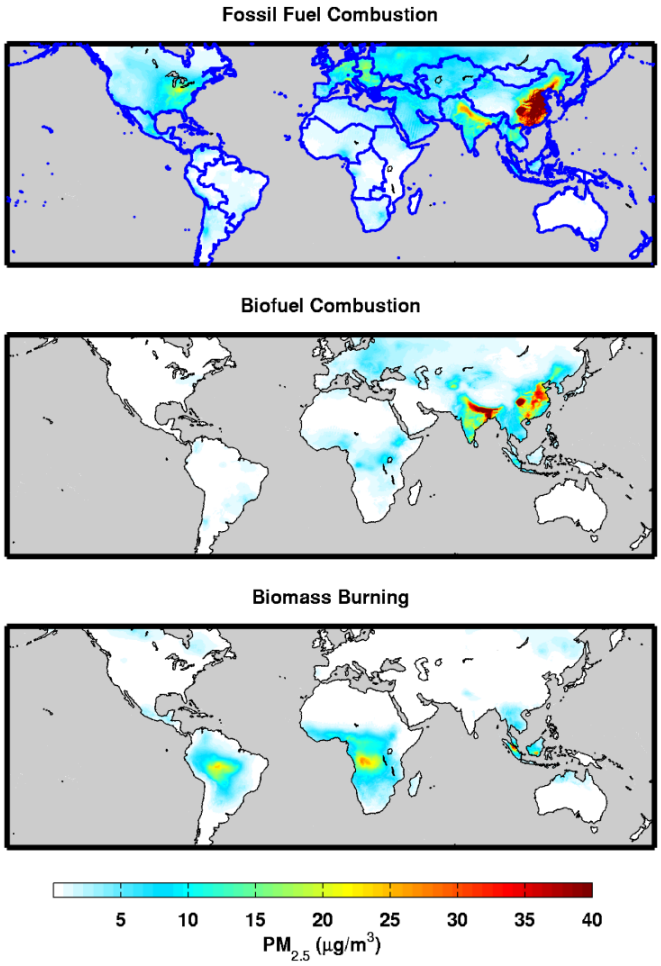

Figure 2-9: Estimate of three major emission sources contributing to $PM_{2.5}$. Gray denotes water. The thick border lines in the top panel represent the GBD (Global Diseases, Injuries, and Risk Factors 2010 study) regions.

GEOS-Chem simulates HO_x-NO_x-VOC-ozone-aerosol chemistry in detail (Bey et al., 2001; Park et al., 2004). Park et al. (2004) describe the simulation of secondary inorganic ions coupled to gas phase chemistry. The simulation of aerosol-gas interactions are through the aerosol extinction effects on photolysis rates (Martin et al., 2003b), and heterogeneous chemistry (Jacob, 2000) with updated N_2O_5 (Evans and Jacob, 2005) and HO_2 (Thornton et al., 2008) uptake by aerosols. The ISORROPIA II thermodynamic scheme (Fountoukis and Nenes, 2007) is used for partitioning gases and aerosols (Pye et al., 2009). GEOS-Chem uses in-cloud sulfate formation using the cloud liquid water content and cloud volume fractions of the GEOS-5 data (Fisher et al., 2011). We artificially limited the nitric acid to two thirds of its value for each timestep to correct for an overestimation in HNO_3 found in comparison with measurements over the eastern U.S. (Heald et al., 2012). GEOS-Chem calculates AOD based on the relative humidity dependent aerosol optical properties as described in Martin et al. (2003b) with an updated growth factor for organic matter, and updates to ammonium sulfate optics. Modification to dust optics is described in Ridley et al. (2012).

The GEOS-Chem simulation uses emission inventories of aerosol and its precursor gases as input. We used regional anthropogenic emission inventories of NO_x and SO_2 over Canada (CAC; http://www.ec.gc.ca/inrp-npri/), the U.S. (Environmental protection Agency-National Emissions Inventory 2005; http://www.epa.gov/ttnchie1/net/2005inventory.html), Mexico (BRAVO; Kuhns et al., 2005), Europe (EMEP; http://www.emep.int/), and East Asia (Zhang et al., 2009) for NO_x; (Lu et al., 2011) for SO_2. Elsewhere, we used anthropogenic emissions from EDGAR v32-FT2000 global inventory for 2000 (Olivier, 2005), and scaled it based on the energy

statistics to subsequent years (van Donkelaar et al., 2008). Anthropogenic NO_x emissions were scaled from 2006 to subsequent years based on the NO_2 column density data retrieved from the OMI satellite sensor (Lamsal et al., 2011). GEOS-Chem includes soil NO_x (Yienger and Levy, 1995; Wang et al., 1998), lightning NO_x (Price and Rind, 1992; Sauvage et al., 2007; Martin et al., 2007; Hudman et al., 2007; Murray et al., 2012), ship SO_2 from the ICOADS inventory (Lee et al., 2011; Vinken e al., 2011), and volcanic emissions (Fisher et al., 2011). Seasonality for NO_x and SO_2 is based on the statistics from regional inventories. GEOS-Chem includes a diurnal variation for NO_x as described in van Donkelaar et al. (2008). Global ammonia emission in GEOS-Chem is from Bouwman et al. (1997) with a seasonality imposed by Park et al. (2004). Spatial and seasonal NH_3 variation over Canada is based on monthly varying agricultural activity statistics provided by the Agriculture Canada (Sheppard et al., 2011). Other regional inventories are over the U.S. (EPA-NEI), Europe (EMEP), and East Asia (Streets et al., 2003). East Asian annual emissions are superimposed with a relative seasonal variation (Fisher et al., 2011, Kharol et al., 2013), and a reduction of 30% (Kharol et al., 2013) motivated by comparison with other inventories (Huang et al., 2012a; 2012b). We doubled NH_3 emissions over California as suggested by Heald et al. (2012) and Walker et al. (2012).

GEOS-Chem carbonaceous aerosols include black carbon (BC), organic carbon (OC), and secondary organic aerosols (SOA) (Park et al., 2003; Wang et al., 2011). The global anthropogenic OC and BC inventory is from Bond et al. (2007), with the Cooke et al. (1999) inventory over North America, and the Lu et al. (2011) inventory over East Asia. We doubled the East Asian OC and BC emissions based on a comparison with top-down inversion of regional inventories by Fu et al. (2012), and recognize there is ongoing

discussion on this topic (Wang et al., 2013). GEOS-Chem simulates the formation of SOA from the oxidation of volatile organic compounds (Henze and Seinfeld, 2006; Liao et al., 2007; Fu et al., 2008). Global biomass burning emission is from the GFED-3 inventory at 3-day temporal resolution (van der Werf et al., 2010; Mu et al., 2011), and global biofuel emission is from Yevich and Logan (49) superimposed with the regional inventories mentioned above. We calculated OM as the sum of model OC and SOA. We used the OM/OC ratio estimated from observations by the OMI satellite sensor and Aerosol Mass Spectrometer to convert OC to OM to account for the presence of non-carbon elements (Philip et al., 2014a).

GEOS-Chem includes the simulation of natural particles such as mineral dust and sea salt. The mineral dust simulation is described by Fairlie et al. (2007). We used the first dust size bin and 37% of the second dust size bin (out of the 4 bins) to get a $PM_{2.5}$ size range. Sea salt emission in the model is described by Alexander et al. (2005) with updates by Jaegle et al. (2011). We use sea salt accumulation mode size range from 0.1 to 1 μm, which in typical coastal conditions represents the approximate $PM_{2.5}$ size range.

GEOS-Chem includes dry deposition (Wang et al., 1998), and wet deposition (Wang et al., 2011; Liu et al., 2001; Amos et al., 2012).

Numerous studies have evaluated the GEOS-Chem ground-level aerosol concentrations and its seasonal variation (e.g., Park et al., 2003; 2004; 2006; Fairlie et al., 2007; Pye et al., 2009; Heald et al., 2012; Walker et al., 2012; Leibensperger et al., 2012; Fu et al., 2012; Zhang et al., 2012a). Vertical profiles of aerosol composition were also compared with various aircraft observations (e.g., van Donkelaar et al., 2008; Drury et al., 2010; Heald et

al., 2011), and with CALIOP satellite observations (van Donkelaar et al., 2010; 2013; Ford and Heald, 2012). Six-year coincident comparisons of GEOS-Chem and CALIOP suggest simulated near-surface to column extinction ratios are often within 25%, but can approach a factor of two in certain seasons and locations (van Donkelaar et al., 2013).

Table 2-3: Global in situ data collected from publications. "NA" represents data not available or filtered out.

Sl. No.	Site/City	Country	Latitude	Longitude	Study Period	SO_4^{2-}	NO_3^-	NH_4^+	OC	BC	Size	Source
			degree	degree		μg/m^3	μg/m^3	μg/m^3	μg/m^3	μg/m^3		
1	Beijing	China	40.3	116.3	Mar 2005 - Feb 2006	15.8	10.1	7.3	34.4	8.3	$PM_{2.5}$	Yang et al., 2011
2	Miyun Resevoir	China	40.5	116.8	Mar 2005 - Feb 2006	13.0	6.4	6.1	21.9	3.8	"	"
3	Chongqing	China	29.6	106.5	Mar 2005 - Feb 2006	25.5	5.3	7.9	42.2	6.5	"	"
4	Dadukou	China	29.5	106.5	Mar 2005 - Feb 2006	23.4	5.1	7.6	47.2	6.4	"	"
5	Jinyun	China	29.8	106.4	Mar 2005 - Feb 2006	24.0	4.8	7.3	41.2	4.7	"	"
6	Hok Tsui	Hong Kong	22.2	114.3	Nov 2004 - Oct 2005	11.9	0.8	3.1	4.3	2.1	"	So et al., 2007
7	Tsuen Wan	Hong Kong	22.4	114.1	Nov 2004 - Oct 2005	13.2	1.6	4.1	7.4	6.0	"	"
8	Mong Kok	Hong Kong	22.3	114.1	Nov 2004 - Oct 2005	12.8	2.4	4.4	11.9	13.7	"	"
9	Delhi	India	28.4	77.1	Mar 2001 - Jan 2002	10.9	6.1	6.4	40.3	10.5	"	Chowdhury, 2004
10	Mumbai	India	22.6	88.3	Mar 2001 - Jan 2002	6.9	1.6	2.0	12.6	4.6	"	"
11	Kolkata	India	18.7	72.8	Mar 2001 - Jan 2002	7.2	2.9	3.6	37.1	12.1	"	"
12	Lahore	Pakistan	31.5	74.3	Jan 2007 - Jan 2008	10.5	6.6	3.6	64.4	11.2	"	Stone et al., 2010
13	Brazil	Brazil	23.0	43.2	Sep 2003 - Sep 2004	1.5	0.3	0.6	NA	2.1	"	Soluri et al., 2007
14	Brazil	Brazil	22.9	43.2	Sep 2003 - Sep 2004	1.9	0.4	0.7	NA	3.1	"	"
15	Brazil	Brazil	22.9	43.2	Sep 2003 - Sep 2004	2.2	0.5	0.7	NA	2.9	"	"
16	Brazil	Brazil	23.0	43.4	Sep 2003 - Sep 2004	1.4	0.3	0.4	NA	1.3	"	"
17	Brazil	Brazil	23.0	43.3	Sep 2003 - Sep 2004	1.8	0.5	0.5	NA	2.7	"	"
18	Brazil	Brazil	22.8	43.4	Sep 2003 - Sep 2004	1.5	0.4	0.5	NA	3.2	"	"
19	Brazil	Brazil	23.0	43.6	Sep 2003 - Sep 2004	1.5	0.4	0.5	NA	1.2	"	"
20	Brazil	Brazil	22.9	43.6	Sep 2003 - Sep 2004	1.7	0.4	0.6	NA	2.4	"	"
21	Brazil	Brazil	22.9	43.4	Sep 2003 - Sep 2004	1.7	0.4	0.6	NA	2.5	"	"
22	Brazil	Brazil	22.9	43.7	Sep 2003 - Sep 2004	1.7	0.3	0.5	NA	1.7	"	"
23	Tel Aviv	Israel	32.1	34.8	Jan 2007 - Dec 2007	5.2	0.7	NA	4.7	1.5	"	Sarnat et al., 2010
24	Haifa	Israel	32.8	35.0	Jan 2007 - Dec 2007	5.2	1.4	NA	3.0	1.0	"	"
25	W. Jerusalem	Israel	31.8	35.2	Jan 2007 - Dec 2007	4.6	1.0	NA	4.1	1.1	"	"
26	Hebron	Palestine	31.5	35.1	Jan 2007 - Dec 2007	3.8	0.9	NA	5.3	1.8	"	"
27	E. Jerusalem	Palestine	31.8	35.2	Jan 2007 - Dec 2007	4.4	0.9	NA	5.2	2.2	"	"
28	Nablus	Palestine	32.2	35.2	Jan 2007 - Dec 2007	4.3	1.0	NA	8.2	5.6	"	"
29	Amman	Jordan	32.0	35.8	Jan 2007 - Dec 2007	4.5	1.0	NA	6.2	2.4	"	"
30	Balearic islands	Spain	39.6	2.6	Jan 2004 - Feb 2005	3.9	0.9	2.0	2.9	0.5	"	Pey et al., 2009
31	Kuwait	Kuwait	29.3	48.0	Feb 2004 - Jan 2005	9.9	1.8	NA	3.7	2.5	"	Brown et al., 2008
32	Chengdu	China	30.7	104.0	Jan 2006 - Dec 2007	40.5	NA	14.0	36.3	10.8	PM_{10}	Zhang et al., 2012b
33	Dalian	China	38.9	121.6	Jan 2006 - Dec 2007	23.3	NA	7.7	20.2	5.3	"	"
34	Dunhuang	China	40.2	94.7	Jan 2006 - Dec 2007	6.6	NA	0.4	26.7	3.6	"	"
35	Gaolanshan	China	36.0	105.9	Jan 2006 - Dec 2007	16.7	NA	6.5	19.1	3.8	"	"
36	Gucheng	China	39.1	115.8	Jan 2006 - Dec 2007	35.5	NA	14.4	38.5	11.0	"	"
37	Jinsha	China	29.6	114.2	Jan 2006 - Dec 2007	26.6	NA	7.6	15.3	3.0	"	"
38	Lhasa	China	29.7	91.1	Jan 2006 - Dec 2007	2.9	NA	0.2	21.7	3.8	"	"
39	LinAn	China	30.3	119.7	Jan 2006 - Dec 2007	21.7	NA	6.8	15.1	4.3	"	"
40	Longfengshan	China	44.7	127.6	Jan 2006 - Dec 2007	10.0	NA	2.5	15.9	2.3	"	"
41	Nanning	China	22.8	108.4	Jan 2006 - Dec 2007	21.6	NA	5.8	17.9	4.0	"	"
42	Panyu	China	23.0	113.4	Jan 2006 - Dec 2007	26.8	NA	8.6	22.3	7.9	"	"
43	Taiyangshan	China	29.2	111.7	Jan 2006 - Dec 2007	28.8	NA	7.9	13.8	2.7	"	"
44	Xian	China	34.4	109.0	Jan 2006 - Dec 2007	46.7	NA	14.4	42.6	12.7	"	"
45	Zhengzhou	China	34.8	113.7	Jan 2006 - Dec 2007	45.0	NA	16.5	29.2	9.2	"	"
46	Akdala	China	47.1	88.0	Jul 2004 - Mar 2005	3.3	NA	0.6	2.9	0.4	"	Qu et al., 2008; 2009
47	Shangri-La, Zhuzhang	China	28.0	99.7	Jul 2004 - Mar 2005	1.6	NA	0.2	3.1	0.3	"	"

2.6.2 DESCRIPTION OF THE GROUND-BASED $PM_{2.5}$ COMPOSITION MEASUREMENTS

We utilized filter-based in situ measurements by several networks, such as, the National Air Pollution Surveillance Network (NAPS) and the Canadian Air and Precipitation Monitoring Network (CAPMoN) over Canada (http://www.on.ec.gc.ca/natchem). The U.S. measurement networks include the Clean Air Status and Trends Network (CASTNET, http://java.epa.gov/castnet/epa_jsp/sites.jsp), the Interagency Monitoring of Protected Visual Environments (IMPROVE, http://vista.cira.colostate.edu/improve/), and the U.S. Environmental Protection Agency Air Quality System (EPA-AQS, http://www.epa.gov/ttn/airs/airsaqs/). The NAPS network provides 24-hr composition every third day across Canada as described in Dabek-Zlotorzynska et al. (2011). We used weekly average sulfate and ammonium ion measurements from the CAPMoN and the CASTNET networks even though they are devoid of $PM_{2.5}$ filters (Zhang et al., 2008). The IMPROVE network provides 24-hr $PM_{2.5}$ composition data except for ammonium for every third day from several national parks in the U.S. The EPA-AQS network mainly operates over rural areas which report 24-hr averages of all the major composition measurements every consecutive third or sixth day. Here, we used the $PM_{2.5}$ composition data from EPA-AQS and IMPROVE networks (2005-2008 mean) reported by Hand et al. (2011). We calculated ammonium from sulfate and nitrate measurements of EPA-AQS and IMPROVE networks by assuming a fully neutralized sulfuric acid by ammonia gas. We averaged the data reported by Hand et al. (2011), and the long-term (2004-2008) in situ measurements from other networks into the 0.1^0 x 0.1^0 grid for comparison with satellite-model composition over North America.

We treated these in situ data as 'truth' to evaluate our product. However, it is worth noting some uncertainties. Carbon measurements are prone to errors due to filter contamination (e.g., Rattigan et al., 2011). The ratio of OM to OC varies from 1.2 to 2.6 depending on the spatial and seasonal differences (e.g., Turpin and Lim, 2001; Simon et al., 2011). Mineral dust concentrations were from the elemental measurements of IMPROVE and EPA-AQS following Malm et al. (1994) even though measurements of five elements alone are inadequate to determine the ambient mineral dust (Hand et al., 2011; Malm and Hand, 2007). Sea salt were from elemental chlorine or chlorine ion measurements, by accounting for 55% chlorine by weight; the selection of sea salt marker as sodium or chlorine is also uncertain (Hand et al., 2011; White, 2008). Hand et al. (2012) obtained relative errors for $PM_{2.5}$ and its chemical components from a comparison of collocated IMPROVE and AQS measurements (17% for $PM_{2.5}$, 5% for ammonium sulfate, 11% for ammonium nitrate, 10% for OC, 12% for EC, 33% for dust, and 77% for sea salt). Finally, the gridded in situ data are prone to representation error as an individual measurement is used to represent a 10 km x 10 km area.

In addition, we collected annually representative inorganic and organic composition measurements from the European Monitoring and Evaluation Programme (EMEP; http://www.emep.int/), the Acid Deposition Monitoring Network in East Asia (EANET; http://www.eanet.cc/), and several field measurements around the world from published papers (e.g., Fu et al., 2012; Zhang et al., 2008 and Cao et al., 2007 for organic measurements, and several others: Table 2-3). We used this dataset to evaluate the global satellite-model composition. We included only sites with all SIA components to achieve a consistent evaluation.

CHAPTER 3: SPATIALLY AND SEASONALLY RESOLVED ESTIMATE OF THE RATIO OF ORGANIC MASS TO ORGANIC CARBON

Authors: Sajeev Philip[1*], Randall V. Martin[1, 2], Jeffrey. R. Pierce[3,1], Jose-Luis Jimenez[4], Qi Zhang[5], Manjula. R. Canagaratna[6], Dominick. V. Spracklen[7], Caroline. R. Nowlan[1], Lok N. Lamsal[8,9], Matthew. J. Cooper[1], and Nickolay. A. Krotkov[9]

[1]Department of Physics and Atmospheric Science, Dalhousie University, Halifax, Nova Scotia, Canada

[2]Harvard-Smithsonian Center for Astrophysics, Cambridge, Massachusetts, USA

[3]Department of Atmospheric Science, Colorado State University, Fort Collins, Colorado, USA

[4]Department of Chemistry and Biochemistry, and CIRES, University of Colorado, Boulder, CO, USA

[5]Department of Environmental Toxicology, University of California, Davis, CA

[6]Aerodyne Research, Billerica, Massachusetts, USA

[7]School of Earth and Environment, University of Leeds, Leeds, UK

[8]Goddard Earth Sciences Technology and Research, Universities Space Research Association, Columbia, Maryland, USA

[9]NASA Goddard Space Flight Center, Greenbelt, Maryland, USA

[*]Sajeev Philip conducted the research and wrote the manuscript

3.1 ABSTRACT

Particulate organic matter is of interest for air quality and climate research, but the relationship between ambient organic mass (OM) and organic carbon (OC) remains ambiguous both in measurements and in modeling. We present a simple method to derive an estimate of the spatially and seasonally resolved global, lower tropospheric, ratio between OM and OC. We assume ambient NO_2 concentrations as a surrogate for fresh emission which mostly determines the continental scale OM/OC ratio. For this, we first develop a parameterization for the OM/OC ratio using the primary organic aerosol (POA) fraction of total OM estimated globally from Aerosol Mass Spectrometer (AMS) measurements, and evaluate it with high mass resolution AMS data. Second, we explore the ability of ground-level NO_2 concentrations derived from the OMI satellite sensor to serve as a proxy for fresh emissions that have a high POA fraction, and apply NO_2 data to derive ambient POA fraction. The combination of these two methods yields an estimate of OM/OC from NO_2 measurements. Although this method has inherent deficiencies over biomass burning, free-tropospheric, and marine environments, elsewhere it offers more information than the currently used global-mean OM/OC ratios. The OMI-derived global OM/OC ratio ranges from 1.3 to 2.1 μg/μgC, with distinct spatial variation between urban and rural regions. The seasonal OM/OC ratio has a summer maximum and a winter

minimum over regions dominated by combustion emissions. This dataset serves as a tool for interpreting organic carbon measurements, and for evaluating the modeling of atmospheric organics. We also develop an additional parameterization for models to estimate the ratio of primary OM to OC from simulated NO_x concentrations.

3.2. INTRODUCTION

Organic aerosols (OA) are a major constituent of fine particulate mass which affects air quality, visibility, and climate. Primary OA (POA) are mostly produced by combustion sources, while secondary OA (SOA) form through oxidation and partitioning of volatile organic compounds from anthropogenic and biogenic sources. Ambient OA is a complex mix of thousands of different organic molecules that introduces difficulties in analytical measurements, leaving large measurement uncertainty (e.g., Kanakidou et al., 2005; Jimenez et al., 2009). OA contains organic carbon (OC) as its major constituent and other elements such as oxygen, hydrogen and nitrogen, which together with OC constitute the total organic aerosol mass. Characterization of OA requires spatially and seasonally resolved information about the ratio of OA with OC (OA/OC, also commonly written as OM/OC, where OM is "organic mass", a synonym of OA).

Traditional ground-based impaction or filter-based instruments routinely measure OC using different analytic methods (e.g., Hand et al., 2012), but not OM due to difficulties in characterizing different components of OM. Other specific techniques that measure OM directly, such as Fourier Transform Infrared spectroscopy (FTIR) (Russell et al., 2009) and solvent extraction techniques (El-Zanan et al., 2005), are not used extensively. A wide range of literature is available on the methods to determine the OM/OC ratio, and it is a

broadly debated issue. A common practice to interpret OC measurements is through the use of a continental mean value for the OM/OC ratio, such as 1.4 (Grosjean and Friedlander, 1975; White and Roberts, 1977), 1.6 (Malm et al., 1994), 1.4–2.1 (Turpin and Lim, 2001), and 1.8 (Hand et al., 2012) for North America. The spatial and seasonal variation in the OM/OC ratio is often neglected in the interpretation of measurement data due to insufficient information (e.g., Hand et al., 2012).

These global-mean values are frequently used in aerosol models to convert between POA and OM (e.g., Park et al., 2003). This is because most global and regional models simulate POA as OC. Despite notable developments for simulating the oxidative aging of OM (Simon and Bhave, 2012), most models do not yet readily predict the OM/OC ratio. A spatially and seasonally varying estimate of the OM/OC ratio should help interpret simulated organic aerosols.

The OM/OC ratio is directly related to the O/C ratio in the organic mass, since the contribution of non-oxygen elements to the OM/OC ratio is generally small, and both ratios increase with chemical aging of OA (Aiken et al., 2008; Pang et al., 2006). OM/OC has seasonal and spatial variation depending on the sources of POA and SOA and their degree of aging. The Aerosol Mass Spectrometer (AMS) offers quantitative determination of the size-resolved submicron OM at high temporal resolution through mass spectrometry (Jimenez et al., 2003; Canagaratna et al., 2007). Factor analysis of the AMS spectra can differentiate POA such as hydrocarbon-like OA (HOA) and several types of oxygenated OA (OOA) (Zhang et al., 2005a) that are typically SOA surrogates (Zhang et al., 2007;

Zhang et al., 2011b). POA has lower OM/OC than SOA, and fresh SOA has lower OM/OC than aged SOA (Aiken et al., 2008).

The oxidative aging of organics may be indirectly estimated through different proxies. Both NO_x and submicron POA are mainly emitted from combustion processes. NO_x is oxidized in the atmosphere with a timescale of about a day. Over regional scales OA is dominated by SOA, and anthropogenic SOA is also formed with a timescale of about a day and in amounts much larger than the originally emitted POA (DeCarlo et al., 2010). Globally most SOA may be due to anthropogenic enhancement of biogenic SOA, which is also thought to have a similar timescale of formation (Goldstein et al., 2009; Spracklen et al., 2011). Once formed, all types of SOA appear to age with a characteristic timescale of about 1–2 days, increasing the OM/OC ratio (Jimenez et al., 2009). Given the similar spatial emission patterns and timescales, we explore ambient NO_2 concentrations as a surrogate for the POA/OA fraction and thus OM/OC ratios.

Here, we introduce a parameterization for OM/OC based on the POA fraction estimated from AMS measurements (section 3.3.1), test global ground-level NO_2 and NO_x concentrations as a proxy for POA fraction, and thus OM/OC (sections 3.3.2 and 3.3.3), and develop a gridded dataset of the seasonally varying OM/OC ratio (section 3.3.4). We describe the spatially and seasonally varying satellite-derived OM/OC in section 3.4.

3.3. MATERIALS AND METHODS

3.3.1 PRIMARY OA FRACTION OF THE AMS DATA TO PREDICT OM/OC

We first explore a method to derive OM/OC. For this, we use the POA fraction of the AMS data as a proxy for combustion emissions (where combustion emissions can then be determined from the measurements of co-emitted species such as NO_x). Aiken et al. (2008) demonstrate a method to use high-resolution time-of-flight AMS ambient OA measurements to directly quantify the OM/OC ratio. Aiken et al. (2008) report a high correlation for OM/OC versus O/C (r = 0.998), quantify the OM/OC ratio for urban POA as ~1.3, and find that for OOA the OM/OC ratio varies from 1.9 to 2.4. Per the timescale discussion above, f_{POA} (the ratio of POA, determined from factor analysis of AMS spectra (Zhang et al., 2011b), to the total measured OA) is expected to be inversely related to OM/OC. We parameterize OM/OC from AMS using f_{POA},

$$OM/OC = 1.3 \times f_{POA} + 2.1 \times (1 - f_{POA}) \quad (3\text{-}1)$$

where OM is the sum of AMS-estimated POA and OOA. This method assumes that POA has an OM/OC ratio of 1.3 and OOA has a value of 2.1. However it should be noted that the OM/OC values for OOA can range from 1.9 to 2.4, and therefore our prescribed value introduces an uncertainty in the OM/OC values estimated using equation 3-1. An independent evaluation with direct OM/OC estimates from the AMS quantifies this uncertainty (±0.2 μg/μgC). This evaluation consisted of collecting nine published high mass resolution campaign-mean AMS-estimated f_{POA} and AMS-measured OM/OC data from field campaigns to evaluate this parameterization. Figure 3-1 shows the scatter plot of AMS OM/OC and f_{POA}. It includes a representation of a typical urban POA with OM/OC ratio of 1.3 (f_{POA} = 1). We plotted equation 3-1 over this scatter plot (black line). The scatter points (OM/OC) are approximately within ±0.2 (μg/μgC) from the solid black line.

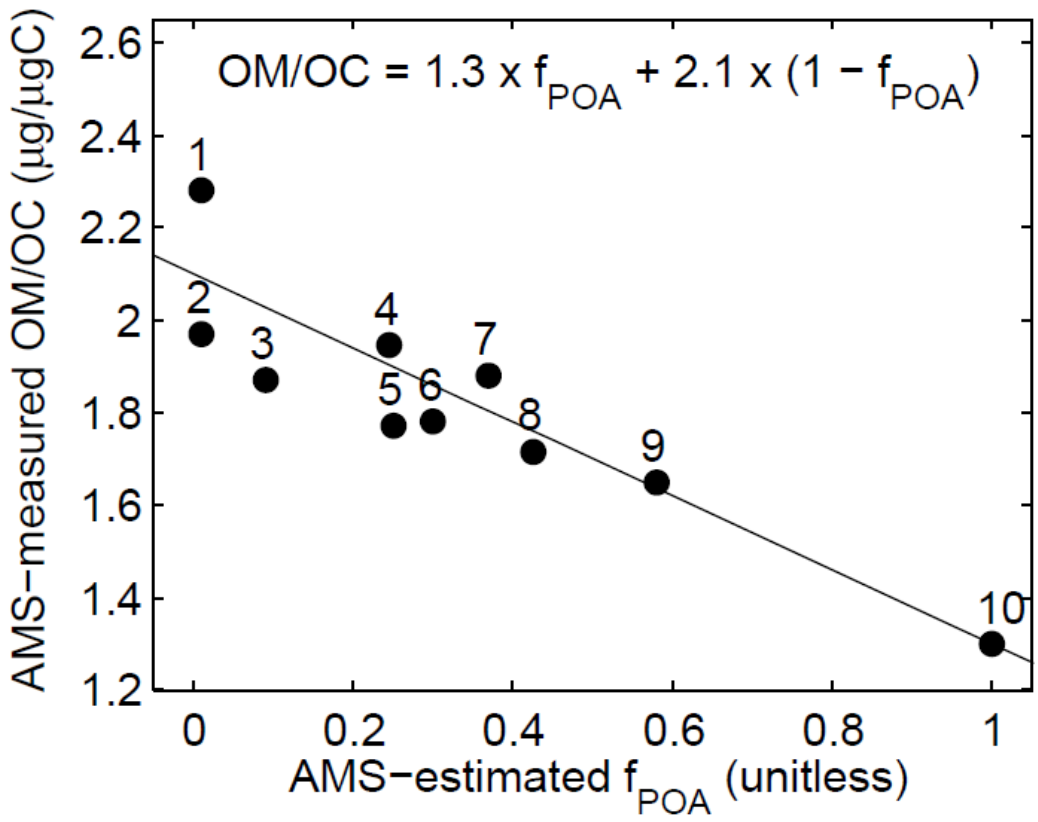

Figure 3-1: Scatter plot of Aerosol Mass Spectrometer (AMS) measured OM/OC ratio, and the corresponding estimated primary organic aerosol fraction (f_{POA}) from several field campaigns around the globe. The dots and the corresponding numbers on the plot represent AMS field campaign-mean values for (1) Whistler, Canada (Sun et al., 2009); (2) Long Island (Personal communication from Qi Zhang); (3) CARES T1 (Setyan et al., 2012); (4) Pearl River Delta, China (Huang et al., 2011); (5) SOAR 1 (Docherty et al., 2011); (6) New York City (Sun et al., 2011); (7) CalNex, Los Angeles (Hayes et al., 2013); (8) Beijing, China (Huang et al., 2010); (9) Fresno, California (Ge et al., 2012); and (10) typical urban POA (Jimenez et al., 2009). The solid black line is equation 3-1 (also in inset).

This confirms the validity of the predicted relation in equation 3-1. Moreover, the high correlation ($r = -0.91$) supports the linear relation between AMS $f_{POA}$and OM/OC in the continental boundary layer across a variety of regions. We can affirm this because there were actually few free-tropospheric, biomass burning or marine boundary layer observations in this dataset. This constraint limits, to a degree, the applicability of equation 3-1 (and its validation) in Figure 3-1; it is noted, for example, that OM/OC values can exceed 2.1 outside of the continental boundary layer (Sun et al., 2009) and from biomass burning (Turpin and Lim, 2001).

Thus, this parameterization may underestimate OM/OC in those cases. Although the relation in equation 3-1 offers another estimate (indirect) of OM/OC over AMS locations, this relation is developed only to generate OM/OC from NO_x measurements (Section 3.4). More reliable methods to estimate OM/OC from AMS are already available (for example, publications listed in Figure 3-1 caption).

Spracklen et al. (2011) and Zhang et al. (2007) collected AMS POA and OOA data for 47 approximately month-long, observation campaigns over 37 locations. However, this dataset does not have reliable high mass resolution OM/OC measurements to evaluate equation 3-1. Nevertheless, this dataset has reliable POA fraction data for a broad range of locations. The prediction model in equation 3-1 can be applied to f_{POA} estimates of these 47 campaign-mean dataset to generate an indirect OM/OC dataset. Figure 3-2 shows these global AMS measurements of OA (top left), POA (top right), f_{POA} (bottom left), and the derived OM/OC ratio (bottom right). f_{POA} is high over regions with fresh anthropogenic emissions. The OM/OC ratio typically ranges from 1.7 to 2.1.

We also considered the OM/OC ratio as estimated through a multiple regression analysis of IMPROVE data (Simon et al., 2011). However, the OM/OC ratio estimated from AMS and IMPROVE measurements differs from each other (r = 0.4, RMSE = 0.13 µg/µgC, number of points = 13), and the difference is not well understood. The O/C from the AMS is a more direct measurement, whereas the OM from IMPROVE is based on the measured OC plus extra mass needed to get closure between the total characterized mass and the total measured mass (Aiken et al., 2008; Simon et al., 2011). The inaccuracy of OC and inorganic mass measurements by IMPROVE filter techniques, and the subtraction of two large numbers introduce errors in the OM/OC calculation (Simon et al., 2011). In addition, filter measurements tend to suffer loss of semivolatile species (especially during warm seasons) and condensation of volatile organic compounds. Real time AMS measurements are less influenced by gas-particle partitioning of semivolatile species. Thus we focus exclusively on AMS data for the remainder of this manuscript.

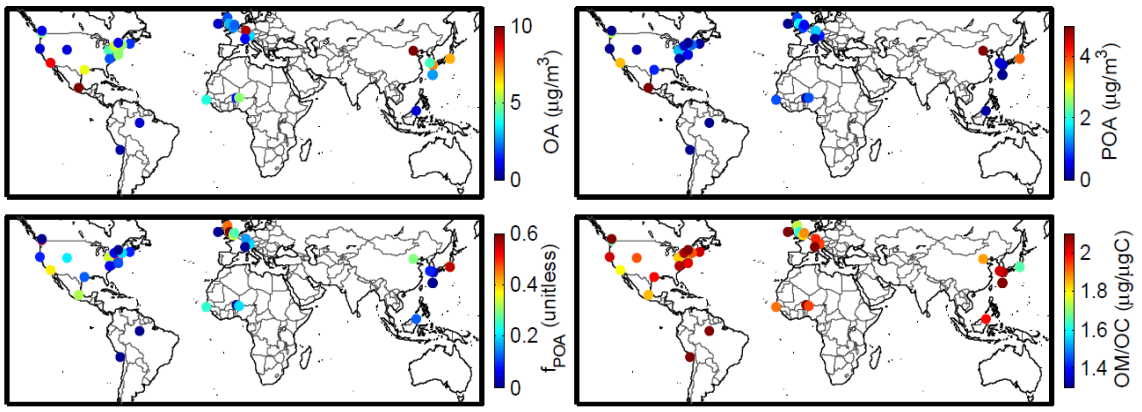

Figure 3-2: Aerosol Mass Spectrometer measured organic aerosol (OA), estimated primary OA (POA), POA fraction (f_{POA}), and predicted organic mass (OM) to organic carbon (OC) ratio using equation 3-1. Data source: Spracklen et al., 2011 and Zhang et al., 2007.

3.3.2 NITROGEN OXIDES AS A PROXY FOR PRIMARY OA FRACTION

Local combustion processes are a major source of primary organic aerosol. Several studies reported the high correlation of AMS-estimated POA with nitrogen oxide species (e.g., Zhang et al., 2005b; Sun et al., 2011; Ge et al., 2012). Therefore, the fractionation of ambient OA to primary and oxygenated components can be determined indirectly from the measurements of NO_x. Given the correlation between POA and NO_x, we explore the relationship between AMS POA fraction measurements, and a spatially coincident modeled NO_x climatology to develop a proxy for the POA fraction and then the OM/OC ratio. We use the GEOS-Chem (http://geos-chem.org) global three-dimensional chemical transport model to test the correlations between AMS-estimated f_{POA} and co-emitted combustion related species. GEOS-Chem includes a detailed simulation of oxidant-aerosol chemistry as described in the Appendix (section 3.7).

We tested the spatial correlation between AMS-estimated f_{POA} and coincident GEOS-Chem simulations of NO_x ($r = 0.73$), NO_2 ($r = 0.74$), hydrophobic OC ($r = 0.42$), BC ($r = 0.57$), and CO ($r = 0.15$). The significant correlation for NO_x supports the use of this species as a proxy for the AMS POA fraction. Therefore, we assume that the typical continental POA fraction is a function of NO_x concentrations.

3.3.3. AMBIENT PRIMARY OA FRACTION ESTIMATE FROM SATELLITE-DERIVED NITROGEN DIOXIDE CONCENTRATION

Given the significant correlation between modeled nitrogen oxides and observed POA fraction, we further compare AMS f_{POA} with satellite retrievals of NO_2 which offer finer spatial information than the model. Advancements in satellite remote sensing over the last

decade yield accurate retrievals of global NO_2 column concentrations at moderate spatial resolution (Boersma et al., 2011; Bucsela et al., 2013). The NO_2 column concentrations are closely related to local NO_x emission (Martin et al., 2003a) and ground-level NO_2 concentrations (Lamsal et al., 2008). We relate these satellite-derived NO_2 concentrations with the POA fraction at ground-level. We begin with NO_2 columns retrieved by Bucsela et al. (2013) for years 2005–2008 from the Dutch–Finnish built Ozone Monitoring Instrument (OMI) sensor aboard the NASA Aura satellite. We retain column data that have cloud fraction < 0.3, solar zenith angle < 78° and near-nadir viewing angle (scan positions 7–53 out of 60).

We use the daily coincident ratio of column density to ground-level concentration simulated with the GEOS-Chem model to derive daily ground-level NO_2 concentrations at a spatial resolution of 0.1° × 0.1° following Lamsal et al. (2008) and Lamsal et al. (2010). Ground-level NO_2 concentrations derived from this approach exhibit significant temporal (r = 0.30–0.96, mean r = 0.69) and spatial (r = 0.78) correlation versus in situ measurements at 307 sites across North America (Lamsal et al., 2013).

We sampled the long-term monthly mean OMI-derived ground-level NO_2 concentration (at a spatial resolution of 0.1° × 0.1°) with the spatially coincident AMS-estimated POA fraction. Figure 3-3 shows the scatter plot of AMS f_{POA} versus OMI NO_2. Similar to model comparisons mentioned above, the correlation for these two species is significant (r = 0.73). Excluding outliers (New York City, summer 2001; New York City, winter 2004; and Vancouver, Canada, August 2001 campaigns) increases it further up (r = 0.87). This

supports the utility of OMI nitrogen dioxide measurements to predict the fractionation of ambient OA.

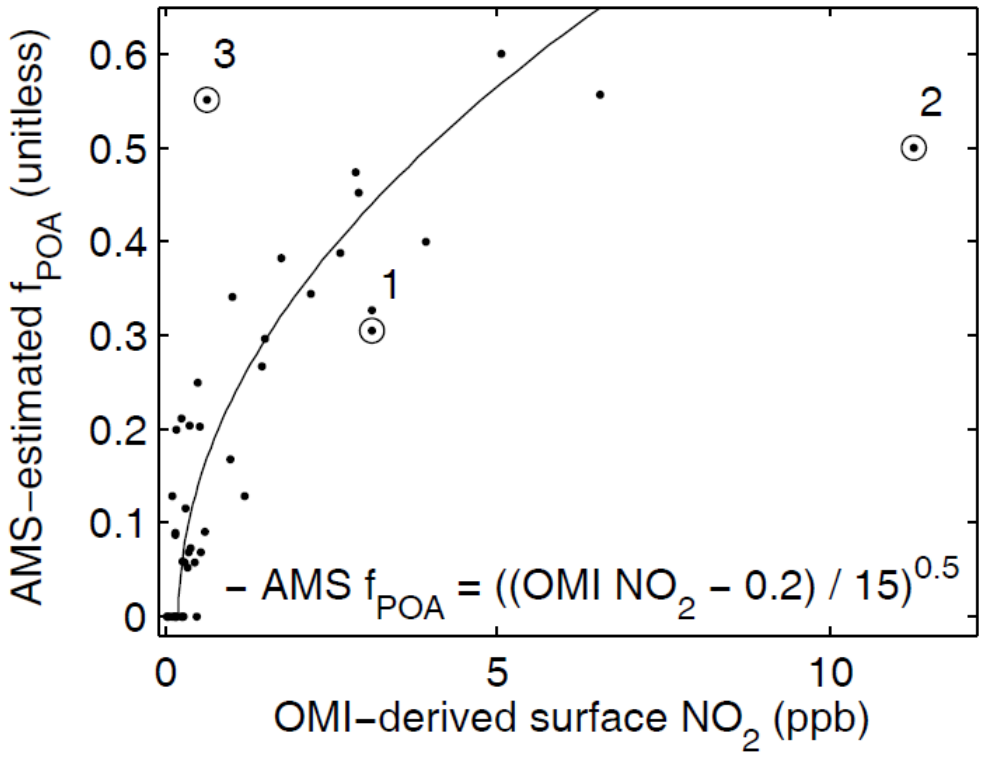

Figure 3-3: Scatter plot of estimated primary organic aerosol fraction (f_{POA}) from the Aerosol Mass Spectrometer (AMS) versus ground-level NO_2 concentrations derived from the OMI satellite instrument. The solid black line is equation 3-2 (also in inset). The circled dots and the corresponding numbers represent three outliers which represent mean values for the New York City, Summer 2001; New York City, Winter 2004; and Vancouver, Canada, August 2001 campaigns respectively.

A linear relation can be used to derive ambient f_{POA} from OMI NO_2 data given their high correlation. We used the correlation statistics obtained for a reduced major axis regression

(Miller and Kahn, 1962) between the AMS f_{POA} and OMI NO_2 (r = 0.73, slope = 11.32, offset = −0.77, N = 47) to fit a line. We then compared f_{POA} estimated from OMI NO_2 (using the linear fit) against the 47 AMS f_{POA} data, and obtained an RMSE of 0.31 (r = 0.73, slope = 1.0, offset = 0, N = 47). However, we note that a fast increase of f_{POA} at low NO_2 concentrations (i.e. a non-linear increase) is more consistent with Figure 3-3. OMI NO_2 is almost constant for f_{POA} between 0 and 0.2, and increasing thereafter. Therefore we test a non-linear relation here.

The ground-level f_{POA} and the OMI NO_2 data (ppb) were fitted with the following non-linear expression,

$$f_{POA} = ((\text{OMI } NO_2 - 0.2) / 15)^{0.5} \quad (3\text{-}2)$$

where f_{POA} values associated with OMI NO_2 values below 0.2 are assigned a value of 0. We reproduced the f_{POA} values from OMI NO_2 data using equation 3-2, compared these computations with the 47 AMS f_{POA}, and obtained a high correlation when the former was linearly regressed against the latter (r = 0.85, slope = 1.11, offset = −0.02, RMSE = 0.25, N = 47). The RMSE of 0.31 for a linear fit exceeds the RMSE of 0.25 for the non-linear fit. Therefore, equation 3-2 is a good approximation of the relation between the fractionation of ambient OA versus NO_2 concentrations over a broad geographic region.

3.3.4. GLOBAL OM/OC FROM SATELLITE-DERIVED AND MODELED NITROGEN OXIDES

Having predicted (equations 3-1 and 3-2) and evaluated the relation for AMS OM/OC versus AMS f_{POA} (Section 3.3.1), and AMS f_{POA} versus OMI NO_2 (Section 3.3.3), it is straightforward to derive seasonally varying maps of the global OM/OC ratio. Equations 3-1 and 3-2 leads to an empirical OM/OC prediction model as,

$$OM/OC = 2.1 - 0.8 \times ((OMI\ NO_2 - 0.2) / 15)^{0.5} \quad (3\text{-}3)$$

We use monthly mean OMI-derived ground-level NO_2 concentrations (ppb) for 2005–2008 (Bucsela et al., 2013) to produce a global climatology of the OM/OC ratio using equation 3-3. For $NO_2 < 0.2$, the OM/OC ratio is 2.1 (i.e. the POA term is set to zero, as indicated above) which is consistent with a ratio over regions characterized by weak primary emission. We imposed a lower limit of 1.3 to avoid unrealistic (f_{POA} exceeding 1) values for extremely high NO_2 conditions. A cross validation of the OMI-derived long-term monthly mean OM/OC product with the 47 AMS-derived OM/OC estimates (from AMS f_{POA} using equation 3-1) shows an RMSE of 0.06 μg/μgC ($r = 0.85$, slope = 1.11, offset = −0.21, $N = 47$).

Similarly, we create a prediction model from the GEOS-Chem NO_x concentrations,

$$OM/OC = 2.1 - 0.8 \times ((NO_x - 0.5) / 18)^{0.6} \quad (3\text{-}4)$$

The GEOS-Chem NO_x estimated OM/OC also has significant agreement ($r = 0.74$, slope = 1.08, offset = −0.15, RMSE = 0.08 μg/μgC) with the AMS data. Hence, model simulations of NO_x also can be used as a proxy for OM/OC.

3.4. DISCUSSION OF THE GLOBAL OM/OC RATIO

Figure 3-4 shows seasonal maps of the predicted OM/OC ratio based on the OMI-derived NO_2 concentration climatology. Maximum OM/OC ratios above 1.9 are found in regions with low NO_x emissions. Urban and industrial regions of the Northern Hemisphere tend to have lower OM/OC ratios. Fresh urban OA emission mainly from transportation leads to lower values for OM/OC in Eastern North America. The southeast U.S. with biogenic SOA production has high OM/OC values. Biomass burning regions have high predicted OM/OC ratios which are coincidently consistent with expectations; future work should extend this parameterization to explicitly represent the enhanced OM/OC from fires. Biases due to soil NO_x emissions are not apparent, due to the diffuse nature of the source. Annual mean values for urban (~1.5 μg/μgC) and rural (~2.0 μg/μgC) regions are broadly consistent with the values recommended by Turpin and Lim (2001). FTIR spectroscopy methods yield annual mean values of 1.9–2.0 μg/μgC over both Pittsburg (Polidori et al., 2008) and a rural site in Hungary (Kiss et al., 2002), which is close to our regional estimate of 1.8 μg/μgC.

The OM/OC ratio has a winter minimum and summer maximum over regions dominated by combustion emissions. The high summer OM/OC in this dataset reflects lower NO_x and f_{POA} in summer compared to winter. In general, high temperatures and sunlight in summer lead to high oxidant availability and enhanced photochemistry. The resulting oxidative aging and enhanced SOA formation increase the summertime OM/OC ratio compared to winter. The lower winter OM/OC is due to lower oxygen content in the aged OA. Simon et al. (2011) also find similar seasonality for the OM/OC ratio despite differences in magnitude. Xing et al. (2013) used chemical analysis of organic compounds extracted from $PM_{2.5}$ to find OM/OC ratios for 14 Chinese cities in summer of

1.75 ± 0.13 μg/μgC compared with our estimate of ~1.8 μg/μgC, and in winter of 1.59 ± 0.18 μg/μgC compared with our estimate of ~1.6 μg/μgC. Hence, we conclude that the global annual mean values for urban and rural regions, and its seasonal variation over urban regions are broadly consistent with the values recommended by several other studies.

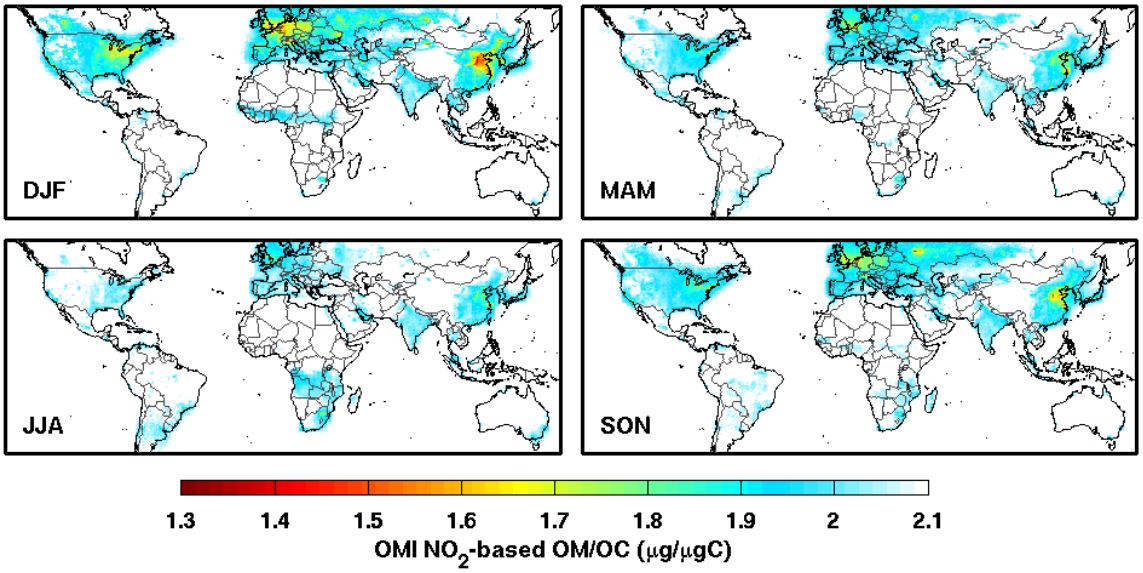

Figure 3-4: Seasonal OM/OC ratio estimated from the prediction model (equation 3-3) using the OMI-derived ground-level NO_2 concentration. Seasons are defined as December–January–February (DJF), March–April–May (MAM), June–July–August (JJA), and September–October–November (SON).

3.5 CONCLUSIONS

We developed a simple technique to estimate the spatial and seasonal variation of the global OM/OC ratio. OMI NO_2 observations were used to represent air mass age and scaled to AMS observations. The resultant dataset appears to generally represent the OM to OC ratio in most of the continental boundary layer. Underestimates are expected in biomass burning,

marine and free-tropospheric environments. Nonetheless the dataset should serve as an improvement over the commonly used global values for OM/OC. This work would benefit from more AMS measurements of the OM/OC ratio across multiple seasons and regions. Ongoing efforts to explicitly simulate oxidative aging of OA should ultimately yield a more complete representation of OM/OC.

3.6 ACKNOWLEDGEMENTS

This work was supported by NSERC. JLJ was supported by DOE (BER/ASR) DE SC0006035/DE-SC0006711/DE-FG02-11ER65293. QZ was supported by DE-FG02-11ER65293. We thank Aaron van Donkelaar and Ian Folkins for useful comments.

3.7 APPENDIX

The GEOS-Chem (version 9-01-03; http://geos-chem.org) is a global three-dimensional chemical transport model driven with assimilated meteorological data from the Goddard Earth Observing System (GEOS-5) at the NASA Global Modeling Assimilation Office (GMAO). We conduct our simulations at a spatial resolution of 2° × 2.5° for the years 2005–2008. The lowest layer of the model is approximately 130 m with a total of 47 levels from the Earth's surface to the top of the atmosphere. We use full mixing of species below the mixed layer depth, with a correction to the GEOS-5 predicted mixed layer depth (Heald et al., 2012; Walker et al., 2012). We use a timestep of 15 min for dynamical processes (transport and convection), and a timestep of 60 min for chemical processes and emissions.

GEOS-Chem contains a detailed simulation of HO_x–NO_x–VOC–ozone–aerosol chemistry (Bey et al., 2001; Park et al., 2004). Mao et al. (2010) describe the GEOS-Chem chemical

mechanism in detail. The simulation of secondary inorganic ions is directly coupled with gas phase chemistry (Park et al., 2004). Aerosol–gas interactions are simulated through heterogeneous chemistry (Jacob, 2000) with updated aerosol uptake of N_2O_5 (Evans and Jacob, 2005) and HO_2 (Thornton et al., 2008), aerosol extinction effects on photolysis rates (Martin et al., 2003b), the partitioning of aerosols from gas using the ISORROPIA II thermodynamic scheme (Fountoukis and Nenes, 2007) as implemented by Pye et al. (2009), and gas–aerosol partitioning of semivolatile products of VOC oxidation (Henze and Seinfeld, 2006; Henze et al., 2008; Liao et al., 2007).

Anthropogenic NO_x emission inventories are from the EDGAR v32-FT2000 global inventory for 2000 (Olivier et al., 2005), with regional overwrites over the U.S. (Environmental protection Agency-National Emissions Inventory 2005), Canada (CAC; http://www.ec.gc.ca/pdb/cac/), Mexico (BRAVO; Kuhns et al., 2005), Europe (EMEP; http://www.emep.int/), and East Asia (Zhang et al., 2009). Emissions are scaled to subsequent years on the basis of energy statistics (van Donkelaar et al., 2008) and after 2006 with OMI NO_2 data (Lamsal et al., 2011). Other major non-anthropogenic land NO_x emissions include biomass burning emissions (GFED-3; Mu et al., 2011) and soil emissions (Yienger and Levy, 1995; Wang et al., 1998).

CHAPTER 4: SENSITIVITY OF CHEMICAL TRANSPORT MODEL SIMULATIONS TO THE DURATION OF CHEMICAL AND TRANSPORT OPERATORS

4.1 ABSTRACT

Chemical transport models involve considerable computational expense. Fine temporal resolution offers accuracy at the expense of computation time. Assessment is needed of the sensitivity of simulation accuracy to the duration of chemical and transport operators. We conduct a series of simulations with the GEOS-Chem chemical transport model at different temporal and spatial resolutions to examine the sensitivity of simulated atmospheric composition to temporal resolution. Subsequently, we compare the tracers simulated with operator durations from 10 min to 60 min as typically used by global chemical transport models, and identify the timesteps that optimize both computational expense and simulation accuracy. We found that longer transport timesteps increase concentrations of emitted species such as nitrogen oxides and carbon monoxide since a more homogeneous distribution reduces loss though chemical reactions and dry deposition. The increased concentrations of ozone precursors increase ozone production at longer transport timesteps. Longer chemical timesteps decrease sulfate and ammonium but increase nitrate due to feedbacks with in-cloud sulfur dioxide oxidation and aerosol thermodynamics. The simulation duration decreases by an order of magnitude from fine (5 min) to coarse (60 min) temporal resolution. We assess the change in simulation accuracy with resolution by comparing the root mean square difference in ground-level concentrations of nitrogen oxides, ozone, carbon monoxide and secondary inorganic aerosols with a finer temporal or spatial resolution taken as truth. Simulation error for these species increases four times

from the shortest (5 min) to longest (60 min) temporal resolution. Chemical timesteps twice that of the transport timestep offer more simulation accuracy per unit computation. However, simulation error from coarser spatial resolution generally exceeds that from longer timesteps, e.g. degrading from 2^o x 2.5^o to 4^o x 5^o increases error by an order of magnitude. We recommend prioritizing fine spatial resolution before considering different temporal resolutions. We encourage the chemical transport model users to specify the durations of operators in publications due to its effect on simulation accuracy.

4.2 INTRODUCTION

Global and regional chemical transport models (CTMs) have a wide range of applications in studies of climate, air quality, and biogeochemical cycling. The last few decades have witnessed rapid development of modeling sophistication to tackle these issues, but that development is associated with increasing computational expense. Eulerian models divide the atmosphere into numerous (10^4-10^8) grid boxes and solve a mass continuity equation to simulate atmospheric composition. The concentrations of the simulated species are sensitive to the temporal resolution of the CTM. Attention is needed to understand how temporal resolution affects model performance.

Numerous studies have examined the sensitivity of simulations to grid resolution for ozone (Jang et al., 1995a; 1995b; Esler et al., 2004; Wild and Prather, 2006), ozone production efficiency (Liang and Jacobson 2000), and ozone sensitivity to precursor emissions (Cohan et al., 2006). Biases can be reduced by simulating sub grid scale processes such as emission plumes from point sources (Sillman et al., 1990; Gillani and Pleim, 1996), aircraft exhaust (Meijer et al., 1997; Kraabol et al., 2002), ship exhaust (Vinken et al., 2011), and lightning

(Cooper et al., 2014). Simulation error increases proportional to grid resolution (Wild and Prather, 2006; Prather et al., 2008). The spatiotemporal variation of tropospheric carbon monoxide is better represented with finer grid resolution (Wang et al., 2004; Chen et al., 2009; Yan et al., 2014). Moreover, fine horizontal resolution is important for air quality exposure assessment and health impact studies (Punger and West, 2013; Fountoukis et al., 2013; Thompson et al., 2014; Li et al., 2015). Fine vertical resolution can better represent convection (Rind et al., 2007; Arteta et al., 2009). Simulations are sensitive to temporal resolution (Mallet et al., 2007; Mallet and Sportisse, 2006), however, few studies have examined this sensitivity.

CTMs solve the continuity equation of around a hundred chemical species, each with number density n, for individual grid boxes defined in the Eulerian model.

$$\frac{\partial n}{\partial t} = -\nabla \cdot nU + P - L \tag{4.1}$$

$\partial n/\partial t$ represents the local temporal evolution of n. $-\nabla \cdot nU$ represents the transport flux divergence term, where U is the wind velocity vector. P and L are the local production and loss terms respectively. Typically, the above equation is discretized in space, and the continuity equation is simulated as a system of coupled non-linear partial differential equations with chemical and transport operators. These operators are usually simulated sequentially through operator splitting (McRae et al., 1982) which is found to increase computational efficiency (Kim and Cho, 1997). The transport operator involves solving the 3-D advection equation using efficient numerical schemes (Prather, 1986; Rood 1987). The Courant number C_r which relates the product of the wind speed u and the transport timestep T to the length of the grid box x,

$$C_r = \frac{u \times T}{x} \tag{4.2}$$

is kept less than unity for stability in advection schemes based on the Courant-Freidrich-Lewy criterion (Courant et al., 1967). Semi-Lagrangian numerical schemes (Lin and Rood, 1996) have been developed to accommodate higher C_r, and thereby allow coarser transport timesteps for faster computation. The chemical operator representing the temporal evolution of local sources and sinks involves numerically solving a system of coupled ordinary differential equations using efficient solvers (Hertel et al., 1993, Jacobson and Turco, 1994; Damian et al., 2002). For computational convenience, production and loss terms are also simulated as individual operators. The order in which operators are applied can affect performance (Sportisse, 2000; Santillana et al., 2016). The operator splitting method requires the coupling between individual operators to be negligible over each timestep. However, reducing timesteps increases computational expense. Attention is needed to accommodate this tradeoff.

We examine the sensitivity of a CTM to temporal resolution by conducting a series of simulations at different temporal and horizontal resolutions. We then identify the optimal temporal resolution for the range of timesteps, from 10 min to 60 min, usually used with global CTMs (e.g., Horowitz et al., 2003; Huijnen et al. 2010). Section 4.3 describes the sensitivity simulations, as well as the method to quantify the simulation error and to identify the optimal simulation timesteps. Comparison of the sensitivity simulations, description of resolution-dependent errors, and the identification of appropriate chemical and transport timesteps is examined in section 4.4.

4.3 MATERIALS AND METHODS

4.3.1 GEOS-CHEM SIMULATIONS

We conduct a series of sensitivity simulations with the GEOS-Chem CTM (version 10-01; www.geos-chem.org) at different temporal and horizontal resolutions to examine the individual sensitivities to chemical and transport timestep durations. The GEOS-Chem model (Bey et al., 2001) is used by about 100 research groups worldwide to simulate the oxidant-aerosol system. GEOS-Chem has the capability to be driven with several generations of assimilated meteorological data from the Goddard Earth Observing System (GEOS) at the NASA Global Modeling Assimilation Office (GMAO). For computational expedience, GEOS-Chem global simulations are often conducted using horizontal resolutions of either 4^o x 5^o or 2^o x 2.5^o degraded from the native resolution of GEOS meteorology. GEOS-Chem also has the capability to run nested regional simulations where the global model provides boundary condition to the regional grids (Wang et al., 2004; Chen et al., 2009; Zhang et al., 2011a; van Donkelaar et al., 2012). We use the GEOS-5 (or GEOS-5.2.0) meteorology available at a native horizontal resolution of 0.5^o x 0.667^o (Rienecker et al., 2008). It includes three-hour averaged 2-D fields like mixed layer depth, and six-hour averaged 3-D fields such as zonal and meridional wind and convective mass flux. The atmosphere is divided into 47 vertical levels with the lowest level being approximately 130 meters above sea level. GEOS-Chem performs tracer advection (A), vertical mixing (V), cloud convection (Z) and wet deposition (W) for every transport timestep (T), as well as dry deposition (D), emissions (E), and chemistry (G) for every chemical timestep (C) in the following order,

$$A(T) \cdot D(C) \cdot E(C) \cdot V(T) \cdot Z(T) \cdot G(C) \cdot W(T) \qquad (4.3)$$

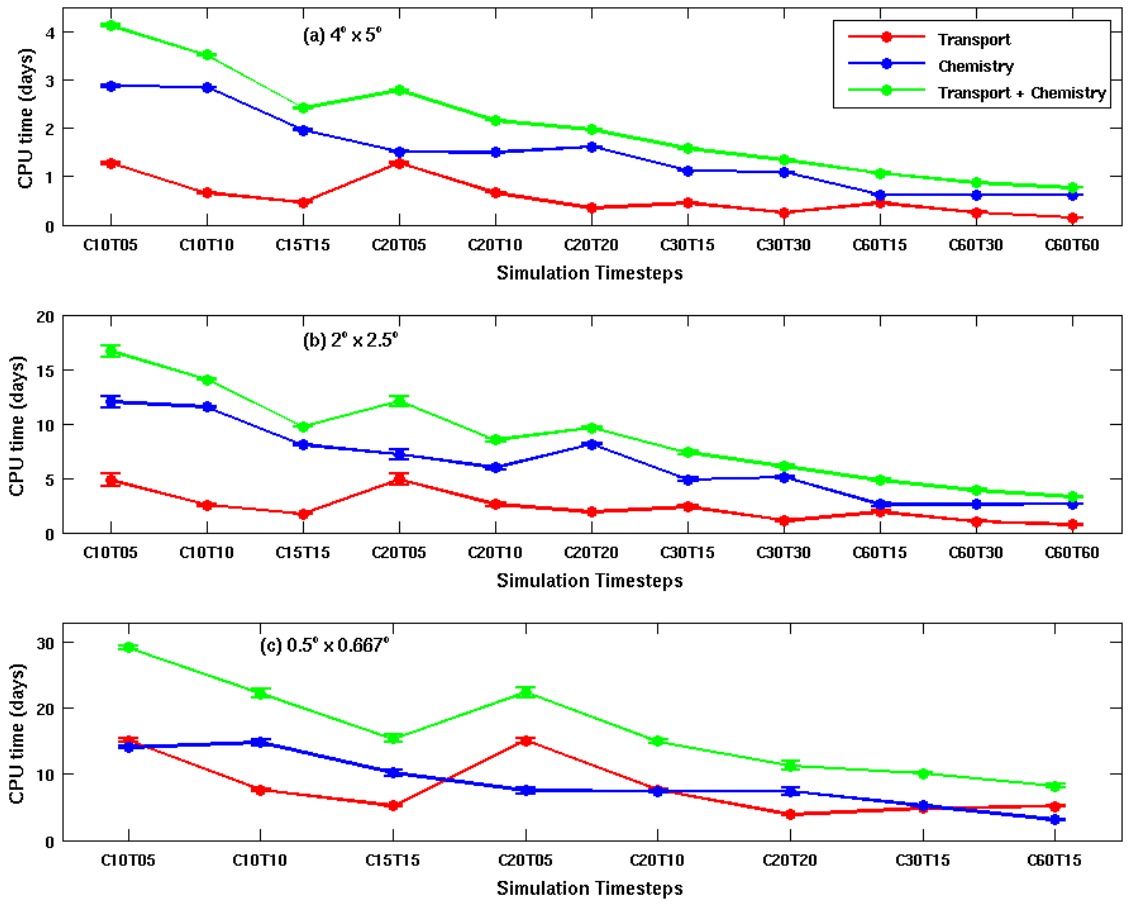

Figure 4-1: CPU time for GEOS-Chem simulations with various timesteps at three horizontal resolutions. Global simulations are at 4° x 5° (top) and 2° x 2.5° (middle) resolutions. The bottom panel contains results for the average of two nested regions North America and East Asia at 0.5° x 0.667° resolution. Colored lines represent the CPU time for simulating transport (red) and chemical (blue) operators, and the sum of the two (green). Error bars represent standard error of five simulations. Simulations are represented in the abscissa as CccTtt with chemical timestep, C = cc minutes, and transport timestep, T = tt minutes.

The traditional transport timesteps are 30 minutes for the 4^o x 5^o resolution, 15 minutes for the 2^o x 2.5^o resolution, 10 min for 0.5^o x 0.667^o resolution, and 5 min for 0.25^o x 0.312^o simulations. The traditional chemical timesteps have varied from either 60 min or twice the transport timestep based on the Strang operator splitting scheme (Strang, 1968) which follows $T \cdot C \cdot T \cdot T \cdot C \cdot T$ order repetitively with $C = 2 \times T$. We also test an alternate splitting scheme which follows $T \cdot C \cdot T \cdot C$ order repetitively with $C = T$.

Advection is based on the multi-dimensional flux-form semi-Lagrangian advection scheme (Lin and Rood, 1996; Lin et al., 1994), with an additional pressure-fixer algorithm implemented for the conservation of tracer mass (Rotman et al., 2004). Transport by convection is coupled (Balkanski et al., 1993; Wu et al., 2007) with gas-aerosol wet deposition (Liu et al., 2001; Wang et al., 2011; Amos et al., 2012). GEOS-Chem uses an internal timestep of 5 min for convective mixing. We use a non-local boundary layer mixing scheme for vertical transport (Holtslag and Boville, 1993, Lin et al., 2010).

Emissions are processed through the HEMCO module (Keller et al., 2014). A resistance-in-series method is used for dry deposition of species (Wesely 1989; Wang et al., 1998; Zhang et al., 2001; Fisher et al., 2011).

GEOS-Chem uses a Sparse Matrix Vectorized GEAR II chemistry solver (Jacobson and Turco, 1994; Jacobson, 1995; 1998). The oxidant-aerosol chemistry simulation includes organic and black carbon (Park et al., 2003), mineral dust (Fairlie et al., 2007), sea salt (Alexander et al., 2005; Jaegle et al., 2011), and the sulfate-nitrate-ammonium system (Park et al., 2004). The photolysis frequency is calculated (Mao et al., 2010) at the middle of the chemical timestep using the Fast-JX algorithm (Bian and Prather, 2002). Simulation

of gas-aerosol interactions are performed by aerosol extinction effects on photolysis rates (Martin et al., 2003b), and heterogeneous chemistry (Jacob, 2000) with aerosol uptake of N_2O_5 (Evans and Jacob, 2005) and HO_2 (Mao et al., 2013). The ISORROPIA II thermodynamic module (Fontoukis and Nenes, 2007) performs aerosol-gas partitioning (Pye et al., 2009).

We conduct simulations for 2010 July at two horizontal resolutions of 4^o x 5^o and 2^o x 2.5^o globally, and 0.5^o x 0.667^o over North America (140^oW–40^oW, 10^oN–70^oN) and East Asia (70^oW–150^oW, 11^oS–55^oN) nested regions. We use the 4^o x 5^o global simulation to archive dynamic boundary conditions every three hours for the nested models. We use one month spin up with each GEOS-Chem simulation to reduce the influence of initial conditions.

4.3.2 COMPUTING PLATFORM

We conduct all simulations on the same computing platform to compare their computational performance. We use the Glooscap cluster of the Atlantic Computational Excellence Network (ACENET) Consortium of Canadian Universities (http://www.ace-net.ca/wiki/Glooscap). The operating system is Linux 4.8. We use Intel Fortran compiler version 12. Each GEOS-Chem simulation is submitted as a 16-thread parallelized job on a single node.

We calculate the CPU time for the month of July for each operator separately using the Fortran-intrinsic routine, CPU_TIME. We found this value identical to the one calculated using the Linux command ‘qacct –j’. We noticed that CPU time can be affected by other jobs on the shared cluster. Therefore, we repeat simulations five times, while excluding

data output operations to minimize sensitivity to system input/output, and use the median to represent CPU time for each simulation.

4.3.3 ASSESSING SIMULATION ERROR

Assessing simulation error versus timestep through comparison with observations is impaired by imperfect model processes, by the sparseness of measurements, and by model-observation representativeness biases. Therefore, we treat the simulation with the finest temporal resolution as the most accurate. We take as 'Truth' the concentrations simulated with a chemical timestep (C) of 10 minutes and a transport time step (T) of 5 minutes (represented as C10T05). Finer resolutions are computationally prohibitive. We define the simulation error E^s_{sim} for species *s* as the root mean squared error of the species concentrations simulated with the finest resolution (*Truth*) and the simulation under consideration (*Sim*), normalized by the concentrations in simulation '*Truth*',

$$E^s_{sim} = \frac{\sqrt{\sum_{i=1}^{i=N} (Truth_i^s - Sim_i^s)^2}}{\sum_{i=1}^{i=N} Truth_i^s} \tag{4.4}$$

where, *i* represents a particular grid box, with a total number of *N* grid boxes of interest. The root mean squared error in the numerator is chosen instead of absolute difference to more heavily penalize extrema. Normalization with the total mass concentration value of the true simulation is intended to cross-compare E^s_{sim} of different species. E^s_{sim} captures the variation of a species *s* from the true simulation.

Here, we focus on four key species relevant to atmospheric chemistry, namely nitrogen oxides (NO_x = NO + NO_2), ozone (O_3), carbon monoxide (CO), and secondary inorganic

aerosols (SIA: sum of sulfate, nitrate and ammonium). These species represent a range of lifetimes from a day (NO_x) to weeks (CO). The focus on SIA is designed to devote more attention to chemically active species than to mineral dust and sea salt. We sample the instantaneous values of simulated ground-level concentrations of these atmospheric species every 60 min to span the diurnal variation of chemical environments. We focus on concentrations in July near the Earth's surface when and where chemical and transport timescales tend to be short.

4.3.4 IDENTIFYING THE OPTIMAL TEMPORAL RESOLUTION

A practical way to select optimal chemical and transport timesteps is to identify the simulation with the lowest error (E^s_{sim}) per unit of computation time. To quantify the simulation accuracy per unit CPU time, we propose a simple metric, the normalized error (*NE*) which which is a quantitative indicator of the tradeoff between the simulation accuracy, and the associated computation expense. This dual mandate of the NE is accomplished by normalizing the simulation error E^s_{sim} for species *s* by the ratio of CPU time for the simulation under consideration (t_{sim}) to the CPU time of the reference simulation (t_{ref}), and taking the mean of four species.

$$NE = \left(\frac{1}{4} \times \sum_s \frac{E^s_{sim}}{E^s_{ref}} \right) \times \left(\frac{t_{sim}}{t_{ref}} \right) \tag{4.5}$$

The time normalization rewards or penalizes CPU times that are less than or greater than the reference CPU time. We normalize E^s_{sim} by the reference E^s_{ref} so that the normalized error for each species is of similar magnitude. The variation of NE across timesteps is

unaffected by the choice of reference simulation; C10T10 is used here. The simulation with the lowest NE can be employed as an indicator of optimal chemical and transport resolution.

4.4 RESULTS AND DISCUSSION

Figure 4-1 shows the computational performance for the series of GEOS-Chem simulations conducted here. The CPU time decreases four times from fine to coarse temporal resolution. The CPU time increases by about a factor of 4 from 4^o x 5^o to 2^o x 2.5^o and another factor of 2 to a single nested simulation at 0.5^o x 0.667^o. Comparison of individual CPU times for chemical and transport operators shows that performing all the chemical operations takes ~4 times that of performing all the transport operations, at the global scale. This factor is reduced for nested simulations due to the additional CPU time for simulating boundary conditions.

Figure 4-2 illustrates the sensitivity of the simulations to chemical and transport operators at 2^o x 2.5^o horizontal resolution. The left columns show the tracer concentrations for the 'true' simulation (C10T05). The middle column shows the difference in tracer concentrations from doubling the transport timestep duration. Increasing the transport timestep tends to increase concentrations of emitted species like CO and NO_x over source regions since tracers are more uniformly mixed by long timesteps before loss processes such as deposition and chemistry occur. More homogeneous fields have lower dry deposition and chemical loss rates. The increase in CO decreases OH over source regions. Increasing concentrations of ozone precursors increases ozone production (P $[O_3]$). Wild and Prather (2006) similarly found that ozone production increases at coarser horizontal

resolution. Increasing the transport timestep duration increases SIA components, especially over the source regions of East Asia, North India, and North America (Figure 4-3).

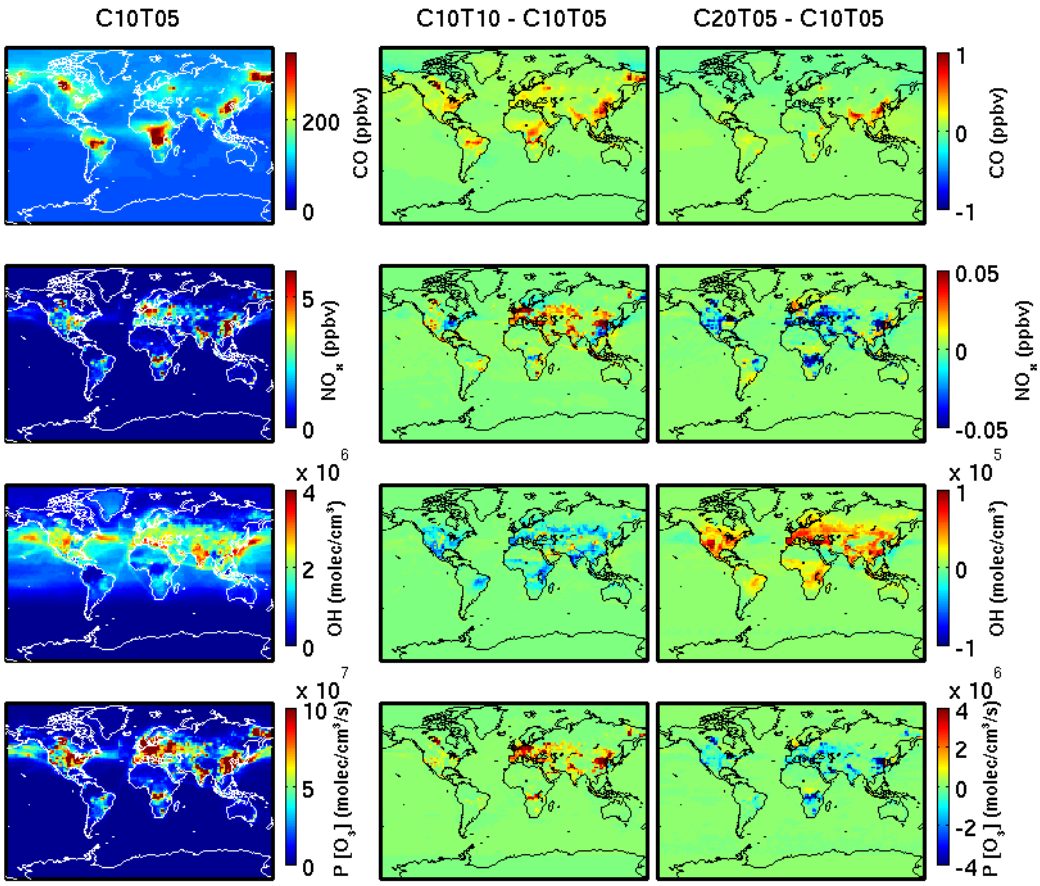

Figure 4-2: Sensitivity of simulated tracers to the duration of chemical and transport operators. The left column contains monthly mean ground-level concentrations simulated with the finest timesteps considered (C10T05) at 2º x 2.5º horizontal resolution. Other columns contain the absolute differences from doubling the transport timestep to C10T10 (middle), and doubling the chemical timestep to C20T05 (right). Each row from top to bottom represents carbon monoxide (CO), nitrogen oxides (NO_x), hydroxyl radical (OH), and the production of ozone (P[O3]). Simulations are represented as CccTtt with chemical timestep, C = cc minutes, and transport timestep, T = tt minutes.

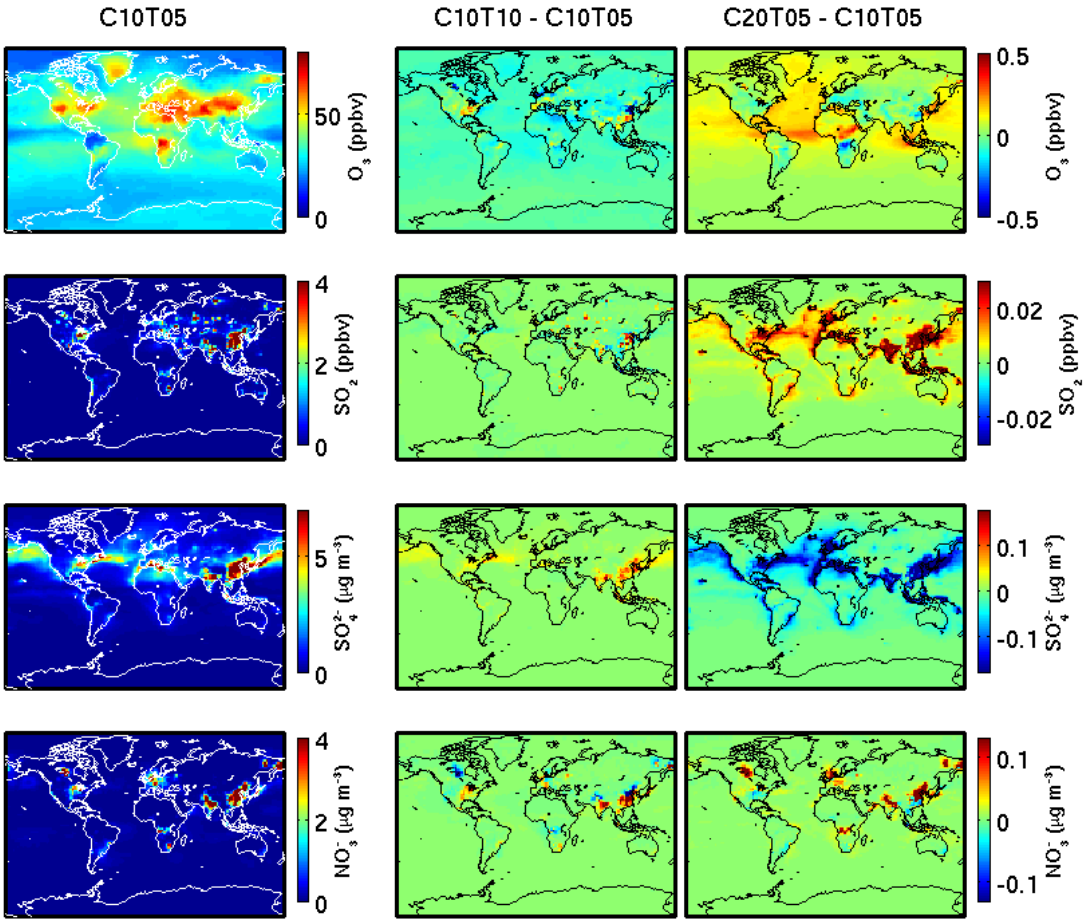

Figure 4-3: As described in Figure 4-2, but each row from top to bottom represents ozone (O_3), sulfur dioxide (SO_2), sulfate (SO_4^{2-}), and nitrate (NO_3^-) respectively.

The right columns in Figure 4-2 and 4-3 show the change in tracer concentrations from increasing the chemical timestep. Hydroxyl radical concentrations increase, NO_x concentrations largely decrease, and P [O_3] decreases with increasing chemical timesteps over source regions. Berntsen and Isaken (1997) found that the error introduced by coarser chemical timesteps is higher in polluted regions than the clean background. This is due to

the increased time lag and invariant production and loss across rapid chemical cycles.

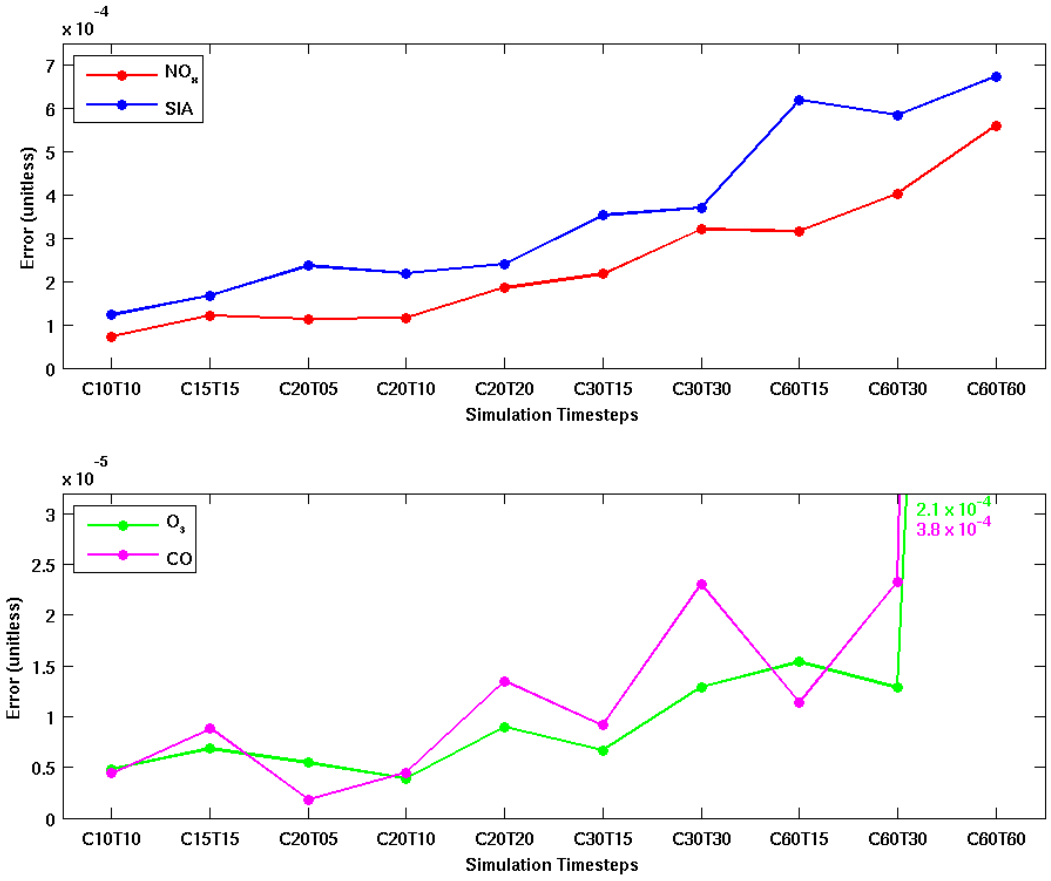

Figure 4-4: Simulation error of different species (E^{s}_{sim} , equation 4-4) for GEOS-Chem with various timesteps at 2° x 2.5° horizontal resolution. Colored lines and dots represent the simulation error for nitrogen oxides (NO_x; red), secondary inorganic aerosols (SIA; blue), ozone (O_3; green), and carbon monoxide (CO; magenta). Simulations are represented in the abscissa as CccTtt with chemical timestep, C = cc minutes, and transport timestep, T = tt minutes.

A longer chemical timestep decreases sulfate and ammonium but increases nitrate over source regions. Inspection of SO_2 and H_2O_2 fields indicates that sulfate formation through

H_2O_2 in clouds decreases at longer chemical timesteps. In turn, SO_2 and NH_3 concentrations increase at longer chemical timesteps due to the corresponding decreases in ammonium sulfate or ammonium bisulfate. The additional free ammonia at longer chemical timesteps tends to promote regional ammonium nitrate formation (Figure 4-3) depending on local thermodynamics. An increase of total SIA mass with the increasing chemical timestep is driven by nitrate and ammonium, and partially compensated by a reduction in sulfate, especially downwind of source regions. We found similar spatial patterns for other timestep combinations, and other horizontal resolutions.

Figures 4-4 shows the simulation error for nitrogen oxides, ozone, carbon monoxide and secondary inorganic aerosols with varying temporal resolution at 2^o x 2.5^o horizontal resolution. Simulation errors for all these major species increase by more than a factor of 5 from the shortest to longest temporal resolution. Errors increase fairly smoothly until the transport timestep exceeds 30 min. The large corresponding Courant numbers are associated with errors that increase errors by an order of magnitude for long lived species such as O_3 and CO. Simulation errors for other horizontal resolutions follows a similar pattern.

Figure 4-5 shows the difference in simulated tracers at 2^o x 2.5^o horizontal resolution for the GEOS-Chem traditional (C30T15) minus the finest timesteps considered (C10T05). The spatial variation for the monthly mean ground-level concentrations is generally within 5-15% for short lived species like NO_x and SIA, and within 1% for longer lived species like O_3 and CO. Santillana et al. (2016) similarly found an upper limit of 10% for operator splitting errors. However, the maximum hourly spatial variation can exceed 50% for short

lived species and 5% for the longer lived species. The spatial pattern of extrema resembles that of the monthly mean, albeit with more heterogeneity from synoptic variation.

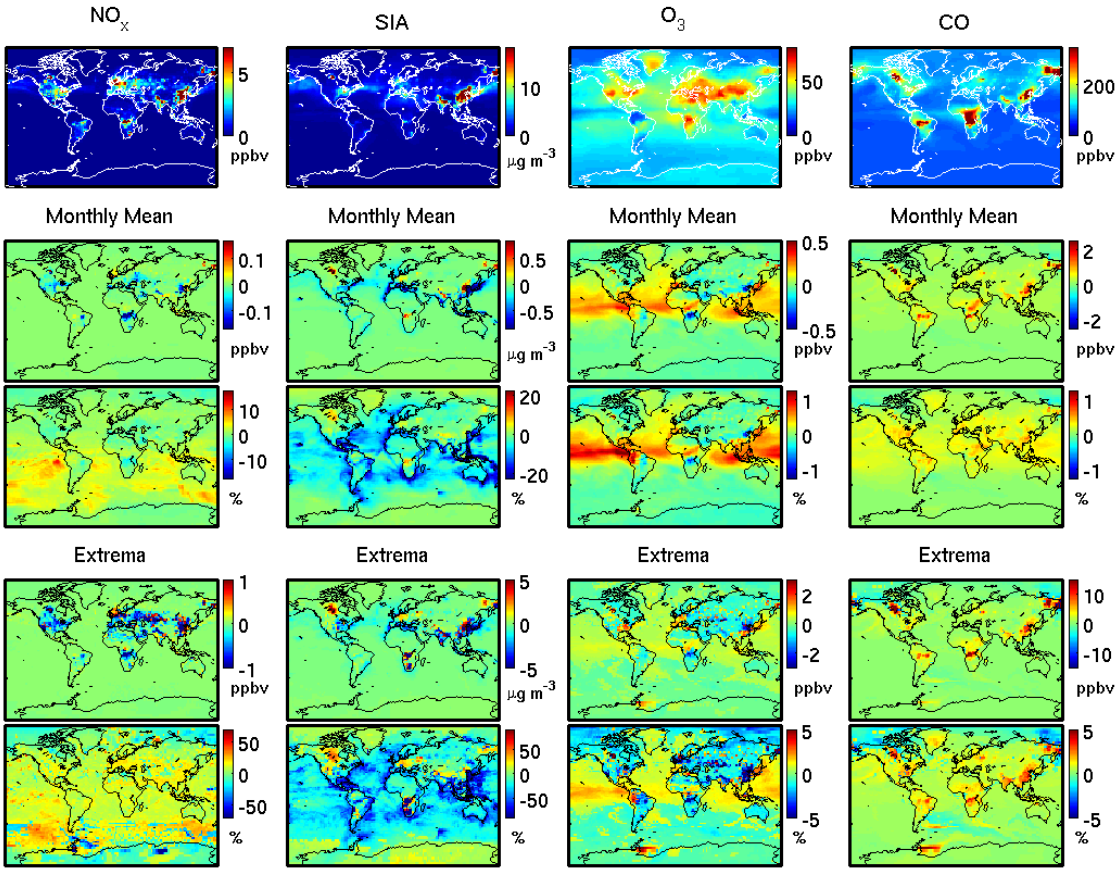

Figure 4-5: Effect on simulated tracers of changing from the GEOS-Chem traditional timesteps (C30T15) to the finest timesteps considered (C10T05). The top row contains ground-level concentrations simulated with the C30T15 timesteps at 2^{o} x 2.5^{o} horizontal resolution. The next two rows contain the monthly mean differences (C30T15 minus C10T05) for absolute (second row) and relative (third row) differences. The two lowest rows contain the maximum differences (C30T15 minus C10T05) for absolute (fourth row) and relative (bottom row) differences. Each column from left to right represents nitrogen oxides (NO_x), secondary inorganic aerosols (SIA), ozone (O_3), and carbon monoxide (CO).

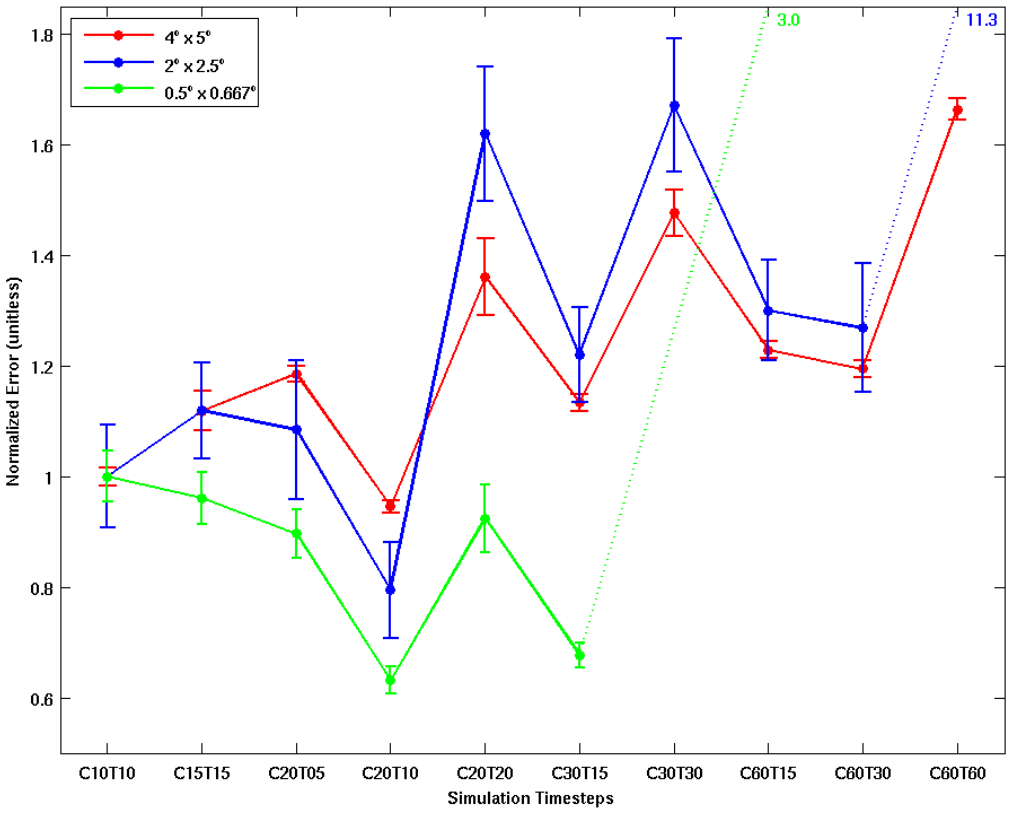

Figure 4-6: Normalized error (NE, equation 4-5) for GEOS-Chem simulations with various spatial and temporal resolutions. Colored lines and dots represent the NE for the global simulations at 4^o x 5^o (red) and 2^o x 2.5^o (blue), and the nested simulations at 0.5^o x 0.667^o (green) horizontal resolutions. Error bars represent standard error in CPU time. Simulations are represented in the abscissa as CccTtt with chemical timestep, C = cc minutes, and transport timestep, T = tt minutes.

We also examined the diurnal variation and vertical profile of extrema. Extrema arise at all times of the day with a slight tendency for larger values for NO_x at night, for ozone near sunrise and sunset, and for SIA and CO near noon. Zonal mean vertical profiles exhibit the largest differences in the lower troposphere for NO_x and SIA, with more homogeneous

differences throughout the troposphere for O_3 and CO. Near the subtropical jets of the upper troposphere O_3 and CO have maximum extrema of up to 3%.

Table 4-1: Mean Error* versus grid resolution with truth at 2^o x 2.5^o horizontal resolution

Species	Simulation Error (1 x 10^{-4})	
	4^o x 5^o resolution	2^o x 2.5^o resolution
Nitrogen Oxides	38.04	1.64
Secondary Inorganic Aerosols	3.06	0.07
Ozone	6.45	0.09
Carbon monoxide	18.47	2.44

* Mean taken for timesteps ≤ 30 min.

Figures 4-6 shows the normalized error for the GEOS-Chem simulations at various spatial and temporal resolutions. The NE is noticeably higher with C = T than C = 2 x T. We confirmed this tendency with different choices of truth (such as C05T05, C10T10, instead of C10T05) or reference (C10T05, instead of C10T10) simulations. This finding supports the traditional approach of using C = 2 x T in prior GEOS-Chem simulations. Applying the chemical operator as frequently as the transport operator (with C = T) appears to increase computation cost with little benefit in accuracy. The NE for all three horizontal resolutions has a minima with a chemical timestep of 20 min and a transport timestep of 10 min (C20T10). A unit of computation time has a similar efficiency for a small range of timesteps from 10 min to 20 min. We found similar patterns in the variation of NE with timesteps with NE calculated for selected domains, such as over Northern Hemisphere, nested model regions, land grid boxes, and over the entire troposphere. We conducted

additional simulations at 4° x 5° horizontal resolution for January 2011 with a spin up of 7 months, and found similar patterns in NE.

The simulation error decreases by 40-50% (Figure 4-4) by changing the resolution from the traditional (C30T15) to the optimal (C20T10) at 2° x 2.5° horizontal resolution. The relative spatial variations are <10% for NO_x and SIA, and <1% for O_3 and CO. However, the CPU time increases by 20% as the result of the increase in temporal resolution.

Table 4-1 shows the simulation error for the 4° x 5° horizontal resolution with truth at 2° x 2.5° resolution (C10T05) to further investigate the tradeoff between temporal and horizontal resolution. The simulation error for all species at 4° x 5° resolution increases by an order of magnitude compared to 2° x 2.5° resolution for any choice of timestep tested here. The error in this configuration is dominated by representativeness differences between 4° x 5° and is insensitive to timestep. Numerical errors due to advection processes generally exceed those from operator splitting (e.g., Prather et al., 2008; Santillana et al., 2016). Thus CTM users could consider the finest spatial resolution available, and subsequently the optimal temporal resolution. We therefore recommend prioritizing horizontal resolution over temporal resolution. The optimal temporal resolution is insensitive to horizontal resolution. We encourage the CTM users to specify the durations of operators in publications due to its effect on simulation accuracy.

4.5 CONCLUSIONS

The computational expense of chemical transport models warrants investigation into their efficiency and accuracy. Solving the continuity equation in CTMs through the operator splitting method offers numerical efficiency, however, few studies have examined the

implications of operator duration on simulation accuracy. We conducted simulations with the GEOS-Chem model for multiple choices of timestep duration from 10 min to 60 min as typically used by global CTMs. We found that longer transport timesteps increase ozone precursors and ozone production over source regions since a more homogeneous distribution reduces loss though chemical reactions and dry deposition. Longer chemical timesteps decrease NO_x and ozone production over source regions. Longer chemical timesteps reduce sulfate and ammonium concentrations while increasing nitrate concentrations due to feedbacks with in-cloud SO_2 oxidation and local aerosol thermodynamics.

We investigated the computational efficiency with the GEOS-Chem model, and found that the simulation duration decreases by an order of magnitude from fine (C10T05) to coarse (C60T60) temporal resolution. The chemical operator consumes about four times the CPU time of the transport operator. We subsequently compared the root mean square differences in the ground-level concentrations of nitrogen oxides, ozone, carbon monoxide and secondary inorganic aerosols with a finer temporal or spatial resolution taken as truth, and estimated the simulation error. Simulation error for these species increases by more than a factor of 5 from the shortest to longest temporal resolution.

In order to account for the tradeoff between simulation accuracy and computational cost, we proposed a metric, normalized error, which quantifies performance in terms of the coupling of temporal resolution and simulation error. In general, we recommend the approach of using C = 2 x T for all horizontal resolutions. The normalized error exhibits a minimum for a chemical timestep of 20 min and transport timestep of 10 min. Nonetheless,

the simulation error from changing spatial resolution exceeds that from changing temporal resolution. We recommend choosing the finest possible spatial resolution before considering different temporal resolutions. We encourage the CTM users to specify the durations of operators in publications due to its effect on simulation accuracy.

4.6 ACKNOWLEDGEMENTS

This work was supported by NSERC and ACENET. We thank Colette Heald, Daniel Jacob and Patrick Kim for useful comments at the early stages of this research.

CHAPTER 5: CONCLUSION

We developed a first estimate of the long-term population exposure to all major $PM_{2.5}$ (particulate matter with aerodynamic diameter less than 2.5 μm) chemical components and emission sectors throughout the world. We inferred global long-term (2004-2008) mean ambient outdoor satellite-model chemical components and sources of $PM_{2.5}$ at a spatial resolution of 0.1^o x 0.1^o from satellite-derived aerosol optical depth observations and chemical transport model simulations. We evaluated the $PM_{2.5}$ chemical component dataset with in situ measurements across North America, and where available in the rest of the world, and found significant agreement.

We found that major contributors to global population-weighted $PM_{2.5}$ concentrations were particulate organic mass (11.9 ± 7.3 μg/m3), secondary inorganic aerosol (11.1 ± 5.0 $\mu g/m^3$), and mineral dust (11.1 ± 7.9 $\mu g/m^3$). Secondary inorganic aerosols were high in East Asia (28 $\mu g/m^3$) and South Asia (11 $\mu g/m^3$), as was particulate organic mass in both South Asia and East Asia (22 $\mu g/m^3$), and mineral dust concentrations in West Africa, North Africa, Middle East, and Central Asia (>20 $\mu g/m^3$).

We found that fossil fuel combustion (17 $\mu g/m^3$), biofuel combustion (11 $\mu g/m^3$) and biomass burning (1.3 $\mu g/m^3$) were the major emission sectors to the population-weighted $PM_{2.5}$. On a regional scale, fossil fuel combustion over East Asia (46 $\mu g/m^3$), biofuel combustion over South Asia (24 $\mu g/m^3$) and East Asia (20 $\mu g/m^3$), and biomass burning over Central Africa (14 $\mu g/m^3$) were noteworthy. Population-weighted $PM_{2.5}$ from biofuel combustion was comparable to that from fossil fuel combustion in South Asia.

These estimates of chemical components and sources of $PM_{2.5}$ offer information about global population exposure and health impacts of $PM_{2.5}$. Crouse et al. (submitted) associated these composition estimates with a Canadian mortality cohort, and found that including $PM_{2.5}$ composition into the model could improve mortality predictions.

We developed a first estimate of the spatially and seasonally resolved global, lower tropospheric, ratio between organic mass (OM) and organic carbon (OC). We first developed a parameterization for the OM/OC ratio using the primary organic aerosol (POA) fraction of total OM estimated globally from Aerosol Mass Spectrometer (AMS) measurements, and evaluated it with high quality AMS data. We explored the ability of ground-level NO_2 concentrations derived from the satellite-borne Ozone Monitoring Instrument to serve as a proxy for fresh emissions that have a high POA fraction, and applied NO_2 data to derive ambient POA fraction. We developed an estimate of OM/OC from the combination of these two methods.

The global OM/OC ratio ranged from 1.3 to 2.1 μg/μgC, with distinct spatial variation between urban and rural regions. The seasonal OM/OC ratio had a summer maximum and a winter minimum over regions dominated by combustion emissions. This dataset serves as an improvement over the commonly used global values for OM/OC, and it represents the OM/OC in most of the continental boundary layer, except for biomass burning, marine and free tropospheric environments.

This global OMI-derived OM/OC dataset can be used to interpret in situ organic carbon measurements (e.g., Attwood et al., 2014). The parameterization developed in this paper

(Philip et al. 2014a) can be included into models for estimating OM/OC online, using simulated NO_x concentrations (e.g., Xu et al., 2015).

In the final section of this thesis, we examined the sensitivity of chemical transport model simulations to temporal resolution. We found that increasing the transport operator timestep increases the concentrations of emitted species such as NO_x and CO since a more homogeneous spatial distribution reduces loss though chemical reactions and dry deposition. The increased concentration of these ozone precursors increases ozone production at longer transport timesteps. Increasing the chemical operator timestep decreases sulfate and ammonium but increases nitrate due to feedbacks with in-cloud SO_2 oxidation and aerosol thermodynamics.

We found that simulation time decreased four times from fine (5 min) to coarse (60 min) temporal resolution, while simulation error increased by more than a factor of 5. The simulation error from reducing spatial resolution exceeded that from reducing temporal resolution. For accurate simulations with respect to computational expense, we recommended a chemical timestep twice that of transport timestep. A chemical timestep of 20 min and transport timestep of 10 min offered the highest accuracy per computational cost for the 4^o x 5^o, 2^o x 2.5^o, and 0.5^o x 0.667^o horizontal resolutions.

There are multiple future directions possible to improve the estimates of global ground-level air quality. Future developments in satellite remote sensing, and in the modeling of aerosol composition such as organic mass are needed to improve the estimates of $PM_{2.5}$ components. Assimilation of satellite observations of trace gases into a chemical transport models could provide constraints on $PM_{2.5}$ composition. Explicitly simulating the oxidative

aging of organic aerosols should ultimately yield a more complete representation of the ratio of organic mass to organic carbon. Satellite and chemical transport model simulations at finer spatial resolutions would better resolve intraurban gradients in $PM_{2.5}$. The computational burden for the chemical operator can be reduced with the development of numerical methods, from the use of efficient algorithms and solvers to adjusting the chemical scheme locally (e.g., Rastigejev et al., 2007; Santillana et al., 2010).

REFERENCES

Aiken, A. C., Decarlo, P. F., Kroll, J. H., Worsnop, D. R., Huffman, J. A., Docherty, K. S., Ulbrich, I. M., Mohr, C., Kimmel, J. R., Sueper, D., Sun, Y., Zhang, Q., Trimborn, A., Northway, M., Ziemann, P. J., Canagaratna, M. R., Onasch, T. B., Alfarra, M. R., Prevot, A. S. H., Dommen, J., Duplissy, J., Metzger, A., Baltensperger, U. and Jimenez, J. L.: O/C and OM/OC ratios of primary, secondary, and ambient organic aerosols with high-resolution time-of-flight aerosol mass spectrometry, Environ. Sci. Technol., 42, 4478-4485, doi:10.1021/es703009q, 2008.

Alexander, B., Park, R. J., Jacob, D. J., Li, Q. B., Yantosca, R. M., Savarino, J., Lee, C. C. W. and Thiemens, M. H.: Sulfate formation in sea-salt aerosols: Constraints from oxygen isotopes, J. Geophys. Res., 110, D10307, doi:10.1029/2004JD005659, 2005.

Allen, G., Sioutas, C., Koutrakis, P., Reiss, R., Lurmann, F. W. and Roberts, P. T.: Evaluation of the TEOM method for measurement of ambient particulate mass in urban areas., J. Air Waste Manag. Assoc., 47, 682-9, doi:10.1080/10473289.1997.10463923, 1997.

Al Saadi, J., Szykman, J., Pierce, R. B., Kittaka, C., Neil, D., Chu, D. A., Remer, L., Gumley, L., Prins, E., Weinstock, L., MacDonald, C., Wayland, R., Dimmick, F. and Fishman, J.: Improving national air quality forecasts with satellite aerosol observations, Bull. Am. Meteorol. Soc., 86, 1249-1261, doi:10.1175/BAMS-86-9-1249, 2005.

Amos, H. M., Jacob, D. J., Holmes, C. D., Fisher, J. A., Wang, Q., Yantosca, R. M., Corbitt, E. S., Galarneau, E., Rutter, A. P., Gustin, M. S., Steffen, A., Schauer, J. J., Graydon, J. A., St Louis, V. L., Talbot, R. W., Edgerton, E. S., Zhang, Y. and Sunderland, E. M.: Gas-particle partitioning of atmospheric Hg(II) and its effect on global mercury deposition, Atmos. Chem. Phys., 12, 591-603, doi:10.5194/acp-12-591-2012, 2012.

Andreae, M. O. and Crutzen, P. J.: Atmospheric aerosols: Biogeochemical sources and role in atmospheric chemistry, Science, 276, 1052-1058, doi:10.1126/science.276.5315.1052, 1997.

Anenberg, S. C., Talgo, K., Arunachalam, S., Dolwick, P., Jang, C. and West, J. J.: Impacts of global, regional, and sectoral black carbon emission reductions on surface air quality and human mortality, Atmos. Chem. Phys., 11, 7253-7267, doi:10.5194/acp-11-7253-2011, 2011.

Arteta, J., Marecal, V. and Riviere, E. D.: Regional modelling of tracer transport by tropical convection – Part 2: Sensitivity to model resolutions, Atmos. Chem. Phys., 9, 7101-7114, doi:10.5194/acp-9-7101-2009, 2009.

Attwood, A. R., Washenfelder, R. A., Brock, C. A., Hu, W., Baumann, K., Campuzano-Jost, P., Day, D. A., Edgerton, E. S., Murphy, D. M., Palm, B. B., McComiskey, A., Wagner, N. L., de Sá, S. S., Ortega, A., Martin, S. T., Jimenez, J. L. and Brown, S. S.: Trends in sulfate and organic aerosol mass in the Southeast U.S.: Impact on aerosol optical depth and radiative forcing, Geophys. Res. Lett., 41, 7701-7709, doi:10.1002/2014GL061669, 2014.

Balakrishnan, K., Ghosh, S., Ganguli, B., Sambandam, S., Bruce, N., Barnes, D. and Smith, K.: State and national household concentrations of $PM_{2.5}$ from solid cookfuel use: Results from measurements and modeling in India for estimation of the global burden of disease, Environ. Health, 12, 77, doi:10.1186/1476-069X-12-77, 2013.

Balkanski, Y. J., Jacob, D. J., Gardner, G. M., Graustein, W. C. and Turekian, K. K.: Transport and residence times of tropospheric aerosols inferred from a global three-dimensional simulation of ^{210}Pb, J. Geophys. Res., 98, 20573-20586, doi:10.1029/93JD02456, 1993.

Bell, M., Dominici, F., Ebisu, K., Zeger, S. and Samet, J.: Spatial and temporal variation in $PM_{2.5}$ chemical composition in the United States for health effects studies, Environ. Health Perspec., 115, 989-995, doi:10.1289/ehp.9621, 2007.

Bell, M., Ebisu, K., Peng, R., Samet, J. and Dominici, F.: Hospital admissions and chemical composition of fine particle air pollution, Am. J. Respir. Crit. Care Med., 179, 1115-1120, doi:10.1164/rccm.200808-1240OC, 2009.

Bell, M. L. and HEI Health Review Committee: Assessment of the health impacts of particulate matter characteristics, Res. Rep. Health Eff. Inst., 5-38, 2012.

Berntsen, T. K. and Isaksen, I. S. A.: A global three-dimensional chemical transport model for the troposphere: 1. Model description and CO and ozone results, J. Geophys. Res., 102, 21239-21280, doi:10.1029/97JD01140, 1997.

Bey, I., Jacob, D. J., Yantosca, R. M., Logan, J. A., Field, B. D., Fiore, A. M., Li, Q. B., Liu, H. G. Y., Mickley, L. J. and Schultz, M. G.: Global modeling of tropospheric chemistry with assimilated meteorology: Model description and evaluation, J. Geophys. Res., 106(D19), 23073–23095, doi:10.1029/2001JD000807, 2001.

Bian, H. and Prather, M. J.: Fast-J2: Accurate simulation of stratospheric photolysis in global chemical models, J. Atmos. Chem., 41, 281-296, doi:10.1023/A:1014980619462, 2002.

Boersma, K. F., Eskes, H. J., Dirksen, R. J., van der A, R. J., Veefkind, J. P., Stammes, P., Huijnen, V., Kleipool, Q. L., Sneep, M., Claas, J., Leitão, J., Richter, A., Zhou, Y. and Brunner, D.: An improved tropospheric NO_2 column retrieval algorithm for the Ozone Monitoring Instrument, Atmos. Meas. Tech., 4, 1905-1928, doi:10.5194/amt-4-1905-2011, 2011.

Bond, T., Bhardwaj, E., Dong, R., Jogani, R., Jung, S., Roden, C., Streets, D. and Trautmann, N.: Historical emissions of black and organic carbon aerosol from energy-related combustion, 1850-2000, Global Biogeochem. Cy., 21, GB2018, doi:10.1029/2006GB002840, 2007.

Bouwman, A. F., Lee, D. S., Asman, W. A. H., Dentener, F. J., VanderHoek, K. W. and Olivier, J. G. J.: A global high-resolution emission inventory for ammonia, Global Biogeochem. Cy., 11, 561-587, doi:10.1029/97GB02266, 1997.

Brauer, M., Amann, M., Burnett, R., Cohen, A., Dentener, F., Ezzati, M., Henderson, S., Krzyzanowski, M., Martin, R., Van Dingenen, R., van Donkelaar, A. and Thurston, G.: Exposure assessment for estimation of the global burden of disease attributable to outdoor air pollution, Environ. Sci. Technol., 46, 652-660, doi:10.1021/es2025752, 2012.

Brook, R. D., Rajagopalan, S., Pope, C. A.,III, Brook, J. R., Bhatnagar, A., Diez-Roux, A. V., Holguin, F., Hong, Y., Luepker, R. V., Mittleman, M. A., Peters, A., Siscovick, D., Smith, S. C.,Jr., Whitsel, L., Kaufman, J. D., Amer Heart Assoc Council Epidemiol, Council Kidney Cardiovasc Dis and Council Nutr Phys Activity Metab: Particulate matter air pollution and cardiovascular disease: An update to the scientific statement from the American Heart Association, Circulation, 121, 2331-2378, doi:10.1161/CIR.0b013e3181dbece1, 2010.

Brown, K., Bouhamra, W., Lamoureux, D., Evans, J. and Koutrakis, P.: Characterization of particulate matter for three sites in Kuwait, J. Air Waste Manag. Assoc., 58, 994-1003, doi:10.3155/1047-3289.58.8.994, 2008.

Bucsela, E. J., Krotkov, N. A., Celarier, E. A., Lamsal, L. N., Swartz, W. H., Bhartia, P. K., Boersma, K. F., Veefkind, J. P., Gleason, J. F. and Pickering, K. E.: A new stratospheric and tropospheric NO_2 retrieval algorithm for nadir-viewing satellite instruments: applications to OMI, Atmos. Meas. Tech., 6, 2607-2626, doi:10.5194/amt-6-2607-2013, 2013.

Burnett, R. T., Brook, J., Dann, T., Delocla, C., Philips, O., Cakmak, S., Vincent, R., Goldberg, M. S. and Krewski, D.: Association between particulate- and gas-phase components of urban air pollution and daily mortality in eight Canadian cities, Inhal. Toxicol., 12:sup4, 15-39, doi:10.1080/08958370050164851, 2000.

Canagaratna, M. R., Jayne, J. T., Jimenez, J. L., Allan, J. D., Alfarra, M. R., Zhang, Q., Onasch, T. B., Drewnick, F., Coe, H., Middlebrook, A., Delia, A., Williams, L. R., Trimborn, A. M., Northway, M. J., DeCarlo, P. F., Kolb, C. E., Davidovits, P. and Worsnop, D. R.: Chemical and microphysical characterization of ambient aerosols with the aerodyne aerosol mass spectrometer, Mass Spectrom. Rev., 26, 185-222, doi:10.1002/mas.20115, 2007.

Cao, J. J., Lee, S. C., Chow, J. C., Watson, J. G., Ho, K. F., Zhang, R. J., Jin, Z. D., Shen, Z. X., Chen, G. C., Kang, Y. M., Zou, S. C., Zhang, L. Z., Qi, S. H., Dai, M. H., Cheng, Y. and Hu, K.: Spatial and seasonal distributions of carbonaceous aerosols over China, J. Geophys. Res., 112, D22S11, doi:10.1029/2006JD008205, 2007.

Cao, J., Xu, H., Xu, Q., Chen, B. and Kan, H.: Fine particulate matter constituents and cardiopulmonary mortality in a heavily polluted Chinese city, Environ. Health Perspec., 120, 373-378, doi:10.1289/ehp.1103671, 2012.

Chen, D., Wang, Y., McElroy, M. B., He, K., Yantosca, R. M. and Le Sager, P.: Regional CO pollution and export in China simulated by the high-resolution nested-grid GEOS-Chem model, Atmos. Chem. Phys., 9, 3825-3839, doi:10.5194/acp-9-3825-2009, 2009.

Chowdhury, M.: Characterization of fine particle air pollution in the Indian subcontinent, PhD thesis, Georgia Institute of Technology, 2004.

Clarisse, L., Clerbaux, C., Dentener, F., Hurtmans, D. and Coheur, P.: Global ammonia distribution derived from infrared satellite observations, Nature Geosci., 2, 479-483, doi:10.1038/ngeo551, 2009.

Cohan, D. S., Hu, Y. and Russell, A. G.: Dependence of ozone sensitivity analysis on grid resolution, Atmos. Environ., 40, 126-135, doi:10.1016/j.atmosenv.2005.09.031, 2006.

Cooke, W. F., Liousse, C., Cachier, H. and Feichter, J.: Construction of a 1° × 1° fossil fuel emission data set for carbonaceous aerosol and implementation and radiative impact in the ECHAM4 model, J. Geophys. Res., 104, 22137-22162, doi:10.1029/1999JD900187, 1999.

Cooper, M., Martin, R. V., Wespes, C., Coheur, P., Clerbaux, C. and Murray, L. T.: Tropospheric nitric acid columns from the IASI satellite instrument interpreted with a chemical transport model: Implications for parameterizations of nitric oxide production by lightning, J. Geophys. Res., 119, 10068-10079, doi:10.1002/2014JD021907, 2014.

Courant, R., Friedrichs, K. and Lewy, H.: On partial difference equations of mathematical physics, IBM J. Res. Dev., 11, 215-234, doi:10.1147/rd.112.0215, 1967.

Crouse, D. L., Philip, S., van Donkelaar, A., Martin, R. V., Jessiman, B., Peters, P. A., Weichenthal, S., Brook, J. R., Hubbell, B. and Burnett, R. T.: A new method to jointly estimate the mortality risk of long-term exposure to fine particulate matter and its components, Submitted.

Dabek-Zlotorzynska, E., Dann, T. F., Kalyani Martinelango, P., Celo, V., Brook, J. R., Mathieu, D., Ding, L. and Austin, C. C.: Canadian National Air Pollution Surveillance (NAPS) $PM_{2.5}$ speciation program: Methodology and $PM_{2.5}$ chemical composition for the years 2003–2008, Atmos. Environ., 45, 673-686, doi:10.1016/j.atmosenv.2010.10.024, 2011.

Damian, V., Sandu, M., Damian M., Potra, F. and Carmichael G. R.: The kinetic preprocessor KPP-a software environment for solving chemical kinetics, Comput. Chem. Eng., 26, 1567-1579, doi:10.1016/S0098-1354(02)00128-X, 2002.

DeCarlo, P. F., Ulbrich, I. M., Crounse, J., de Foy, B., Dunlea, E. J., Aiken, A. C., Knapp, D., Weinheimer, A. J., Campos, T., Wennberg, P. O. and Jimenez, J. L.: Investigation of the sources and processing of organic aerosol over the Central Mexican Plateau from aircraft measurements during MILAGRO, Atmos. Chem. Phys., 10, 5257-5280, doi:10.5194/acp-10-5257-2010, 2010.

Docherty, K. S., Aiken, A. C., Huffman, J. A., Ulbrich, I. M., DeCarlo, P. F., Sueper, D., Worsnop, D. R., Snyder, D. C., Peltier, R. E., Weber, R. J., Grover, B. D., Eatough, D. J., Williams, B. J., Goldstein, A. H., Ziemann, P. J. and Jimenez, J. L.: The 2005 Study of Organic Aerosols at Riverside (SOAR-1): instrumental intercomparisons and fine particle composition, Atmos. Chem. Phys., 11, 12387-12420, doi:10.5194/acp-11-12387-2011, 2011.

Dockery, D. W., Pope, C. A., Xu, X., Spengler, J. D., Ware, J. H., Fay, M. E., Ferris, B. G. and Speizer, F. E.: An association between air pollution and mortality in six U.S. cities, N. Engl. J. Med., 329, 1753-1759, doi:10.1056/NEJM199312093292401, 1993.

Drury, E., Jacob, D. J., Spurr, R. J. D., Wang, J., Shinozuka, Y., Anderson, B. E., Clarke, A. D., Dibb, J., McNaughton, C. and Weber, R.: Synthesis of satellite (MODIS), aircraft (ICARTT), and surface (IMPROVE, EPA-AQS, AERONET) aerosol observations over eastern North America to improve MODIS aerosol retrievals and constrain surface aerosol concentrations and sources, J. Geophys. Res., 115, D14204, doi:10.1029/2009JD012629, 2010.

El-Zanan, H. S., Lowenthal, D. H., Zielinska, B., Chow, J. C. and Kumar, N.: Determination of the organic aerosol mass to organic carbon ratio in IMPROVE samples, Chemosphere, 60, 485-496, doi:10.1016/j.chemosphere.2005.01.005, 2005.

Engel Cox, J., Holloman, C., Coutant, B. and Hoff, R.: Qualitative and quantitative evaluation of MODIS satellite sensor data for regional and urban scale air quality, Atmos. Environ., 38, 2495-2509, doi:10.1016/j.atmosenv.2004.01.039, 2004.

Esler, J. G., Roelofs, G. J., Kohler, M. O. and O'Connor, F. M.: A quantitative analysis of grid-related systematic errors in oxidising capacity and ozone production rates in chemistry transport models, Atmos. Chem. Phys., 4, 1781-1795, doi:10.5194/acp-4-1781-2004, 2004.

Evans, M. J. and Jacob, D. J.: Impact of new laboratory studies of N_2O_5 hydrolysis on global model budgets of tropospheric nitrogen oxides, ozone, and OH, Geophys. Res. Lett., 32, L09813, doi:10.1029/2005GL022469, 2005.

Fairlie, T. D., Duncan Fairlie, T., Jacob, D. J. and Park, R. J.: The impact of transpacific transport of mineral dust in the United States, Atmos. Environ., 41, 1251-1266, doi:10.1016/j.atmosenv.2006.09.048, 2007.

Fiore, A. M., Dentener, F. J., Wild, O., Cuvelier, C., Schultz, M. G., Hess, P., Textor, C., Schulz, M., Doherty, R. M., Horowitz, L. W., MacKenzie, I. A., Sanderson, M. G., Shindell, D. T., Stevenson, D. S., Szopa, S., Van Dingenen, R., Zeng, G., Atherton, C., Bergmann, D., Bey, I., Carmichael, G., Collins, W. J., Duncan, B. N., Faluvegi, G., Folberth, G., Gauss, M., Gong, S., Hauglustaine, D., Holloway, T., Isaksen, I. S. A., Jacob, D. J., Jonson, J. E., Kaminski, J. W., Keating, T. J., Lupu, A., Marmer, E., Montanaro, V., Park, R. J., Pitari, G., Pringle, K. J., Pyle, J. A., Schroeder, S., Vivanco, M. G., Wind, P., Wojcik, G., Wu, S. and Zuber, A.: Multimodel estimates of intercontinental source-receptor relationships for ozone pollution, J. Geophys. Res., 114, D04301, 10.1029/2008JD010816, 2009.

Fisher, J. A., Jacob, D. J., Wang, Q., Bahreini, R., Carouge, C. C., Cubison, M. J., Dibb, J. E., Diehl, T., Jimenez, J. L., Leibensperger, E. M., Lu, Z., Meinders, M. B. J., Pye, H. O. T., Quinn, P. K., Sharma, S., Streets, D. G., van Donkelaar, A. and Yantosca, R. M.: Sources, distribution, and acidity of sulfate-ammonium aerosol in the Arctic in winter-spring, Atmos. Environ., 45, 7301-7318, doi:10.1016/j.atmosenv.2011.08.030, 2011.

Ford, B. and Heald, C. L.: An A-train and model perspective on the vertical distribution of aerosols and CO in the Northern Hemisphere, J. Geophys. Res., 117, D06211, doi:10.1029/2011JD016977, 2012.

Fountoukis, C., Koraj, D., Denier van der Gon, H.A.C., Charalampidis, P. E., Pilinis, C. and Pandis, S. N.: Impact of grid resolution on the predicted fine PM by a regional 3-D chemical transport model, Atmos. Environ., 68, 24-32, doi:10.1016/j.atmosenv.2012.11.008, 2013.

Fountoukis, C. and Nenes, A.: ISORROPIA II: a computationally efficient thermodynamic equilibrium model for K^+-Ca^{2+}-Mg^{2+}-NH_4^+-Na^+-SO_4^{2-}-NO_3^--Cl^--H_2O aerosols, Atmos. Chem. Phys., 7, 4639-4659, doi:10.5194/acp-7-4639-2007, 2007.

Fu, T.-M., Cao, J. J., Zhang, X. Y., Lee, S. C., Zhang, Q., Han, Y. M., Qu, W. J., Han, Z., Zhang, R., Wang, Y. X., Chen, D. and Henze, D. K.: Carbonaceous aerosols in China: top-down constraints on primary sources and estimation of secondary contribution, Atmos. Chem. Phys., 12, 2725-2746, doi:10.5194/acp-12-2725-2012, 2012.

Fu, T.-M., Jacob, D. J., Wittrock, F., Burrows, J. P., Vrekoussis, M. and Henze, D. K.: Global budgets of atmospheric glyoxal and methylglyoxal, and implications for formation of secondary organic aerosols, J. Geophys. Res., 113, D15303, doi:10.1029/2007JD009505, 2008.

Ge, X., Setyan, A., Sun, Y. and Zhang, Q.: Primary and secondary organic aerosols in Fresno, California during wintertime: Results from high resolution aerosol mass spectrometry, J. Geophys. Res., 117, D19301, doi:10.1029/2012JD018026, 2012.

Gillani, N. V. and Pleim, J. E.: Sub-grid-scale features of anthropogenic emissions of NO_x and VOC in the context of regional Eulerian models, Atmos. Environ., 30, 2043-2059, doi:10.1016/1352-2310(95)00201-4, 1996.

Goldstein, A. H., Koven, C. D., Heald, C. L. and Fung, I. Y.: Biogenic carbon and anthropogenic pollutants combine to form a cooling haze over the southeastern United States, Proc. Natl. Acad. Sci. U. S. A., 106, 8835-8840, doi:10.1073/pnas.0904128106, 2009.

Grosjean, D. and Friedlander, S. K.: Gas-particle distribution factors for organic and other pollutants in Los-Angeles atmosphere, J. Air Pollut. Control Assoc., 25, 1038-1044, doi:10.1080/00022470.1975.10470176, 1975.

Han, Y. M., Han, Z. W., Cao, J. J., Chow, J. C., Watson, J. G., An, Z. S., Liu, S. X. and Zhang, R. J.: Distribution and origin of carbonaceous aerosol over a rural high-mountain lake area, Northern China and its transport significance, Atmos. Environ., 42, 2405-2414, doi:10.1016/j.atmosenv.2007.12.020, 2008.

Hand J. L., Copeland, S. A., Day, D. E., Dillner, A. M., Indresand, H., Malm, W. C., McDade, C. E., Moore, C. T., Pitchford, M. L., Schichtel, B. A. and Watson, J. G.: IMPROVE (Interagency Monitoring of Protected Visual Environments): Spatial and seasonal patterns and temporal variability of haze and its constituents in the United States, Rep. V, Coop. Inst. For Res. In the Atmos., Fort Collins, Colorado, 2011.

Hand, J. L., Schichtel, B. A., Pitchford, M. L., Malm, W. C. and Frank, N. H.: Seasonal composition of remote and urban fine particulate matter in the United States, J. Geophys. Res., 117, D05209, doi:10.1029/2011JD017122, 2012.

Hansen, J. and Travis, L.: Light scattering in planetary atmospheres, Space Science Reviews, 16, 527-610, doi:10.1007/BF00168069, 1974.

Heald, C. L., Collett Jr., J. L., Lee, T., Benedict, K. B., Schwandner, F. M., Li, Y., Clarisse, L., Hurtmans, D. R., Van Damme, M., Clerbaux, C., Coheur, P.-F., Philip, S., Martin, R. V. and Pye, H. O. T.: Atmospheric ammonia and particulate inorganic nitrogen over the United States, Atmos. Chem. Phys., 12, 10295-10312, doi:10.5194/acp-12-10295-2012, 2012.

Heald, C. L., Coe, H., Jimenez, J. L., Weber, R. J., Bahreini, R., Middlebrook, A. M., Russell, L. M., Jolleys, M., Fu, T. -., Allan, J. D., Bower, K. N., Capes, G., Crosier, J., Morgan, W. T., Robinson, N. H., Williams, P. I., Cubison, M. J., DeCarlo, P. F. and Dunlea, E. J.: Exploring the vertical profile of atmospheric organic aerosol: comparing 17 aircraft field campaigns with a global model, Atmos. Chem. Phys., 11, 12673-12696, doi:10.5194/acp-11-12673-2011, 2011.

Health Effects Institute: Understanding the health effects of components of the particulate matter mix: Progress and next steps, Perspectives 2, Health Effects Institute, Boston, MA, 2004.

Henze, D. K. and Seinfeld, J. H.: Global secondary organic aerosol from isoprene oxidation, Geophys. Res. Lett., 33, L09812, doi:10.1029/2006GL025976, 2006.

Henze, D. K., Seinfeld, J. H., Ng, N. L., Kroll, J. H., Fu, T.-M., Jacob, D. J. and Heald, C. L.: Global modeling of secondary organic aerosol formation from aromatic hydrocarbons: high- vs. low-yield pathways, Atmos. Chem. Phys., 8, 2405-2420, doi:10.5194/acp-8-2405-2008, 2008.

Hertel, O., Berkowicz, R., Christensen, J. and Hov, Ø.: Test of two numerical schemes for use in atmospheric transport-chemistry models, Atmos. Environ., 27, 2591-2611, doi:10.1016/0960-1686(93)90032-T, 1993.

Hoff, R. M. and Christopher, S. A.: Remote sensing of particulate pollution from space: Have we reached the promised land?, J. Air Waste Manag. Assoc., 59, 645-675, doi:10.3155/1047-3289.59.6.645, 2009.

Hoppel, W. A., Frick, G. M. and Larson, R. E.: Effect of nonprecipitating clouds on the aerosol size distribution in the marine boundary layer, Geophys. Res. Lett., 13, 125-128, doi:10.1029/GL013i002p00125, 1986.

Holben, B. N., Eck, T. F., Slutsker, I., Tanre, D., Buis, J. P., Setzer, A., Vermote, E., Reagan, J. A., Kaufman, Y. J., Nakajima, T., Lavenu, F., Jankowiak, I. and Smirnov, A.: AERONET - A federated instrument network and data archive for aerosol characterization, Remote Sens. Environ., 66, 1-16, doi:10.1016/S0034-4257(98)00031-5, 1998.

Holtslag, A. A. M. and Boville, B. A.: Local versus nonlocal boundary-layer diffusion in a global climate model, J. Clim., 6, 1825-1842, doi:10.1175/1520-0442(1993)006<1825:LVNBLD>2.0.CO;2, 1993.

Hopke, P. K., Cohen, D. D., Begum, B. A., Biswas, S. K., Ni, B., Pandit, G. G., Santoso, M., Chung, Y., Davy, P., Markwitz, A., Waheed, S., Siddique, N., Santos, F. L., Pabroa, P. C. B., Seneviratne, M. C. S., Wimolwattanapun, W., Bunprapob, S., Vuong, T. B., Duy Hien, P. and Markowicz, A.: Urban air quality in the Asian region, Sci. Total Environ., 404, 103-112, doi:10.1016/j.scitotenv.2008.05.039, 2008.

Horowitz, L. W., Walters, S., Mauzerall, D. L., Emmons, L. K., Rasch, P. J., Granier, C., Tie, X., Lamarque, J., Schultz, M. G., Tyndall, G. S., Orlando, J. J. and Brasseur, G. P.: A global simulation of tropospheric ozone and related tracers: Description and evaluation of MOZART, version 2, J. Geophys. Res., 108(D24), 4784, doi:10.1029/2002JD002853, 2003.

Huang, K., Zhuang, G., Lin, Y., Fu, J. S., Wang, Q., Liu, T., Zhang, R., Jiang, Y., Deng, C., Fu, Q., Hsu, N. C. and Cao, B.: Typical types and formation mechanisms of haze in an Eastern Asia megacity, Shanghai, Atmos. Chem. Phys., 12, 105-124, doi:10.5194/acp-12-105-2012, 2012a.

Huang, X. -., He, L. -., Hu, M., Canagaratna, M. R., Kroll, J. H., Ng, N. L., Zhang, Y. -., Lin, Y., Xue, L., Sun, T. -., Liu, X. -., Shao, M., Jayne, J. T. and Worsnop, D. R.: Characterization of submicron aerosols at a rural site in Pearl River Delta of China using an Aerodyne High-Resolution Aerosol Mass Spectrometer, Atmos. Chem. Phys., 11, 1865-1877, doi:10.5194/acp-11-1865-2011, 2011.

Huang, X. -., He, L. -., Hu, M., Canagaratna, M. R., Sun, Y., Zhang, Q., Zhu, T., Xue, L., Zeng, L. -., Liu, X. -., Zhang, Y. -., Jayne, J. T., Ng, N. L. and Worsnop, D. R.: Highly time-resolved chemical characterization of atmospheric submicron particles during 2008 Beijing Olympic Games using an Aerodyne High-Resolution Aerosol Mass Spectrometer, Atmos. Chem. Phys., 10, 8933-8945, doi:10.5194/acp-10-8933-2010, 2010.

Huang, X., Song, Y., Li, M., Li, J., Huo, Q., Cai, X., Zhu, T., Hu, M. and Zhang, H.: A high-resolution ammonia emission inventory in China, Global Biogeochem. Cy., 26, GB1030, doi:10.1029/2011GB004161, 2012b.

Hudman, R. C., Jacob, D. J., Turquety, S., Leibensperger, E. M., Murray, L. T., Wu, S., Gilliland, A. B., Avery, M., Bertram, T. H., Brune, W., Cohen, R. C., Dibb, J. E., Flocke, F. M., Fried, A., Holloway, J., Neuman, J. A., Orville, R., Perring, A., Ren, X., Sachse, G. W., Singh, H. B., Swanson, A. and Wooldridge, P. J.: Surface and lightning sources of nitrogen oxides over the United States: Magnitudes, chemical evolution, and outflow, J. Geophys. Res., 112, D12S05, doi:10.1029/2006JD007912, 2007.

Huijnen, V., Williams, J., van Weele, M., van Noije, T., Krol, M., Dentener, F., Segers, A., Houweling, S., Peters, W., de Laat, J., Boersma, F., Bergamaschi, P., van Velthoven, P., Le Sager, P., Eskes, H., Alkemade, F., Scheele, R., Nédélec, P. and Pätz, H. -.: The global chemistry transport model TM5: description and evaluation of the tropospheric chemistry version 3.0, Geosci. Model Dev., 3, 445-473, doi:10.5194/gmd-3-445-2010, 2010.

Hyer, E. J., Reid, J. S. and Zhang, J.: An over-land aerosol optical depth data set for data assimilation by filtering, correction, and aggregation of MODIS Collection 5 optical depth retrievals, Atmos. Meas. Tech., 4, 379-408, doi:10.5194/amt-4-379-2011, 2011.

IPCC: Climate Change 2013: The Physical Science Basis. Contribution of Working Group I to the Fifth Assessment Report of the Intergovernmental Panel on Climate Change [Stocker, T.F., D. Qin, G.-K. Plattner, M. Tignor, S.K. Allen, J. Boschung, A. Nauels, Y. Xia, V. Bex and P.M. Midgley (eds.)], Cambridge University Press, Cambridge, United Kingdom and New York, NY, USA, 1535 pp., 2013.

Ito, K., Mathes, R., Ross, Z., Nadas, A., Thurston, G. and Matte, T.: Fine particulate matter constituents associated with cardiovascular hospitalizations and mortality in New York City, Environ. Health Perspec., 119, 467-473, doi:10.1289/ehp.1002667, 2011.

Jacob, D. J.: Heterogeneous chemistry and tropospheric ozone, Atmos. Environ., 34, 2131-2159, doi:10.1016/S1352-2310(99)00462-8, 2000.

Jacobson, M. Z.: Improvement of SMVGEAR II on vector and scalar machines through absolute error tolerance control, Atmos. Environ., 32, 791-796, doi:10.1016/S1352-2310(97)00315-4, 1998.

Jacobson, M. Z.: Computation of global photochemistry with SMVGEAR II, Atmos. Environ., 29, 2541-2546, doi:10.1016/1352-2310(95)00194-4, 1995.

Jacobson, M. and Turco, R. P.: SMVGEAR - A SPARSE-MATRIX, VECTORIZED GEAR CODE FOR ATMOSPHERIC MODELS, Atmos. Environ., 28, 273-284, doi:10.1016/1352-2310(94)90102-3, 1994.

Jaegle, L., Quinn, P. K., Bates, T. S., Alexander, B. and Lin, J.: Global distribution of sea salt aerosols: new constraints from in situ and remote sensing observations, Atmos. Chem. Phys., 11, 3137-3157, doi:10.5194/acp-11-3137-2011, 2011.

Jang, J. C., Jeffries, H. E. and Tonnesen, S.: Sensitivity of ozone to model grid resolution — II. Detailed process analysis for ozone chemistry, Atmos. Environ., 29, 3101-3114, doi:10.1016/1352-2310(95)00119-J, 1995a.

Jang, J. C., Jeffries, H. E., Byun, D. and Pleim, J. E.: Sensitivity of ozone to model grid resolution — I. Application of high-resolution regional acid deposition model, Atmos. Environ., 29, 3085-3100, doi:10.1016/1352-2310(95)00118-I, 1995b.

Jimenez, J. L., Canagaratna, M. R., Donahue, N. M., Prevot, A. S. H., Zhang, Q., Kroll, J. H., DeCarlo, P. F., Allan, J. D., Coe, H., Ng, N. L., Aiken, A. C., Docherty, K. S., Ulbrich, I. M., Grieshop, A. P., Robinson, A. L., Duplissy, J., Smith, J. D., Wilson, K. R., Lanz, V. A., Hueglin, C., Sun, Y. L., Tian, J., Laaksonen, A., Raatikainen, T., Rautiainen, J., Vaattovaara, P., Ehn, M., Kulmala, M., Tomlinson, J. M., Collins, D. R., Cubison, M. J., Dunlea, E. J., Huffman, J. A., Onasch, T. B., Alfarra, M. R., Williams, P. I., Bower, K., Kondo, Y., Schneider, J., Drewnick, F., Borrmann, S., Weimer, S., Demerjian, K., Salcedo, D., Cottrell, L., Griffin, R., Takami, A., Miyoshi, T., Hatakeyama, S., Shimono, A., Sun, J. Y., Zhang, Y. M., Dzepina, K., Kimmel, J. R., Sueper, D., Jayne, J. T., Herndon, S. C., Trimborn, A. M., Williams, L. R., Wood, E. C., Middlebrook, A. M., Kolb, C. E., Baltensperger, U. and Worsnop, D. R.: Evolution of organic aerosols in the atmosphere, Science, 326, 1525-1529, doi:10.1126/science.1180353, 2009.

Jimenez, J. L., Jayne, J. T., Shi, Q., Kolb, C. E., Worsnop, D. R., Yourshaw, I., Seinfeld, J. H., Flagan, R. C., Zhang, X., Smith, K. A., Morris, J. W. and Davidovits, P.: Ambient aerosol sampling using the Aerodyne Aerosol Mass Spectrometer, J. Geophys. Res., 108(D7), 8425, doi:10.1029/2001JD001213, 2003.

Kahn, R. A., Li, W. -., Moroney, C., Diner, D. J., Martonchik, J. V. and Fishbein, E.: Aerosol source plume physical characteristics from space-based multiangle imaging, J. Geophys. Res., 112, D11205, doi:10.1029/2006JD007647, 2007.

Kanakidou, M., Seinfeld, J. H., Pandis, S. N., Barnes, I., Dentener, F. J., Facchini, M. C., Van Dingenen, R., Ervens, B., Nenes, A., Nielsen, C. J., Swietlicki, E., Putaud, J. P., Balkanski, Y., Fuzzi, S., Horth, J., Moortgat, G. K., Winterhalter, R., Myhre, C. E. L., Tsigaridis, K., Vignati, E., Stephanou, E. G. and Wilson, J.: Organic aerosol and global climate modelling: a review, Atmos. Chem. Phys., 5, 1053-1123, doi:10.5194/acp-5-1053-2005, 2005.

Keller, C. A., Long, M. S., Yantosca, R. M., Da Silva, A. M., Pawson, S. and Jacob, D. J.: HEMCO v1.0: a versatile, ESMF-compliant component for calculating emissions in atmospheric models, Geosci. Model Dev., 7, 1409-1417, doi:10.5194/gmd-7-1409-2014, 2014.

Kharol, S. K., Martin, R. V., Philip, S., Vogel, S., Henze, D. K., Chen, D., Wang, Y., Zhang, Q. and Heald, C. L.: Persistent sensitivity of Asian aerosol to emissions of nitrogen oxides, Geophys. Res. Lett., 40, 1021-1026, doi:10.1002/grl.50234, 2013.

Kim, J. and Cho, S. Y.: Computation accuracy and efficiency of the time-splitting method in solving atmospheric transport/chemistry equations, Atmos. Environ., 31, 2215-2224, doi:10.1016/S1352-2310(97)88636-0, 1997.

Kim, P. S., Jacob, D. J., Fisher, J. A., Travis, K., Yu, K., Zhu, L., Yantosca, R. M., Sulprizio, M. P., Jimenez, J. L., Campuzano-Jost, P., Froyd, K. D., Liao, J., Hair, J. W., Fenn, M. A., Butler, C. F., Wagner, N. L., Gordon, T. D., Welti, A., Wennberg, P. O., Crounse, J. D., St. Clair, J. M., Teng, A. P., Millet, D. B., Schwarz, J. P., Markovic, M. Z., and Perring, A. E.: Sources, seasonality, and trends of Southeast US aerosol: an integrated analysis of surface, aircraft, and satellite observations with the GEOS-Chem chemical transport model, Atmos. Chem. Phys. Discuss., 15, 17651-17709, doi:10.5194/acpd-15-17651-2015, 2015.

Kim, S., Peel, J. L., Hannigan, M. P., Dutton, S. J., Sheppard, L., Clark, M. L. and Vedal, S.: The temporal lag structure of short-term associations of fine particulate matter chemical constituents and cardiovascular and respiratory hospitalizations, Environ. Health Perspec., 120, 1094-1099, doi:10.1289/ehp.1104721, 2012.

Kiss, G., Varga, B., Galambos, I. and Ganszky, I.: Characterization of water-soluble organic matter isolated from atmospheric fine aerosol, J. Geophys. Res., 107(D21), 8339, doi:10.1029/2001JD000603, 2002.

Kloog, I., Koutrakis, P., Coull, B. A., Lee, H. J. and Schwartz, J.: Assessing temporally and spatially resolved $PM_{2.5}$ exposures for epidemiological studies using satellite aerosol optical depth measurements, Atmos. Environ., 45, 6267-6275, doi:10.1016/j.atmosenv.2011.08.066, 2011.

Kocak, M., Mihalopoulos, N. and Kubilay, N.: Chemical composition of the fine and coarse fraction of aerosols in the northeastern Mediterranean, Atmos. Environ., 41, 7351-7368, doi:10.1016/j.atmosenv.2007.05.011, 2007.

Kraabøl, A. G., Berntsen, T. K., Sundet, J. K. and Stordal, F.: Impacts of NO_x emissions from subsonic aircraft in a global three-dimensional chemistry transport model including plume processes, J. Geophys. Res., 107(D22), 4655, doi:10.1029/2001JD001019, 2002.

Kuhns, H., Knipping, E. M. and Vukovich, J. M.: Development of a United States-Mexico emissions inventory for the Big Bend Regional Aerosol and Visibility Observational (BRAVO) Study, J. Air Waste Manag. Assoc., 55, 677-92, doi:10.1080/10473289.2005.10464648, 2005.

Lamsal, L. N., Martin, R. V., Padmanabhan, A., van Donkelaar, A., Zhang, Q., Sioris, C. E., Chance, K., Kurosu, T. P. and Newchurch, M. J.: Application of satellite observations for timely updates to global anthropogenic NO_x emission inventories, Geophys. Res. Lett., 38, L05810, doi:10.1029/2010GL046476, 2011.

Lamsal, L. N., Martin, R. V., Parrish, D. D. and Krotkov, N. A.: Scaling relationship for NO_2 pollution and urban population size: A satellite perspective, Environ. Sci. Technol., 47, 7855-61, doi:10.1021/es400744g, 2013.

Lamsal, L. N., Martin, R. V., van Donkelaar, A., Celarier, E. A., Bucsela, E. J., Boersma, K. F., Dirksen, R., Luo, C. and Wang, Y.: Indirect validation of tropospheric nitrogen dioxide retrieved from the OMI satellite instrument: Insight into the seasonal variation of nitrogen oxides at northern midlatitudes, J. Geophys. Res., 115, D05302, doi:10.1029/2009JD013351, 2010.

Lamsal, L. N., Martin, R. V., van Donkelaar, A., Steinbacher, M., Celarier, E. A., Bucsela, E., Dunlea, E. J. and Pinto, J. P.: Ground-level nitrogen dioxide concentrations inferred from the satellite-borne Ozone Monitoring Instrument, J. Geophys. Res., 113, D16308, doi:10.1029/2007JD009235, 2008.

Lee, C., Martin, R. V., van Donkelaar, A., Dickerson, R. R., Hains, J. C., Krotkov, N., Richter, A., Vinnikov, K. and Schwab, J. J.: SO_2 emissions and lifetimes: Estimates from inverse modeling using in situ and global, space-based (SCIAMACHY and OMI) observations, J. Geophys. Res., 116, D06304, doi:10.1029/2010JD014758.

Leibensperger, E. M., Mickley, L. J., Jacob, D. J., Chen, W. -., Seinfeld, J. H., Nenes, A., Adams, P. J., Streets, D. G., Kumar, N. and Rind, D.: Climatic effects of 1950–2050 changes in U.S. anthropogenic aerosols– Part 1: Aerosol trends and radiative forcing, Atmos. Chem. Phys., 12, 3333-3348, doi:10.5194/acp-12-3333-2012, 2012.

Lepeule, J., Laden, F., Dockery, D. and Schwartz, J.: Chronic exposure to fine particles and mortality: An extended follow-up of the Harvard Six Cities Study from 1974 to 2009, Environ. Health Perspec., 120, 965-970, doi:10.1289/ehp.1104660, 2012.

Levy, R. C., Remer, L. A., Mattoo, S., Vermote, E. F. and Kaufman, Y. J.: Second-generation operational algorithm: Retrieval of aerosol properties over land from inversion of Moderate Resolution Imaging Spectroradiometer spectral reflectance, J. Geophys. Res., 112, D13211, doi:10.1029/2006JD007811, 2007.

Li, Y., Henze, D. K., Jack, D. and Kinney, P.: The influence of air quality model resolution on health impact assessment for fine particulate matter and its components, Air Qual., Atmos. Health, 1-18, doi: 10.1007/s11869-015-0321-z, 2015

Liang, J. and Jacobson, M. Z.: Effects of subgrid segregation on ozone production efficiency in a chemical model, Atmos. Environ., 34, 2975-2982, doi:10.1016/S1352-2310(99)00520-8, 2000.

Liao, H., Henze, D. K., Seinfeld, J. H., Wu, S. and Mickley, L. J.: Biogenic secondary organic aerosol over the United States: Comparison of climatological simulations with observations, J. Geophys. Res., 112, D06201, doi:10.1029/2006JD007813, 2007.

Lim, S. S., Vos, T., Flaxman, A. D., Danaei, G., Shibuya, K., Adair-Rohani, H., AlMazroa, M. A., Amann, M., Anderson, H. R., Andrews, K. G., Aryee, M., Atkinson, C., Bacchus, L. J., Bahalim, A. N., Balakrishnan, K., Balmes, J., Barker-Collo, S., Baxter, A., Bell, M. L., Blore, J. D., Blyth, F., Bonner, C., Borges, G., Bourne, R., Boussinesq, M., Brauer, M., Brooks, P., Bruce, N. G., Brunekreef, B., Bryan-Hancock, C., Bucello, C., Buchbinder, R., Bull, F., Burnett, R. T., Byers, T. E., Calabria, B., Carapetis, J., Carnahan, E., Chafe, Z., Charlson, F., Chen, H., Chen, J. S., Cheng, A. T., Child, J. C., Cohen, A., Colson, K. E., Cowie, B. C., Darby, S., Darling, S., Davis, A., Degenhardt, L., Dentener, F., Des Jarlais, D. C., Devries, K., Dherani, M., Ding, E. L., Dorsey, E. R., Driscoll, T., Edmond, K., Ali, S. E., Engell, R. E., Erwin, P. J., Fahimi, S., Falder, G., Farzadfar, F., Ferrari, A., Finucane, M. M., Flaxman, S., Fowkes, F. G. R., Freedman, G., Freeman, M. K., Gakidou, E., Ghosh, S., Giovannucci, E., Gmel, G., Graham, K., Grainger, R., Grant, B., Gunnell, D., Gutierrez, H. R., Hall, W., Hoek, H. W., Hogan, A., Hosgood III, H. D., Hoy, D., Hu, H., Hubbell, B. J., Hutchings, S. J., Ibeanusi, S. E., Jacklyn, G. L., Jasrasaria, R., Jonas, J. B., Kan, H., Kanis, J. A., Kassebaum, N., Kawakami, N., Khang, Y., Khatibzadeh, S., Khoo, J., Kok, C., Laden, F., Lalloo, R., Lan, Q., Lathlean, T., Leasher, J. L., Leigh, J., Li, Y., Lin, J. K., Lipshultz, S. E., London, S., Lozano, R., Lu, Y., Mak, J., Malekzadeh, R., Mallinger, L., Marcenes, W., March, L., Marks, R., Martin, R., McGale, P., McGrath, J., Mehta, S., Memish, Z. A., Mensah, G. A., Merriman, T. R., Micha, R., Michaud, C., Mishra, V., Hanafiah, K. M., Mokdad, A. A., Morawska, L., Mozaffarian, D., Murphy, T., Naghavi, M., Neal, B., Nelson, P. K., Nolla, J. M., Norman, R., Olives, C., Omer, S. B., Orchard, J., Osborne, R., Ostro, B., Page, A., Pandey, K. D., Parry, C. D., Passmore, E., Patra, J., Pearce, N., Pelizzari, P. M., Petzold, M., Phillips, M. R., Pope, D., Pope III, C. A., Powles, J., Rao, M., Razavi, H., Rehfuess, E. A., Rehm, J. T., Ritz, B., Rivara, F. P., Roberts, T., Robinson, C., Rodriguez-Portales, J. A., Romieu, I., Room, R., Rosenfeld, L. C., Roy, A., Rushton, L., Salomon, J. A., Sampson, U., Sanchez-Riera, L., Sanman, E., Sapkota, A., Seedat, S., Shi, P., Shield, K., Shivakoti, R., Singh, G. M., Sleet, D. A., Smith, E., Smith, K. R., Stapelberg, N. J., Steenland, K., Stöckl, H., Stovner, L. J., Straif, K., Straney, L., Thurston, G. D., Tran, J. H., Van Dingenen, R., van Donkelaar, A., Veerman, J. L., Vijayakumar, L., Weintraub, R., Weissman, M. M., White, R. A., Whiteford, H., Wiersma, S. T., Wilkinson, J. D., Williams, H. C., Williams, W., Wilson, N., Woolf, A. D., Yip, P., Zielinski, J. M., Lopez, A. D., Murray, C. J. and Ezzati, M.: A comparative risk assessment of burden of disease and injury attributable to 67 risk factors and risk factor clusters in 21 regions, 1990–2010: a systematic analysis for the Global Burden of Disease Study 2010, The Lancet, 380, 2224-2260, doi:10.1016/S0140-6736(12)61766-8, 2012.

Lin, J. and McElroy, M. B.: Impacts of boundary layer mixing on pollutant vertical profiles in the lower troposphere: Implications to satellite remote sensing, Atmos. Environ., 44, 1726-1739, doi:10.1016/j.atmosenv.2010.02.009, 2010.

Lin, S., Chao, W. C., Sud, Y. C. and Walker, G. K.: A class of the van Leer-type transport schemes and its application to the moisture transport in a general circulation model, Mon. Weather Rev., 122, 1575-1593, doi:10.1175/1520-0493(1994)122<1575:ACOTVL>2.0.CO;2, 1994.

Lin, S. and Rood, R. B.: Multidimensional flux-form semi-lagrangian transport schemes, Mon. Weather Rev., 124, 2046-2070, doi:10.1175/1520-0493(1996)124<2046:MFFSLT>2.0.CO;2, 1996.

Liu, S. C., Trainer, M., Fehsenfeld, F. C., Parrish, D. D., Williams, E. J., Fahey, D. W., Hübler, G. and Murphy, P. C.: Ozone production in the rural troposphere and the implications for regional and global ozone distributions, J. Geophys. Res., 92, 4191-4207, doi:10.1029/JD092iD04p04191, 1987.

Liu, H. Y., Jacob, D. J., Bey, I. and Yantosca, R. M.: Constraints from ^{210}Pb and ^{7}Be on wet deposition and transport in a global three-dimensional chemical tracer model driven by assimilated meteorological fields, J. Geophys. Res., 106, 12109-12128, doi:10.1029/2000JD900839, 2001.

Liu, Y., Park, R. J., Jacob, D. J., Li, Q. B., Kilaru, V. and Sarnat, J. A.: Mapping annual mean ground-level $PM_{2.5}$ concentrations using Multiangle Imaging Spectroradiometer aerosol optical thickness over the contiguous United States, J. Geophys. Res., 109, D22206, doi:10.1029/2004JD005025, 2004.

Liu, Y., Koutrakis, P. and Kahn, R.: Estimating fine particulate matter component concentrations and size distributions using satellite-retrieved fractional aerosol optical depth: part 1--method development, J. Air Waste Manag. Assoc., 57, 1351-9, doi:10.3155/1047-3289.S7.11.1351, 2007.

Lu, R., Turco, R. P. and Jacobson, M. Z.: An integrated air pollution modeling system for urban and regional scales: 1. Structure and performance, J. Geophys. Res., 102, 6063-6079, doi:10.1029/96JD03501, 1997.

Lu, Z., Zhang, Q. and Streets, D. G.: Sulfur dioxide and primary carbonaceous aerosol emissions in China and India, 1996-2010, Atmos. Chem. Phys., 11, 9839-9864, doi:10.5194/acp-11-9839-2011, 2011.

Mallet, V., Pourchet, A., Quélo, D. and Sportisse, B.: Investigation of some numerical issues in a chemistry-transport model: Gas-phase simulations, J. Geophys. Res., 112, D15301, doi:10.1029/2006JD008373, 2007.

Mallet, V. and Sportisse, B.: Uncertainty in a chemistry-transport model due to physical parameterizations and numerical approximations: An ensemble approach applied to ozone modeling, J. Geophys. Res., 111, D01302, doi:10.1029/2005JD006149, 2006.

Malm, W. C. and Hand, J. L.: An examination of the physical and optical properties of aerosols collected in the IMPROVE program, Atmos. Environ., 41, 3407-3427, doi:10.1016/j.atmosenv.2006.12.012, 2007.

Malm, W. C., Sisler, J. F., Huffman, D., Eldred, R. A. and Cahill, T. A.: Spatial and seasonal trends in particle concentration and optical extinction in the United States, J. Geophys. Res., 99, 1347-1370, doi:10.1029/93JD02916, 1994.

Mao, J., Fan, S., Jacob, D. J. and Travis, K. R.: Radical loss in the atmosphere from Cu-Fe redox coupling in aerosols, Atmos. Chem. Phys., 13, 509-519, doi:10.5194/acp-13-509-2013, 2013.

Mao, J., Jacob, D. J., Evans, M. J., Olson, J. R., Ren, X., Brune, W. H., St Clair, J. M., Crounse, J. D., Spencer, K. M., Beaver, M. R., Wennberg, P. O., Cubison, M. J., Jimenez, J. L., Fried, A., Weibring, P., Walega, J. G., Hall, S. R., Weinheimer, A. J., Cohen, R. C., Chen, G., Crawford, J. H., McNaughton, C., Clarke, A. D., Jaegle, L., Fisher, J. A., Yantosca, R. M., Le Sager, P. and Carouge, C.: Chemistry of hydrogen oxide radicals (HO_x) in the Arctic troposphere in spring, Atmos. Chem. Phys., 10, 5823-5838, doi:10.5194/acp-10-5823-2010, 2010.

Martin, R. V.: Satellite remote sensing of surface air quality, Atmos. Environ., 42, 7823-7843, doi:10.1016/j.atmosenv.2008.07.018, 2008.

Martin, R. V., Jacob, D. J., Chance, K., Kurosu, T. P., Palmer, P. I. and Evans, M. J.: Global inventory of nitrogen oxide emissions constrained by space-based observations of NO_2 columns, J. Geophys. Res., 108(D17), 4537, doi:10.1029/2003JD003453, 2003a.

Martin, R. V., Jacob, D. J., Yantosca, R. M., Chin, M. and Ginoux, P.: Global and regional decreases in tropospheric oxidants from photochemical effects of aerosols, J. Geophys. Res., 108(D3), 4097, doi:10.1029/2002JD002622, 2003b.

Martin, R. V., Sauvage, B., Folkins, I., Sioris, C. E., Boone, C., Bernath, P. and Ziemke, J.: Space-based constraints on the production of nitric oxide by lightning, J. Geophys. Res., 112, D09309, doi:10.1029/2006JD007831, 2007.

McMurry, P.: A review of atmospheric aerosol measurements, Atmos. Environ., 34, 1959-1999, doi:10.1016/S1352-2310(99)00455-0, 2000.

McRae, G. J., Goodin, W. R. and Seinfeld, J. H.: Numerical solution of the atmospheric diffusion equation for chemically reacting flows, J. Comput. Phys., 45, 1-42, doi:10.1016/0021-9991(82)90101-2, 1982.

Meijer, E. W., van Velthoven, P. F. J., Wauben, W. M. F., Beck, J. P. and Velders, G. J. M.: The effects of the conversion of nitrogen oxides in aircraft exhaust plumes in global models, Geophys. Res. Lett., 24, 3013-3016, doi:10.1029/97GL53156, 1997.

Miller, R. L. and Kahn, J. S.: Statistical analysis in the geological sciences, 205 pp., John Wiley and Sons, New York, 1962.

Mishchenko, M. I., Cairns, B., Hansen, J. E., Travis, L. D., Kopp, G., Schueler, C. F., Fafaul, B. A., Hooker, R. J., Maring, H. B. and Itchkawich, T.: Accurate monitoring of terrestrial aerosols and total solar irradiance: Introducing the Glory mission, Bull. Am. Meteorol. Soc., 88, 677-691, doi:10.1175/BAMS-88-5-677, 2007.

Mu, M., Randerson, J. T., van der Werf, G. R., Giglio, L., Kasibhatla, P., Morton, D., Collatz, G. J., DeFries, R. S., Hyer, E. J., Prins, E. M., Griffith, D. W. T., Wunch, D., Toon, G. C., Sherlock, V. and Wennberg, P. O.: Daily and 3-hourly variability in global fire emissions and consequences for atmospheric model predictions of carbon monoxide, J. Geophys. Res., 116, D24303, doi:10.1029/2011JD016245, 2011.

Murray, L. T., Jacob, D. J., Logan, J. A., Hudman, R. C. and Koshak, W. J.: Optimized regional and interannual variability of lightning in a global chemical transport model constrained by LIS/OTD satellite data, J. Geophys. Res., 117, D20307, doi:10.1029/2012JD017934, 2012.

National Research Council: Integrated science assessment for particulate matter (Final Report), U. S. Environmental Protection Agency, Washington, DC, EPA/600/R-08/139F, 2009.

Olivier, J. G. J., Van Aardenne, J. A., Dentener, F. J., Pagliari, V., Ganzeveld, L. N. and Peters J. A. H. W.: Recent trends in global greenhouse gas emissions: regional trends 1970-2000 and spatial distribution of key sources in 2000. Env. Sc., 2 (2-3), 81-99, doi:10.1080/15693430500400345, 2005.

Ostro, B., Lipsett, M., Reynolds, P., Goldberg, D., Hertz, A., Garcia, C., Henderson, K. D. and Bernstein, L.: Long-term exposure to constituents of fine particulate air pollution and mortality: Results from the California Teachers Study, Environ. Health Perspec., 118, 363-369, doi:10.1289/ehp.0901181, 2010.

Paciorek, C. J. and Liu, Y.: Limitations of remotely sensed aerosol as a spatial proxy for fine particulate matter, Environ. Health Perspec., 117, 904-909, doi:10.1289/ehp.0800360, 2009.

Pang, Y., Turpin, B. J. and Gundel, L. A.: On the importance of organic oxygen for understanding organic aerosol particles, Aerosol Sci. Tech., 40, 128-133, doi:10.1080/02786820500423790, 2006.

Park, R. J., Jacob, D. J., Field, B. D., Yantosca, R. M. and Chin, M.: Natural and transboundary pollution influences on sulfate-nitrate-ammonium aerosols in the United States: Implications for policy, J. Geophys. Res., 109, D15204, doi:10.1029/2003JD004473, 2004.

Park, R. J., Jacob, D. J., Chin, M. and Martin, R. V.: Sources of carbonaceous aerosols over the United States and implications for natural visibility, J. Geophys. Res., 108(D12), 4355, doi:10.1029/2002JD003190, 2003.

Park, R. J., Jacob, D. J., Kumar, N. and Yantosca, R. M.: Regional visibility statistics in the United States: Natural and transboundary pollution influences, and implications for the Regional Haze Rule, Atmos. Environ., 40, 5405–5423, doi:10.1016/j.atmosenv.2006.04.059, 2006.

Perrone, M. R., Piazzalunga, A., Prato, M. and Carofalo, I.: Composition of fine and coarse particles in a coastal site of the central Mediterranean: Carbonaceous species contributions, Atmos. Environ., 45, 7470–7477, doi:10.1016/j.atmosenv.2011.04.030, 2011.

Pey, J., Querol, X. and Alastuey, A.: Variations of levels and composition of PM_{10} and $PM_{2.5}$ at an insular site in the Western Mediterranean, Atmos. Res., 94, 285–299, doi:10.1016/j.atmosres.2009.06.006, 2009.

Philip, S., Martin, R. V., Pierce, J. R., Jimenez, J. L., Zhang, Q., Canagaratna, M. R., Spracklen, D. V., Nowlan, C. R., Lamsal, L. N., Cooper, M. J. and Krotkov, N. A.: Spatially and seasonally resolved estimate of the ratio of organic mass to organic carbon, Atmos. Environ., 87, 34-40, doi:10.1016/j.atmosenv.2013.11.065, 2014a.

Philip, S., Martin, R. V., van Donkelaar, A., Lo, J. W., Wang, Y., Chen, D., Zhang, Q., Lu, Z., Bittman, S., Kasibhatla, P. S., Streets, D. G. and Macdonald, D. J.: Global chemical composition of ambient fine particulate matter for exposure assessment, Environ. Sci. Technol., 48, 13060-13068, doi:10.1021/es502965b, 2014b.

Polidori, A., Turpin, B. J., Davidson, C. I., Rodenburg, L. A. and Maimone, F.: Organic $PM_{2.5}$: Fractionation by polarity, FTIR spectroscopy, and OM/OC ratio for the Pittsburgh aerosol, Aerosol Sci. Tech., 42, 233-246, doi:10.1080/02786820801958767, 2008.

Pope, C. A. III, Ezzati, M. and Dockery, D. W.: Fine-particulate air pollution and life expectancy in the United States, N. Engl. J. Med., 360, 376-386, doi:10.1056/NEJMsa0805646, 2009.

Prather, M. J., Zhu, X., Strahan, S. E., Steenrod, S. D. and Rodriguez, J. M.: Quantifying errors in trace species transport modeling, Proc. Natl. Acad. Sci. U. S. A., 105, 19617-19621, doi:10.1073/pnas.0806541106, 2008.

Prather, M. J.: Numerical advection by conservation of second-order moments, J. Geophys. Res., 91, 6671-6681, doi:10.1029/JD091iD06p06671, 1986.

Price, C. and Rind, D.: A simple lightning parameterization for calculating global lightning distributions, J. Geophys. Res., 97, 9919-9933, doi:10.1029/92JD00719, 1992.

Punger, E. M. and West, J. J.: The effect of grid resolution on estimates of the burden of ozone and fine particulate matter on premature mortality in the USA, Air Qual., Atmos. Health, 6, 563-573, doi:10.1007/s11869-013-0197-8, 2013.

Pye, H. O. T., Liao, H., Wu, S., Mickley, L. J., Jacob, D. J., Henze, D. K. and Seinfeld, J. H.: Effect of changes in climate and emissions on future sulfate-nitrate-ammonium aerosol levels in the United States, J. Geophys. Res., 114, D01205, doi:10.1029/2008JD010701, 2009.

Qu, W. J., Zhang, X. Y., Arimoto, R., Wang, D., Wang, Y. Q., Yan, L. W. and Li, Y.: Chemical composition of the background aerosol at two sites in southwestern and northwestern China: Potential influences of regional transport, Tellus B, 60, 657-673, doi:10.1111/j.1600-0889.2008.00342-x, 2008.

Qu, W., Zhang, X., Arimoto, R., Wang, Y., Wang, D., Sheng, L. and Fu, G.: Aerosol background at two remote CAWNET sites in western China, Sci. Total Environ., 407, 3518–3529, doi:10.1016/j.scitotenv.2009.02.012, 2009.

Ramanathan, V. and Carmichael, G.: Global and regional climate changes due to black carbon, Nature Geosci., 1, 221-227, doi:10.1038/ngeo156, 2008.

Rastigejev, Y., Brenner, M. P. and Jacob, D. J.: Spatial reduction algorithm for atmospheric chemical transport models, Proc. Natl. Acad. Sci. U. S. A., 104, 13875-13880, doi:10.1073/pnas.0705649104, 2007.

Rattigan, O. V., Felton, H. D., Bae, M., Schwab, J. J. and Demerjian, K. L.: Comparison of long-term $PM_{2.5}$ carbon measurements at an urban and rural location in New York, Atmos. Environ., 45, 3228-3236, doi:10.1016/j.atmosenv.2011.03.048, 2011.

Ridley, D. A., Heald, C. L. and Ford, B.: North African dust export and deposition: A satellite and model perspective, J. Geophys. Res., 117, D02202, doi:10.1029/2011JD016794, 2012.

Rienecker, M. M., Suarez, M. J., Todling, R., Bacmeister, J., Takacs, L., Liu, H.-C., Gu, W., Sienkiewicz, M., Koster, R. D., Gelaro, R., Stajner, I., and Nielsen, J. E.: The GEOS-5 Data Assimilation System-Documentation of versions 5.0.1 and 5.1.0, and 5.2.0. NASA Tech. Rep. Series on Global Modeling and Data Assimilation, NASA/TM-2008-104606, Vol. 27, 92 pp., Goddard Space Flight Center, Greenbelt, Maryland, U.S.A., 2008.

Rind, D., Lerner, J., Jonas, J. and McLinden, C.: Effects of resolution and model physics on tracer transports in the NASA Goddard Institute for Space Studies general circulation models, J. Geophys. Res., 112, D09315, doi:10.1029/2006JD007476, 2007.

Rood, R. B.: Numerical advection algorithms and their role in atmospheric transport and chemistry models, Rev. Geophys., 25, 71-100, doi:10.1029/RG025i001p00071, 1987.

Rotman, D. A., Atherton, C. S., Bergmann, D. J., Cameron-Smith, P. J., Chuang, C. C., Connel, P. S., Dignon, J. E., Franz, A., Grant, K. E., Kinnison, D. E., Molenkamp, C. R., Proctor, D. D. and Tannahill, J. R.: IMPACT, the LLNL 3-D global atmospheric chemical transport model for the combined troposphere and stratosphere: Model description and analysis of ozone and other trace gases, J. Geophys. Res., 109, D04303, doi:10.1029/2002JD003155, 2004.

Russell, L. M., Takahama, S., Liu, S., Hawkins, L. N., Covert, D. S., Quinn, P. K. and Bates, T. S.: Oxygenated fraction and mass of organic aerosol from direct emission and atmospheric processing measured on the R/V Ronald Brown during TEXAQS/GoMACCS 2006, J. Geophys. Res., 114, D00F05, doi:10.1029/2008JD011275, 2009.

Saide, P. E., Carmichael, G. R., Liu, Z., Schwartz, C. S., Lin, H. C., da Silva, A. M. and Hyer, E.: Aerosol optical depth assimilation for a size-resolved sectional model: impacts of observationally constrained, multi-wavelength and fine mode retrievals on regional scale analyses and forecasts, Atmos. Chem. Phys., 13, 10425-10444, doi:10.5194/acp-13-10425-2013, 2013.

Santillana, M., Le Sager, P., Jacob, D. J. and Brenner, M. P.: An adaptive reduction algorithm for efficient chemical calculations in global atmospheric chemistry models, Atmos. Environ., 44, 4426-4431, doi:10.1016/j.atmosenv.2010.07.044, 2010.

Santillana, M., Zhang, L. and Yantosca, R.: Estimating numerical errors due to operator splitting in global atmospheric chemistry models: Transport and chemistry, J. Comput. Phys., 305, 372-386, doi:10.1016/j.jcp.2015.10.052, 2016.

Sarnat, J. A., Moise, T., Shpund, J., Liu, Y., Pachon, J. E., Qasrawi, R., Abdeen, Z., Brenner, S., Nassar, K., Saleh, R. and Schauer, J. J.: Assessing the spatial and temporal variability of fine particulate matter components in Israeli, Jordanian, and Palestinian cities, Atmos. Environ., 44, 2383-2392, doi:10.1016/j.atmosenv.2010.04.007, 2010.

Sauvage, B., Martin, R. V., van Donkelaar, A. and Ziemke, J. R.: Quantification of the factors controlling tropical tropospheric ozone and the South Atlantic maximum, J. Geophys. Res., 112, D11309, doi:10.1029/2006JD008008, 2007.

Schaaf, C. B., Gao, F., Strahler, A. H., Lucht, W., Li, X. W., Tsang, T., Strugnell, N. C., Zhang, X. Y., Jin, Y. F., Muller, J. P., Lewis, P., Barnsley, M., Hobson, P., Disney, M., Roberts, G., Dunderdale, M., Doll, C., d'Entremont, R. P., Hu, B. X., Liang, S. L., Privette, J. L. and Roy, D.: First operational BRDF, albedo nadir reflectance products from MODIS, Remote Sens. Environ., 83, 135-148, doi:10.1016/S0034-4257(02)00091-3, 2002.

Seinfeld, J. H. and Pandis, S. N.: Atmospheric chemistry and physics: From air pollution to climate change, Second Edition, John Wiley & Sons, Inc., ISBN:978-0-471-72018-8, 2006.

Setyan, A., Zhang, Q., Merkel, M., Knighton, W. B., Sun, Y., Song, C., Shilling, J. E., Onasch, T. B., Herndon, S. C., Worsnop, D. R., Fast, J. D., Zaveri, R. A., Berg, L. K., Wiedensohler, A., Flowers, B. A., Dubey, M. K. and Subramanian, R.: Characterization of submicron particles influenced by mixed biogenic and anthropogenic emissions using high-resolution aerosol mass spectrometry: results from CARES, Atmos. Chem. Phys., 12, 8131-8156, doi:10.5194/acp-12-8131-2012, 2012.

Sheppard, S. C., Bittman, S., Swift, M. L. and Tait, J.: Modelling monthly NH_3 emissions from dairy in 12 Ecoregions of Canada, Can. J. Anim. Sci., 91, 649-661, doi:10.4141/CJAS2010-005, 2011.

Sillman, S., Logan, J. A. and Wofsy, S. C.: A regional scale model for ozone in the United States with subgrid representation of urban and power plant plumes, J. Geophys. Res., 95, 5731-5748, doi:10.1029/JD095iD05p05731, 1990.

Simon, H., Bhave, P. V., Swall, J. L., Frank, N. H. and Malm, W. C.: Determining the spatial and seasonal variability in OM/OC ratios across the US using multiple regression, Atmos. Chem. Phys., 11, 2933-2949, doi:10.5194/acp-11-2933-2011, 2011.

Simon, H. and Bhave, P. V.: Simulating the degree of oxidation in atmospheric organic particles, Environ. Sci. Technol., 46, 331-339, doi:10.1021/es202361w, 2012.

So, K. L., Guo, H. and Li, Y. S.: Long-term variation of $PM_{2.5}$ levels and composition at rural, urban, and roadside sites in Hong Kong: Increasing impact of regional air pollution, Atmos. Environ., 41, 9427-9434, doi:10.1016/j.atmosenv.2007.08.053, 2007.

Soluri, D. S., Godoy, M. L. D. P., Godoy, J. M. and Roldao, L. A.: Multi-site $PM_{2.5}$ and $PM_{2.5\text{-}10}$ aerosol source apportionment in Rio de Janeiro, Brazil, J. Braz. Chem. Soc., 18, 838-845, doi:10.1590/S0103-50532007000400025, 2007.

Son, J., Lee, J., Kim, K., Jung, K. and Bell, M. L.: Characterization of fine particulate matter and associations between particulate chemical constituents and mortality in Seoul, Korea, Environ. Health Perspec., 120, 872-878, doi:10.1289/ehp.1104316, 2012.

Sportisse, B.: An analysis of operator splitting techniques in the stiff case, J. Comput. Phys., 161, 140-168, doi:10.1006/jcph.2000.6495, 2000.

Spracklen, D. V., Jimenez, J. L., Carslaw, K. S., Worsnop, D. R., Evans, M. J., Mann, G. W., Zhang, Q., Canagaratna, M. R., Allan, J., Coe, H., McFiggans, G., Rap, A. and Forster, P.: Aerosol mass spectrometer constraint on the global secondary organic aerosol budget, Atmos. Chem. Phys., 11, 12109-12136, doi:10.5194/acp-11-12109-2011, 2011.

Stone, E., Schauer, J., Quraishi, T. A. and Mahmood, A.: Chemical characterization and source apportionment of fine and coarse particulate matter in Lahore, Pakistan, Atmos. Environ., 44, 1062-1070, doi:10.1016/j.atmosenv.2009.12.015, 2010.

Strang, G.: On the construction and comparison of difference schemes, SIAM J. Numer. Anal., 5, 506-517, doi:10.1137/0705041, 1968.

Streets, D. G., Bond, T. C., Carmichael, G. R., Fernandes, S. D., Fu, Q., He, D., Klimont, Z., Nelson, S. M., Tsai, N. Y., Wang, M. Q., Woo, J. H. and Yarber, K. F.: An inventory of gaseous and primary aerosol emissions in Asia in the year 2000, J. Geophys. Res., 108, 8809, doi:10.1029/2002JD003093, 2003.

Streets, D. G., Canty, T., Carmichael, G. R., de Foy, B., Dickerson, R. R., Duncan, B. N., Edwards, D. P., Haynes, J. A., Henze, D. K., Houyoux, M. R., Jacob, D. J., Krotkov, N. A., Lamsal, L. N., Liu, Y., Lu, Z., Martin, R. V., Pfister, G. G., Pinder, R. W., Salawitch, R. J. and Wecht, K. J.: Emissions estimation from satellite retrievals: A review of current capability, Atmos. Environ., 77, 1011-1042, doi:10.1016/j.atmosenv.2013.05.051, 2013.

Sun, Y., Zhang, Q., Macdonald, A. M., Hayden, K., Li, S. M., Liggio, J., Liu, P. S. K., Anlauf, K. G., Leaitch, W. R., Steffen, A., Cubison, M., Worsnop, D. R., van Donkelaar, A., and Martin, R. V.: Size-resolved aerosol chemistry on Whistler Mountain, Canada with a high-resolution aerosol mass spectrometer during INTEX-B, Atmos. Chem. Phys., 9, 3095-3111, doi:10.5194/acp-9-3095-2009, 2009.

Sun, Y., Zhang, Q., Zheng, M., Ding, X., Edgerton, E. S. and Wang, X.: Characterization and source apportionment of water-soluble organic matter in atmospheric fine particles ($PM_{2.5}$) with high-resolution Aerosol Mass Spectrometry and GC-MS, Environ. Sci. Technol., 45, 4854-4861, doi:10.1021/es200162h, 2011.

Thompson, T. M., Saari, R. K. and Selin, N. E.: Air quality resolution for health impact assessment: influence of regional characteristics, Atmos. Chem. Phys., 14, 969-978, doi:10.5194/acp-14-969-2014, 2014.

Thornton, J. A., Jaegle, L. and McNeill, V. F.: Assessing known pathways for HO_2 loss in aqueous atmospheric aerosols: Regional and global impacts on tropospheric oxidants, J. Geophys. Res., 113, D05303, doi:10.1029/2007JD009236, 2008.

Tiwari, S., Srivastava, A. K., Bisht, D. S., Bano, T., Singh, S., Behura, S., Srivastava, M. K., Chate, D. M. and Padmanabhamurty, B.: Black carbon and chemical characteristics of PM_{10} and $PM_{2.5}$ at an urban site of North India, J. Atmos. Chem., 62, 193-209, doi:10.1007/s10874-010-9148-z, 2009.

Turpin, B. J. and Lim, H.: Species contributions to $PM_{2.5}$ mass concentrations: Revisiting common assumptions for estimating organic mass, Aerosol Sci. Tech., 35, 602-610, doi:10.1080/02786820119445, 2001.

U.S. EPA: Integrated science assessment for particulate matter (Final Report), Washington, DC, EPA/600/R-08/139F, 2009.

van der Werf, G. R., Morton, D. C., DeFries, R. S., Giglio, L., Randerson, J. T., Collatz, G. J. and Kasibhatla, P. S.: Estimates of fire emissions from an active deforestation region in the southern Amazon based on satellite data and biogeochemical modelling, Biogeosciences, 6, 235-249, doi:10.5194/bg-6-235-2009, 2009.

van Donkelaar, A., Martin, R. V., Brauer, M., Kahn, R., Levy, R., Verduzco, C. and Villeneuve, P. J.: Global estimates of ambient fine particulate matter concentrations from satellite-based aerosol optical depth: Development and application, Environ. Health Perspec., 118, 847-855, doi:10.1289/ehp.0901623, 2010.

van Donkelaar, A., Zhang, L., Chen, D., Martin, R. V., Pasch, A. N., Szykman, J. J. and Wang, Y. X.: Improving the accuracy of daily satellite-derived ground-level fine aerosol concentration estimates for North America, Environ. Sci. Technol., 46, 11971-11978, doi:10.1021/es3025319, 2012.

van Donkelaar, A., Martin, R. V., Leaitch, W. R., Macdonald, A. M., Walker, T. W., Streets, D. G., Zhang, Q., Dunlea, E. J., Jimenez, J. L., Dibb, J. E., Huey, L. G., Weber, R. and Andreae, M. O.: Analysis of aircraft and satellite measurements from the Intercontinental Chemical Transport Experiment (INTEX-B) to quantify long-range transport of East Asian sulfur to Canada, Atmos. Chem. Phys., 8, 2999-3014, doi:10.5194/acp-8-2999-2008, 2008.

van Donkelaar, A., Martin, R. V. and Park, R. J.: Estimating ground-level $PM_{2.5}$ using aerosol optical depth determined from satellite remote sensing, J. Geophys. Res., 111, D21201, doi:10.1029/2005JD006996, 2006.

van Donkelaar, A., Martin, R. V., Spurr, R. J. D., Drury, E., Remer, L. A., Levy, R. C. and Wang, J.: Optimal estimation for global ground-level fine particulate matter concentrations, J. Geophys. Res., 118, 5621-5636, doi:10.1002/jgrd.50479, 2013.

Vinken, G. C. M., Boersma, K. F., Jacob, D. J. and Meijer, E. W.: Accounting for non-linear chemistry of ship plumes in the GEOS-Chem global chemistry transport model, Atmos. Chem. Phys., 11, 11707-11722, doi:10.5194/acp-11-11707-2011, 2011.

Walker, J. M., Philip, S., Martin, R. V. and Seinfeld, J. H.: Simulation of nitrate, sulfate, and ammonium aerosols over the United States, Atmos. Chem. Phys., 12, 11213-11227, doi:10.5194/acp-12-11213-2012, 2012.

Wang, Q., Jacob, D. J., Fisher, J. A., Mao, J., Leibensperger, E. M., Carouge, C. C., Le Sager, P., Kondo, Y., Jimenez, J. L., Cubison, M. J. and Doherty, S. J.: Sources of carbonaceous aerosols and deposited black carbon in the Arctic in winter-spring: implications for radiative forcing, Atmos. Chem. Phys., 11, 12453-12473, doi:10.5194/acp-11-12453-2011, 2011.

Wang, Y., Jacob, D. J. and Logan, J. A.: Global simulation of tropospheric O_3-NO_x-hydrocarbon chemistry: 1. Model formulation, J. Geophys. Res., 103, 10713-10725, doi:10.1029/98JD00158, 1998.

Wang, J. and Christopher, S. A.: Intercomparison between satellite-derived aerosol optical thickness and $PM_{2.5}$ mass: Implications for air quality studies, Geophys. Res. Lett., 30, 2095, doi:10.1029/2003GL018174, 2003.

Wang, X., Wang, Y., Hao, J., Kondo, Y., Irwin, M., Munger, J. W. and Zhao, Y.: Top-down estimate of China's black carbon emissions using surface observations: Sensitivity to observation representativeness and transport model error, J. Geophys. Res., 118, 5781-5795, doi:10.1002/jgrd.50397, 2013.

Wang, Y. X., McElroy, M. B., Jacob, D. J. and Yantosca, R. M.: A nested grid formulation for chemical transport over Asia: Applications to CO, J. Geophys. Res., 109, D22307, doi:10.1029/2004JD005237, 2004.

Wang, Z. S., Chien, C. and Tonnesen, G. S.: Development of a tagged species source apportionment algorithm to characterize three-dimensional transport and transformation of precursors and secondary pollutants, J. Geophys. Res., 114, D21206, doi:10.1029/2008JD010846, 2009.

Wesely, M. L.: Parameterization of surface resistances to gaseous dry deposition in regional-scale numerical models, Atmos. Environ., 23, 1293-1304, doi:10.1016/0004-6981(89)90153-4, 1989.

White, W. H. and Roberts, P. T.: Nature and origins of visibility-reducing aerosols in Los-Angeles Air Basin, Atmos. Environ., 11, 803-812, doi:10.1016/0004-6981(77)90042-7, 1977.

White, W. H.: Chemical markers for sea salt in IMPROVE aerosol data, Atmos. Environ., 42, 261-274, doi:10.1016/j.atmosenv.2007.09.040, 2008.

WHO Regional Office for Europe (2013): Review of evidence on health aspects of air pollution – REVIHAAP project: Technical report. Copenhagen: WHO Regional Office for Europe (http://www.euro.who.int/__data/assets/pdf_file/0004/193108/REVIHAAP-Final-technical-report-final-version.pdf?ua=1), 2013.

Wild, O. and Prather, M. J.: Global tropospheric ozone modeling: Quantifying errors due to grid resolution, J. Geophys. Res., 111, D11305, doi:10.1029/2005JD006605, 2006.

Winker, D. M., Hunt, W. H. and McGill, M. J.: Initial performance assessment of CALIOP, Geophys. Res. Lett., 34, L19803, doi:10.1029/2007GL030135, 2007.

Wu, S., Mickley, L. J., Jacob, D. J., Logan, J. A., Yantosca, R. M. and Rind, D.: Why are there large differences between models in global budgets of tropospheric ozone?, J. Geophys. Res., 112, D05302, doi:10.1029/2006JD007801, 2007.

Xing, L., Fu, T., Cao, J. J., Lee, S. C., Wang, G. H., Ho, K. F., Cheng, M. -. and You, C.: Seasonal and spatial variability of the OM/OC mass ratios and high regional correlation between oxalic acid and zinc in Chinese urban organic aerosols, Atmos. Chem. Phys., 13, 4307-4318, doi:10.5194/acp-13-4307-2013, 2013.

Xu, J., Martin, R. V., van Donkelaar, A., Kim, J., Choi, M., Zhang, Q., Geng, G., Liu, Y., Ma, Z., Huang, L., Wang, Y., Chen, H., Che, H., Lin, P., and Lin, N.: Estimating ground-level $PM_{2.5}$ in Eastern China using aerosol optical depth determined from the GOCI satellite instrument, Atmos. Chem. Phys. Discuss., 15, 17251-17281, doi:10.5194/acpd-15-17251-2015, 2015.

Yan, Y. -., Lin, J. -., Kuang, Y., Yang, D. and Zhang, L.: Tropospheric carbon monoxide over the Pacific during HIPPO: two-way coupled simulation of GEOS-Chem and its multiple nested models, Atmos. Chem. Phys., 14, 12649-12663, doi:10.5194/acp-14-12649-2014, 2014.

Yang, F., Tan, J., Zhao, Q., Du, Z., He, K., Ma, Y., Duan, F., Chen, G. and Zhao, Q.: Characteristics of $PM_{2.5}$ speciation in representative megacities and across China, Atmos. Chem. Phys., 11, 5207-5219, doi:10.5194/acp-11-5207-2011, 2011.

Yevich, R. and Logan, J. A.: An assessment of biofuel use and burning of agricultural waste in the developing world, Global Biogeochem. Cy., 17, 1095, doi:10.1029/2002GB001952, 2003.

Yienger, J. J. and Levy, H.: Empirical-model of global soil-biogenic NO_x emissions, J. Geophys. Res., 100, 11447-11464, doi:10.1029/95JD00370, 1995.

Zhang, L., Jacob, D. J., Knipping, E. M., Kumar, N., Munger, J. W., Carouge, C. C., van Donkelaar, A., Wang, Y. X. and Chen, D.: Nitrogen deposition to the United States: distribution, sources, and processes, Atmos. Chem. Phys., 12, 4539-4554, 10.5194/acp-12-4539-2012, 2012a.

Zhang, L., Jacob, D. J., Downey, N. V., Wood, D. A., Blewitt, D., Carouge, C. C., van Donkelaar, A., Jones, D. B. A., Murray, L. T. and Wang, Y.: Improved estimate of the policy-relevant background ozone in the United States using the GEOS-Chem global model with $1/2° \times 2/3°$ horizontal resolution over North America, Atmos. Environ., 45, 6769-6776, doi:10.1016/j.atmosenv.2011.07.054, 2011a.

Zhang, J. and Reid, J. S.: MODIS aerosol product analysis for data assimilation: Assessment of over-ocean level 2 aerosol optical thickness retrievals, J. Geophys. Res., 111, D22207, doi:10.1029/2005JD006898, 2006.

Zhang, L., Vet, R., Wiebe, A., Mihele, C., Sukloff, B., Chan, E., Moran, M. D., and Iqbal, S.: Characterization of the size-segregated water-soluble inorganic ions at eight Canadian rural sites, Atmos. Chem. Phys., 8, 7133-7151, doi:10.5194/acp-8-7133-2008, 2008.

Zhang, L. M., Gong, S. L., Padro, J. and Barrie, L.: A size-segregated particle dry deposition scheme for an atmospheric aerosol module, Atmos. Environ., 35, 549-560, doi:10.1016/S1352-2310(00)00326-5, 2001.

Zhang, Q., Alfarra, M. R., Worsnop, D. R., Allan, J. D., Coe, H., Canagaratna, M. R. and Jimenez, J. L.: Deconvolution and quantification of hydrocarbon-like and oxygenated organic aerosols based on aerosol mass spectrometry, Environ. Sci. Technol., 39, 4938-4952, doi:10.1021/es048568l, 2005a.

Zhang, Q., Jimenez, J. L., Canagaratna, M. R., Allan, J. D., Coe, H., Ulbrich, I., Alfarra, M. R., Takami, A., Middlebrook, A. M., Sun, Y. L., Dzepina, K., Dunlea, E., Docherty, K., DeCarlo, P. F., Salcedo, D., Onasch, T., Jayne, J. T., Miyoshi, T., Shimono, A., Hatakeyama, S., Takegawa, N., Kondo, Y., Schneider, J., Drewnick, F., Borrmann, S., Weimer, S., Demerjian, K., Williams, P., Bower, K., Bahreini, R., Cottrell, L., Griffin, R. J., Rautiainen, J., Sun, J. Y., Zhang, Y. M. and Worsnop, D. R.: Ubiquity and dominance of oxygenated species in organic aerosols in anthropogenically-influenced Northern Hemisphere midlatitudes, Geophys. Res. Lett., 34, L13801, doi:10.1029/2007GL029979, 2007.

Zhang, Q., Streets, D. G., Carmichael, G. R., He, K. B., Huo, H., Kannari, A., Klimont, Z., Park, I. S., Reddy, S., Fu, J. S., Chen, D., Duan, L., Lei, Y., Wang, L. T., and Yao, Z. L.: Asian emissions in 2006 for the NASA INTEX-B mission, Atmos. Chem. Phys., 9, 5131-5153, doi:10.5194/acp-9-5131-2009, 2009.

Zhang, Q., Worsnop, D. R., Canagaratna, M. R. and Jimenez, J. L.: Hydrocarbon-like and oxygenated organic aerosols in Pittsburgh: insights into sources and processes of organic aerosols, Atmos. Chem. Phys., 5, 3289-3311, doi:10.5194/acp-5-3289-2005, 2005b.

Zhang, Q., Jimenez, J. L., Canagaratna, M. R., Ulbrich, I. M., Ng, N. L., Worsnop, D. R. and Sun, Y.: Understanding atmospheric organic aerosols via factor analysis of aerosol mass spectrometry: a review, Anal. Bioanal. Chem., 401, 3045-3067, doi:10.1007/s00216-011-5355-y, 2011b.

Zhang, X. Y., Wang, Y. Q., Niu, T., Zhang, X. C., Gong, S. L., Zhang, Y. M. and Sun, J. Y.: Atmospheric aerosol compositions in China: spatial/temporal variability, chemical signature, regional haze distribution and comparisons with global aerosols, Atmos. Chem. Phys., 12, 779-799, doi:10.5194/acp-12-779-2012, 2012b.

Zhou, J., Ito, K., Lall, R., Lippmann, M. and Thurston, G.: Time-series analysis of mortality effects of fine particulate matter components in Detroit and Seattle, Environ. Health Perspec., 119, 461-466, doi:10.1289/ehp.1002613, 2011.

APPENDIX A: COPYRIGHT PERMISSION

A1: COPYRIGHT PERMISSION FOR CHAPTER 2

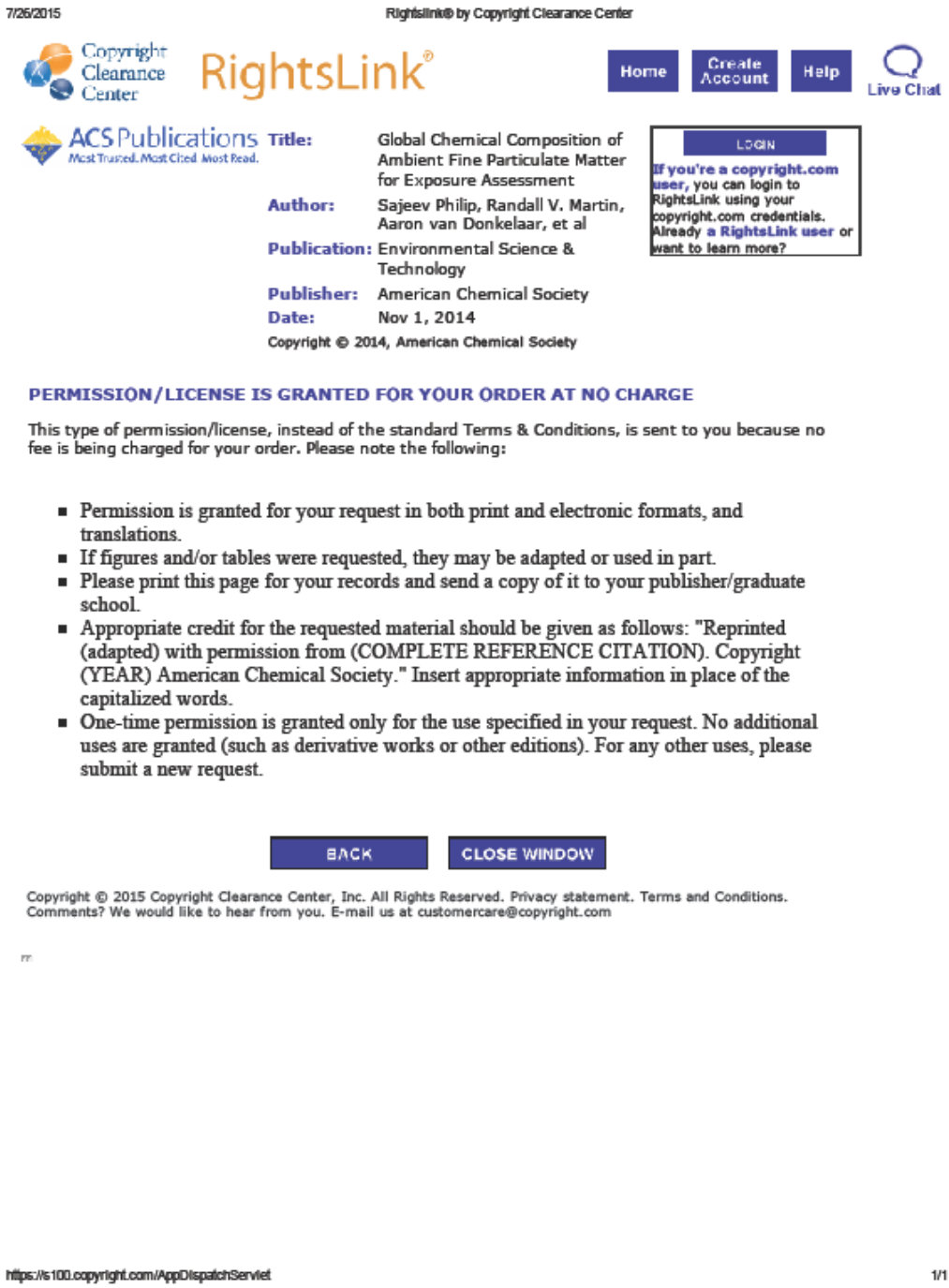

7/26/2015 RightsLink® by Copyright Clearance Center

Copyright Clearance Center RightsLink®

Home | Create Account | Help | Live Chat

ACS Publications Most Trusted. Most Cited. Most Read.

Title: Global Chemical Composition of Ambient Fine Particulate Matter for Exposure Assessment

Author: Sajeev Philip, Randall V. Martin, Aaron van Donkelaar, et al

Publication: Environmental Science & Technology

Publisher: American Chemical Society

Date: Nov 1, 2014

Copyright © 2014, American Chemical Society

LOGIN

If you're a copyright.com user, you can login to RightsLink using your copyright.com credentials. Already a RightsLink user or want to learn more?

PERMISSION/LICENSE IS GRANTED FOR YOUR ORDER AT NO CHARGE

This type of permission/license, instead of the standard Terms & Conditions, is sent to you because no fee is being charged for your order. Please note the following:

- Permission is granted for your request in both print and electronic formats, and translations.
- If figures and/or tables were requested, they may be adapted or used in part.
- Please print this page for your records and send a copy of it to your publisher/graduate school.
- Appropriate credit for the requested material should be given as follows: "Reprinted (adapted) with permission from (COMPLETE REFERENCE CITATION). Copyright (YEAR) American Chemical Society." Insert appropriate information in place of the capitalized words.
- One-time permission is granted only for the use specified in your request. No additional uses are granted (such as derivative works or other editions). For any other uses, please submit a new request.

BACK | CLOSE WINDOW

Copyright © 2015 Copyright Clearance Center, Inc. All Rights Reserved. Privacy statement. Terms and Conditions. Comments? We would like to hear from you. E-mail us at customercare@copyright.com

https://s100.copyright.com/AppDispatchServlet 1/1

A1: COPYRIGHT PERMISSION FOR CHAPTER 3

Order Completed

Thank you very much for your order.

This is a License Agreement between Sajeev Philip ("You") and Elsevier ("Elsevier"). The license consists of your order details, the terms and conditions provided by Elsevier, and the payment terms and conditions.

Get the printable license.

License Number	3676600843075
License date	Jul 26, 2015
Licensed content publisher	Elsevier
Licensed content publication	Atmospheric Environment
Licensed content title	Spatially and seasonally resolved estimate of the ratio of organic mass to organic carbon
Licensed content author	S. Philip,R.V. Martin,J.R. Pierce,J.L. Jimenez,Q. Zhang,M.R. Canagaratna,D.V. Spracklen,C.R. Nowlan,L.N. Lamsal,M.J. Cooper,N.A. Krotkov
Licensed content date	April 2014
Licensed content volume number	87
Licensed content issue number	n/a
Number of pages	7
Type of Use	reuse in a thesis/dissertation
Portion	full article
Format	both print and electronic
Are you the author of this Elsevier article?	Yes
Will you be translating?	No
Title of your thesis/dissertation	INSIGHT INTO GLOBAL GROUND-LEVEL AIR QUALITY USING SATELLITES, MODELING AND IN SITU MEASUREMENTS
Expected completion date	Nov 2015
Estimated size (number of pages)	120
Elsevier VAT number	GB 494 6272 12
Permissions price	0.00 USD
VAT/Local Sales Tax	0.00 USD / 0.00 GBP
Total	0.00 USD